Synthetic lethality by inhibition of PARP in ATM-deficient lymphoid cells:

Reduced proliferation, replication induced DNA damage, G_2 delay and cell death

Idun Dale Rein

2012

OSLO AND AKERSHUS UNIVERSITY COLLEGE OF APPLIED SCIENCES

Oslo University Hospital

SYNTHETIC LETHALITY BY INHIBITION OF PARP IN ATM-DEFICIENT LYMPHOID CELLS:

Reduced proliferation, replication induced DNA damage, G_2 delay and cell death

Thesis submitted for the Master degree (60 ECTS):
by

Idun Dale Rein

Master of Biomedicine
Faculty of Health Sciences
2012

**Department of Radiation Biology,
Institute of Cancer Research,
Oslo University Hospital
and
Oslo University College**

OSLO AND AKERSHUS
UNIVERSITY COLLEGE
OF APPLIED SCIENCES

Oslo
University Hospital

ACKNOWLEDGMENTS

The work presented in this thesis was carried out at the department of Radiation Biology, Institute for Cancer Research, Oslo University Hospital, from August 2011 until May 2012.

I would like to use this opportunity to thank my insightful and enthusiastic supervisor senior scientist Trond Stokke. Throughout this work, he has tirelessly taken the time to discuss every aspect of my results and thesis, which have been both challenging and highly beneficial. His belief in me and extraordinary involvement in both practical and theoretical subjects of all sorts has been a source of inspiration.

I would also like to thank all the wonderful members of the Molecular Radiation Biology research group, which I have been lucky enough to be a part of for the past four years. They make each day a little better, with their experience, helpfulness and support. A special "thank you" to PhD Kirsti Solberg Landsverk for her generous introduction into flow cytometry and lymphoma cell experiments. I deeply appreciate her resourcefulness and knowledge as well as her practical experience in the many aspects of research and life in general. Moreover, I value her sense of humor and positivity.

The rest of the department of Radiation Biology is also entitled to my gratitude for making me feel at home and appreciated. I hope to have many more years of living life both at and outside of work with these fabulous people.

Thanks to the program for Master of Biomedicine at Oslo University College for facilitating my master education and for providing excellent lecturers from which I have learned so much.

Last, but not least, I would like to thank my family and friends for supporting my decision to become a student again and for trying to understand my gibberish talk of pathways, proteins and experiments. I would not be able to go through this without you.

Oslo, May 2011

Idun Dale Rein

ABSTRACT

Cells that are deficient in proteins involved in homologous recombination repair (HRR) have been shown to be hypersensitive to PARP inhibitors. While a cell may tolerate PARP inhibition or HRR defects alone, the combination is lethal. This phenomenon is termed *synthetic lethality*. The function of HRR signaling protein ATM is lost in 50% of mantle cell lymphomas (MCL). MCL is an aggressive and currently incurable subtype of Non-Hodgkins lymphoma. PARP inhibition might prove to be a valuable treatment option for ATM deficient MCL cases.

In this master thesis, we have investigated the alterations in cell growth, cell cycle distribution and DNA damage levels, as well as mode of cell death caused by PARP inhibitor treatment of ATM deficient lymphoid cells. Four lymphoid cancer cell lines (Reh, U698, JVM-2 and Granta-519) were continuously exposed to the clinically relevant PARP inhibitor (olaparib/AZD-2281), and/or ATM inhibitor (KU-55933).

Cell growth was reduced or inhibited in all cell lines exposed to both ATM inhibitor and PARP inhibitor. The ATM inhibitor alone had little effect on the measured parameters in general, but increased the doubling time for all cell lines, and extended mitosis of U698 and Granta-519 cells. PARP inhibition caused a dose dependent-increase of DNA double strand breaks (DSB) during S phase. A G_2 phase delay was induced by combined PARP and ATM inhibition. The cells repaired the DSBs associated with γH2AX foci during the prolonged G_2 phase and entered mitosis without foci. Granta-519 and Reh cells became apoptotic from G_2 or M in response to PARP and ATM inhibition, possibly because of high levels of DSBs. PARP and ATM inhibited U698 and JVM-2 cells suffered from mitotic catastrophe before necrosis. TP53 deficient U698 cells endoreduplicated extensively, while JVM-2 (wildtype *TP53*) cells arrested after failed cytokinesis.

ATM deficient/inhibited lymphoid cells are sensitized to PARP inhibitors in a cell line specific manner, possibly because of other underlying genetic aberrations. We propose that the synthetic lethality of PARP and ATM inhibition was caused by repeated cycles of incorrect or failed repair of DNA DSBs that occurred during replication. Even though the HRR deficient cells have repaired the DSBs (possibly by error-prone non-homologous end joining), they may still accumulate translocations and/or other structural chromosome-defects that lead to apoptosis or mitotic catastrophe.

SAMMENDRAG

Celler som har defekter i homolog rekombinasjon reparasjon-signalveien (HRR) har vist seg å være hypersensitive for behandling med PARP-inhibitorer. En celle kan tåle PARP inhibering eller HRR defekter hver for seg, men kombinasjonen er dødelig. Dette fenomenet kalles syntetisk letalitet. Tap av ATM funksjon (HRR signaleringsprotein) er funnet i 50% av alle mantelcelle-lymfomer (MCL). MCL er en aggressiv og p.d.d. uhelbredelig undergruppe av Non-Hodgkins-lymfom, der bruk av PARP inhibitorer kan vise seg å være en verdifull behandlingsmulighet for undergruppen som har ATM-forstyrrelser.

I denne masteroppgaven har vi undersøkt endringer i cellevekst, cellesyklus og DNA-skade, samt celledød-mekanisme etter PARP inhibitor behandling. Fire lymfoide kreftcellelinjer (Reh, U698, JVM-2 og Granta-519) ble kontinuerlig behandlet med en klinisk relevant PARP-inhibitor (olaparib/AZD-2281) og/eller ATM-inhibitor(KU-55933).

Celleveksten ble redusert eller fullstendig hemmet i all cellelinjene etter samtidig ATM og PARP inhibering. Alene hadde ATM inhibitoren gjennomgående liten effekt på de fleste målte parametere, men økte doblingstiden i alle cellelinjene og forlenget mitosen for U698 og Granta-519 celler. PARP inhibering medførte en doseavhengig økning av DNA dobbeltrådbrudd under S-fase. G_2-fase ble forlenget som følge av kombinert PARP og ATM inhibering. Cellene reparerte γH2AX-foci assosierte dobbeltrådbrudd i den forlengede G_2 fasen og entret mitose uten slike foci. Granta-519 og Reh celler ble apoptotiske etter behandling med PARP og ATM inhibitorer, muligens på grunn av et høyt antall dobbeltrådbrudd. PARP og ATM inhiberte U698 og JVM-2 celler ble nekrotiske etter mitotisk katastrofe. De TP53-defekte U698 cellene endoreduplikerte, i motsetning til JVM-2 celler (har villtype *TP53*) som arresterte etter mislykket celledeling.

ATM-defekte/inhiberte lymfoide kreftceller er sensitive for PARP inhibitorer. Effekten var cellelinje-spesifikk, noe som tyder på at andre genetiske ulikheter påvirket resultatet. Våre resultater tilsier at den syntetiske letale effekten av PARP og ATM inhibering ble forårsaket av gjentatte sykler med mislykket reparasjon av replikasjons-induserte DNA dobbeltrådbrudd. Selv om de HRR-defekte cellene har reparert dobbeltrådbruddene (trolig med ikke-homolog endespleising), kan translokasjoner og/eller misdannelser i kromosom-struktur akkumulere og lede til apoptose eller mitotisk katastrofe.

ABBREVIATIONS

ADP	Adenosine diphosphate
ATM	Ataxia telangiectasia mutated
ATMi	ATM inhibitor, KU-55933
B-CLL	B-cell chronic lymphocytic leukemia
BER	Base excision repair
BRCA	Breast cancer susceptibility protein
CCN	Cyclin
CDK	Cyclin-dependent kinase
DDR	DNA damage response
DNA	Deoxyribonucleic acid
DSB	Double strand break
dsDNA	Double stranded DNA
HRR	Homologous recombination repair
IR	Ionizing radiation
MCL	Mantle cell lymphoma
MMR	Mismatch excision repair
mRNA	Messenger ribonucleic acid
NER	Nucleotide excision repair
NHEJ	Non-homologous end joining
PAR	Poly(ADP-ribose)
PARP	Poly(ADP-ribose) polymerase
PARPi	PARP inhibitor, Olaparib (AZD2281)
pATM	Phospho-ATM
pHistone	Phospho-Histone
RNA	Ribonucleic acid
RP	Restriction point
SAC	Spindle assembly checkpoint
shRNA	Small hairpin RNA
siRNA	Small interfering RNA
SSB	Single strand break
SSBR	Single strand break repair
ssDNA	Single stranded DNA
TdT	Terminal deoxynucleotidyl transferase
TUNEL	TdT dUTP nick end labelling

CONTENTS

1 INTRODUCTION

1.1 AIM OF STUDY

Two studies published in 2005 demonstrating the profound sensitivity to PARP inhibitors in treatment of BRCA-defective cells[1,2] spurred a promising development. The term "synthetic lethality"[3] has been used to describe the effect of combined loss of function of BRCA1/2 and PARP. Depletion of other homologous recombination repair (HRR) proteins, like the DNA damage signal transducer, ataxia telangiectasia mutated (ATM), have also proved synthetically lethal in combination with PARP inhibition[4-9]. The tolerable side effect-profile of PARP inhibitors has made them rapidly available and attractive for clinical use. In contrast to the speed of clinical implementation, the knowledge of the underlying mechanisms has advanced far less rapidly. Recent studies have highlighted the poorly understood complexity of the DNA repair processes, in which PARP are involved[10-14], establishing the need for further functional studies.

Patients diagnosed with mantle cell lymphoma (MCL) have the worst prognosis of malignant non-Hodgkins B-cell lymphoma patients (**figure 1-1**). MCL patients are presently being treated with high doses of chemotherapy, mainly rituximab (anti-CD20) and CHOP (cyclophosphamide, hydrodoxydaunomycin, oncovin, and prednisone), resulting in a median survival of only 4-5 years[15]. The relapse rate is high and after remission, MCLs have commonly developed chemo-resistance. MCL and its leukemia equivalent chronic lymphocytic leukemia (CLL) have frequent deletions and/or mutations of *ATM*[16-19]. Fifty percent of MCL cases have disabling *ATM* alterations[20,21]. While the frequency of *ATM* loss in CLL is around 20%[17,19], the prognosis of this patient subgroup is inferior to that of ATM-proficient CLL patients[18]. Loss of ATM function could therefore prove to be a tumor specific target for MCL treatment.

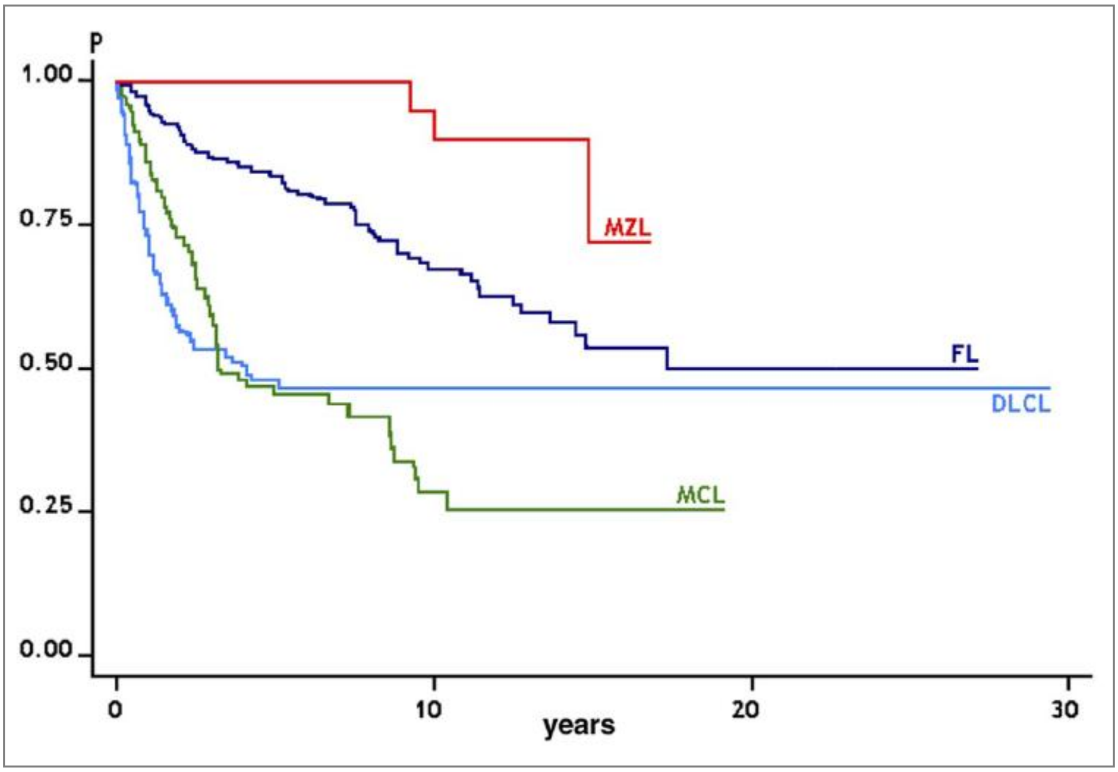

Figure 1-1: Cancer-specific survival of the main B-cell lymphoma subtypes in the series of the Oncology Institute of Southern Switzerland, 1980-2006. MCL indicates mantle cell lymphoma; FL, follicular lymphoma; MZL, marginal zone lymphoma; and DLCL, diffuse large cell lymphoma. This figure was published in Blood 2009, in an article by Michele Ghielmini and Emanuele Zucca [22].

PARP-inhibitors may be used to treat patients with ATM-deficient lymphoid neoplasias. Preclinical studies of the use of PARP inhibitors in ATM-deficient cell lines and xenografts have had promising results, but these studies mainly focused on the end point of cell death[4,6-9]. As the basic mechanism of synthetic lethality is not well understood, we decided to examine the details of certain biological aspects of PARP inhibition. First, we wanted to establish *in vitro* assays for studying synthetic lethality and to use these to investigate the basic mechanisms of PARP inhibition in ATM-deficient cells. We have focused on determining the kinetics of the following phenotypes of lymphoid cancer cell lines during 72h PARP inhibitor treatment:

- Cell growth alterations
- Cell cycle alterations
- Induction of DNA DSBs
- Mode of cell death

1.2 BACKGROUND

1.2.1 CANCER

The cumulative risk of developing cancer by the age of 75 is 34,5% for men and 27,9% for women in Norway (2005-2009)[23]. Although more than 65% of these patients survive for at least 5 years after diagnosis (1970-2009)[23], cancer is the number one cause of death in Norwegian males and the second most common cause of death in the female population (2011)[24]. Cancer is uncontrolled cell growth and termed malignant neoplasia (Greek for “new growth/formation”). Cancer cells are characteristically insensitive to anti-growth signals and self-sufficient in pro-growth signals. A cancer cell must be able to divide limitlessly and avoid cell death and senescence. For a solid tumor to grow above $1mm^3$, it must be able to develop blood vessels (angiogenesis). Further growth of the tumor requires ability to invade surrounding tissue and possibly metastasize to distal locations. These original six hallmarks of cancer[25] have recently been complimented by four new hallmarks[26]. Among the newly added hallmarks are “avoiding destruction by the immune system” and “genetic instability and mutation”. When a *de novo* genetic alteration translates into a growth advantage for a cell during malignant transformation, the change will be one of the many steps of the miniature evolutionary process that is cancer development.

1.2.2 GENETIC ABERRATIONS

Most genetic aberrations are silent (non-functional), while some might be incompatible with cell survival, others are corrected by DNA repair mechanisms. However, unrepaired, carcinogenic errors may accumulate and thereby create malignant lesions. The most common genetic aberrations are subtle sequence changes like base substitutions and small deletions or insertions. However, genetic aberrations also include chromosomal translocations, and amplifications or deletions of large chromosome segments and whole chromosomes.

Exchange of a single nucleotide, called a point mutation, is the simplest form of genetic alteration and may be caused by either exogenous or endogenous agents. If a nucleotide in a coding DNA sequence becomes permanently substituted, this may lead to an amino acid-exchange in the resulting peptide, i.e. a missense mutation. Insertions or deletions of a few nucleotides may lead to changes in the reading frame of the affected gene. In most cases, these changes result in a premature stop codon and subsequent truncated mRNA transcripts (nonsense mutations). Translocations may occur within a chromosome or between two or more non-homologous chromosomes. Some genetic material may be lost during this process, due to unsuccessful ligation of the translocated DNA-ends (unbalanced translocation). Even if the translocation is balanced, there is a possibility of creating fusion genes if the chromosome fusion sites involve coding regions. Alternatively, a gene may be transcriptionally regulated by the enhancer/promoter elements of another gene. An example of the latter is the t(11,14)(q13;q32) translocation, which is one of the hallmarks of mantle cell lymphoma (MCL)[27,28]. This translocation juxtaposes *CCND1* (CyclinD1) on 11q with the *IGH* (immunoglobulin heavy chain) locus on 14q. The *IGH* enhancer element is placed upstream of *CCND1*, causing enhanced transcription of *CCND1*. The resulting enhanced level of CCND1 promotes cell cycle progression into S phase. Amplifications and deletions change the copy number of the genes in the affected region, thus disturbing the expression of gene-dose regulated genes.

Studies of cancer development have led to definition of two broad classes of implicated genes. *Proto-oncogenes* are often amplified, as overexpression of these genes leads to growth promotion. Gain of function-mutations, which lead to hyperactivation of the resulting protein, is another way of disturbing the normal function of the protein. A proto-oncogene becomes an *oncogene* when the function of the resulting protein is malignantly altered. Some highly growth-promoting virus-genes inserted in the mammalian genome are innately oncogenes and can in some cases drive oncogenesis. Deletions or loss of function-mutations in genes that restricts growth, the *tumor-suppressor* genes, are in some cases not efficient unless all copies of a specific gene are affected (e.g. *RB1*). Other tumor-suppressor genes are gene-dose regulated and affected by mutation/deletion of a single allele (e.g. *TP53*). DNA maintenance genes (*caretaker* genes) are also implied in cancer development, as they guard genomic integrity. Inactivation of DNA repair associated genes (through mutations or deletions) will lead to increased acquisition of DNA damage.

1.2.3 DNA DAMAGE REPAIR

Maintenance of genomic integrity is essential in normal proliferation, during development of organisms and in prevention of malignant transformation. The DNA molecule can be altered in many ways by perpetual attacks of both endogenous and exogenous agents (e.g. metabolites, free radicals, ionizing radiation). During one day, up to one million insults to the genetic material needs to be resolved in a single cell. Cells have developed a complex machinery of repair and checkpoint pathways to prevent genomic alterations in response to these insults. If the amount of DNA damage is too extensive, programmed cell death (apoptosis) may be induced. These pathways make up the DNA damage response (DDR)[29], and they ensure the transfer of reliable genetic information throughout the generations.

In addition to extensive proofreading and correction of base substitutions by DNA polymerase δ and ε in mammalian cells[30], high fidelity DNA excision-repair systems evolved early in evolution to protect the genome. Base excision repair (BER) will for instance correct depurinated nucleotides and the most common point mutation (when a thymine is formed from a deamination of a 5-methyl cytosine). In mammalian cells APEX1[31], XRCC1[32] and DNA ligase III[33] are essential BER proteins. In all eukaryotic cells, functional BER requires a DNA glycosylase, an AP endonuclease or AP DNA lyase, a DNA polymerase, and a DNA ligase. Nucleotide base excision repair (NER) is activated in response to chemically altered bases that leads to distortions of the α-helical structure of dsDNA. Approximately 25 nucleotides around the site of damage are excised during NER, in contrast to BER, which only excises the altered nucleotide. The DNA mismatch excision repair (MMR) corrects replication errors, such as base pair-mismatches and small insertions or deletions.

Single strand break repair (SSBR) is sometimes referred to as a separate entity of DNA repair. However, SSB structure is an intermediate during BER, and the machinery implicated in SSBR is the same as in BER. While BER, NER and MMR require intact complimentary DNA strands to guide their repair, some DNA repair mechanisms are able to repair the more severe DNA damage, DNA double-strand breaks (DSBs).

Genomic information is protected by the robust structure of dsDNA with a sugar-phosphate backbone of each strand. Extensive force is thereby required to create a DSB. Incidentally, DSBs are among the DNA damage events that occur most seldom. Identification and stabilization of DSBs are the first steps in the repair process. Phosphorylation of Serine139 of H2AX histones (γH2AX) close to the DNA breakage site occurs within seconds after a DSB[34]. Induction of γH2AX after DSBs leads to chromatin decondensation[35] and recruitment of DDR-proteins[36]. Ionizing radiation, some chemotherapeutics, as well as replication fork collapse can cause DSBs. DSBs (identified by γH2AX foci) are often found in S and G_2 phase of untreated normal and cancer-derived cells, they are, however, rare events in unperturbed G_1[37] and mitotic cells[38]. Thus, it follows that DSBs are repaired before mitotic entry is allowed. The S- and G_2-associated γH2AX foci have been shown to decrease after treatment with reactive oxygen species (ROS) scavengers, thus indicating that DSBs arise during DNA replication and is caused by ROS from cell metabolism[39].

Among the many proteins that participate in the DNA damage response, ataxia telangiectasia mutated (ATM) is one of the key players. The congenital human condition, ataxia telangiectasia (A-T), is an autosomal recessive disorder caused by inherited mutations in both *ATM* alleles. Homozygous A-T patients display many defects in their nervous- and immune-system, and have an increased risk of developing neoplasias. The MRN complex (MRE11-RAD50-NBS1) senses DSBs and recruits the inactive ATM homodimer[40]. Binding of ATM to NBS1 is essential to enable subsequent activation of ATM[41-43]. ATM is fully activated by autophosphorylation of serine1981, followed by dimer dissociation[44]. ATM is capable of inducing several signaling cascades, phosphorylating CHEK2[45], TP53[46,47], Histone H2AX[48], ATR[49] and CtIP[50].

MRN and ATM is necessary for induction of homologous recombination DSB repair through ATR[49,51] and CtIP[50]. CtIP is recruited to damage sites by active ATM, where CtIP promotes the nuclease activity of MRE11[50]. ATR is recruited to DNA damage, via its binding partner ATRIP, by ssDNA coated with Replication protein A (RPA). ATR can further activate CHEK1. CHEK1 is thought to phosphorylate RAD51[52] and BRCA2[53]. NBS1 and ATM are required for this recruitment of ATR to RPA-coated ssDNA in S and G_2[51]. Additionally, ATM was recently found to be required for efficient HRR of DSBs in G_2 after irradiation[54].

Homologous recombination repair (HRR) is considered a highly accurate mechanism of DSB repair (**figure 1-2**, right panel). The accuracy is a result of utilizing the homologous sequence from its sister chromatid as template to guide repair, and HRR is therefore restricted to S and G_2. MRN mediates resectioning of the DNA ends after a DSB. This generates a small 3'-overhang of ssDNA on each end. RPA is bound to the ssDNA[55], inhibiting further resectioning and protecting the vulnerable ends. Recruitment of the recombinase RAD51 will substitute the RPA coating and further attract BRCA1, BRCA2, RAD52 and RAD54 (creating a nucleoprotein filament) [56]. The nucleoprotein filament will search for a homologous sequence and invade the sequence (strand invasion), once coated with RAD51. The intermediate structure is called a displacement loop (D-loop). After DNA synthesis of the 3'-invading strand the D-loop is converted into a cross-shaped structure called a Holiday junction. Further DNA synthesis effectively restores both the displaced and the invading strand. Finally, resolution of the recombination structure requires processing by several helicases and nucleases.

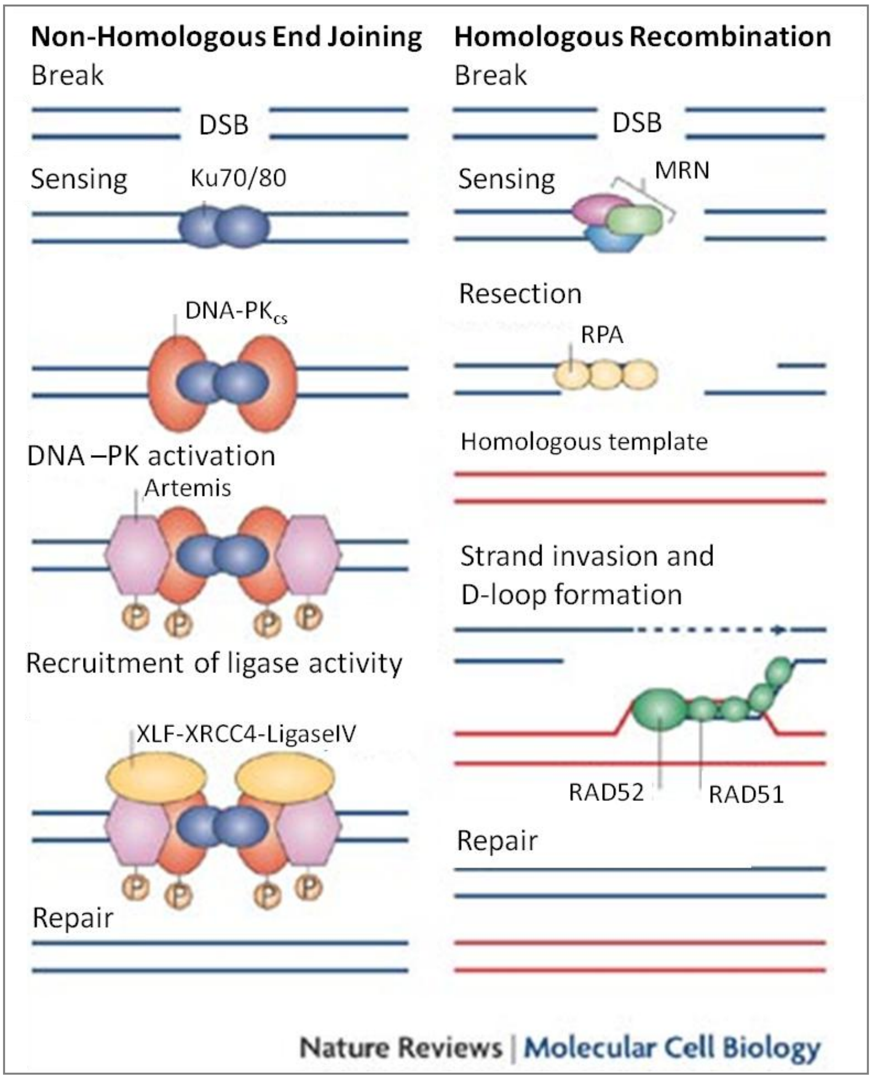

Figure 1-2: Non-homologous end joining and homologous recombination repair. The figure is adapted from a review article by Tom Misteli and Evi Soutoglou (2009)[57].

In G_0/G_1 phase, the cell is dependent on non-homologous end joining repair (NHEJ) to resolve DSBs (**figure 1-2** left panel). NHEJ does not require sequence homology and the DSB DNA ends must be perfectly compatible for accurate repair. Loss of nucleotides and even translocations are some of the results of inappropriate NHEJ repair of incompatible ends. NHEJ is also found to be processed through initial binding and modification through the MRN complex[58-61] (not shown in figure 1-2). However, the ends will subsequently bind the Ku70/80 heterodimer. DNA bound Ku70/80 recruits DNA-PK$_{cs}$ (catalytic subunit), forming DNA-PK[62,63] . Activated DNA-PK will tether the broken ends together[64] and mediate recruitment of other end processing and repair proteins such as Artemis[65].

Finally, a complex of DNA ligase IV, XRCC4 and XLF seals the break[66,67]. Competition of Ku70/80 and HRR for DSB ends is proposed to regulate the choice between the two repair mechanisms when sister chromatids are available[68,69]. It is still debated whether this is a competition or a collaboration[70], as unique roles for the two pathways based on their repair kinetics have been reported. Kim et al. found that rapid and transient NHEJ factor assembly[71] precedes, without inhibiting, the slower, yet persistent retention of HRR factors at the site of damage[58].

The diversity of DNA repair mechanisms forms a robust system that can withstand loss of one pathway as the remaining pathways continue to maintain genomic integrity. Loss of more than one pathway may on the other hand be lethal, which will be further discussed in section 1.2.7.

1.2.4 THE CELL CYCLE

DNA repair is essential for maintaining genome integrity. However, fixation of some types of damage may occur if the cell proceeds in the cell cycle. Eukaryotic cells have therefore evolved checkpoints that delay cell cycle progression until repair is completed. This will be discussed after a brief description of the normal cell cycle and its regulation.

The mammalian cell cycle is a closely regulated process divided into four phases G_1 (gap phase 1), S (DNA synthesis), G_2 (gap phase 2) and M (mitosis) shown in **figure 1-3**. Mitosis is divided into prophase, prometaphase, metaphase, anaphase and telophase, and, finally, the phase of cell division is called cytokinesis. All chromosomes are condensed into sister chromatids during prophase. In prometaphase, the nuclear envelope breaks down to allow the microtubules that are emerging from the spindle poles to attach to the chromatids. The chromatids align at the spindle equator in metaphase, and anaphase is only initiated if all sister chromatids are attached to a microtubule from each pole (i.e. spindle assembly checkpoint). Destruction of sister chromatid cohesion marks the start of anaphase, and the separated chromatids are pulled to opposite spindle poles. During telophase, the segregated chromosomes become decondensed and two separate nuclei form. Cytokinesis is the final stage, where the cell is cleaved into two daughter cells. The state of quiescence, often referred to as G_0, is the withdrawal from active cell cycle. If stimulated, the cell is able to re-enter the cell cycle from resting in G_0. Quiescence differs from the proposed irreversible and non-proliferative state of senescence[72].

The main players in the regulation of cell cycle progression are the cyclin dependent kinases (CDKs), and their activation is initiated by binding to a cyclin partner (CCN). The CCNs are expressed, repressed and/or degraded at different stages of the cell cycle, while the levels of CDKs are almost constant. Different CDK/CCN complexes are responsible for a multitude of coordinated cell cycle events, and their activity is again controlled by other kinases, phosphatases and ubiquitin-ligases.

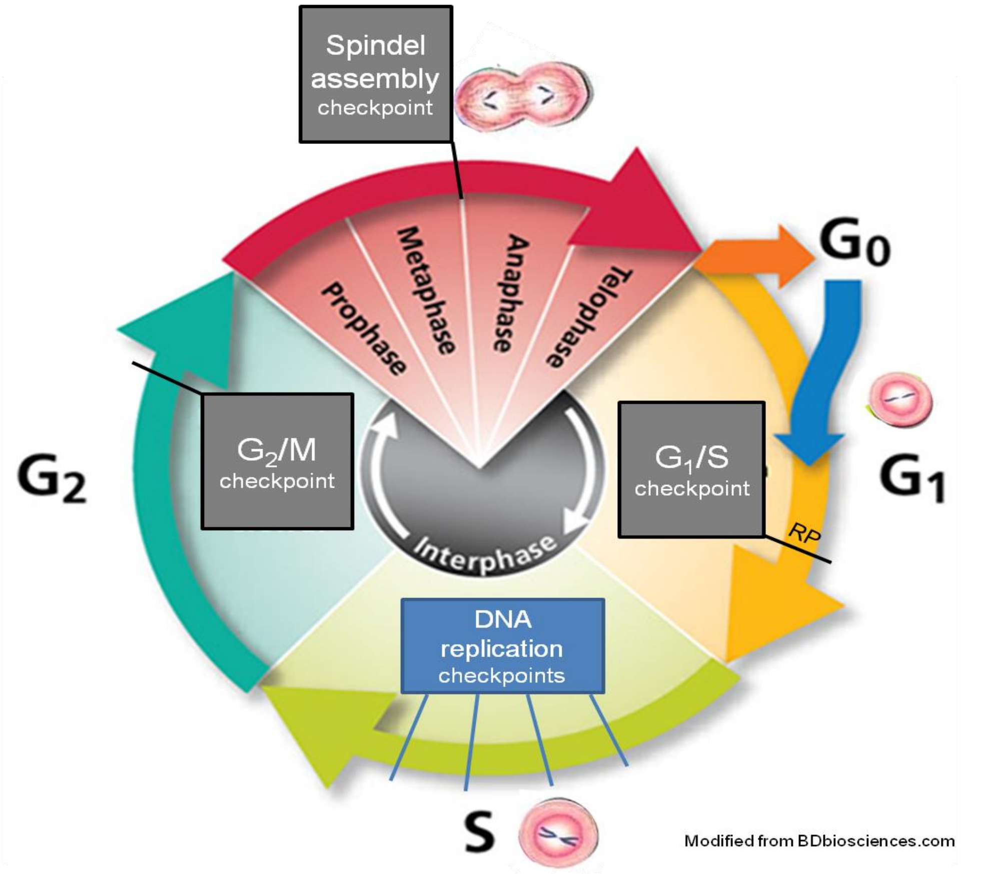

Figure 1-3: The mammalian cell cycle, with regulatory checkpoints.

The cell will not start DNA replication if the environmental conditions, such as growth factors or inhibitory signals, are unfavorable. The cell decides in late G_1

whether to start duplicating its DNA. The point of commitment to DNA replication is irreversible, and called the restriction point (RP). When the cell commences DNA replication it must complete the task, and in the absence of DNA damage, the cell cycle is completed without further growth factor signaling. The mechanisms of cell cycle progression mainly consist of binary "switches", as the incompletion of mitosis or replication, for instance, would be disastrous.

The switches are part of the evolved cell-cycle control system, known as checkpoints [73]. The proper order and completion of the major transitions of the unperturbed cell cycle are controlled by the following checkpoints (**figure 1-3**):

1. G_1/S-transition: the restriction point
2. Re-replication: replication origins cannot be fired more than once
3. G_2/M-transition: DNA replication must be completed before mitotic entry
4. Spindle assembly checkpoint (SAC): All centromeres must be connected to a kinetochore from each spindle to ensure faithful chromosome segregation

DNA damage activates checkpoints in G_1/S, S, G_2/M and in metaphase. Induction of the checkpoints cause a halt of cell cycle progression (arrest) until the damage is repaired. The exception is the intra-S checkpoint (not related to the re-replication checkpoint described above), which causes a cell cycle delay. This intra-S checkpoint actively slows down replication forks and suppresses origin firing[74]. The G_1/S DNA damage checkpoint guards against replication of a damaged template, and may employ the same downstream effectors as the RP. Mitotic entry with DNA damage is prevented by a G_2/M checkpoint. Severe DNA damage will cause improper chromosome segregation, the cell is protected from this by the metaphase to anaphase-transition DNA damage-checkpoint, which employs effectors of SAC, e.g. MAD2[75] and AURKB[76].

The DNA damage checkpoints is initiated in the following order: Sensor proteins recognize DNA damage and relay the signal to transducers (mostly kinases).The transducers regulate the effector proteins that induce cell cycle arrest, DNA repair and apoptosis either indirectly (through transcription) or directly. The members of the phosphatidyl-inositol kinase-like kinase (PIKK) family of protein kinases ATM, ATR and DNA-PK_{cs} are central transducers in this signaling network, and they are involved in both overlapping and distinct pathways[12,77]. CHEK2 and TP53 are among the targets for ATM phosphorylation. While CHEK2 is a transducer itself, it can positively reinforce some of ATMs functions (e.g. TP53 phosphorylation[78]), but it has other separate functions as well, e.g. inhibition of Cdc25 phosphatases that activate CCN-CDK complexes[79-81]. We have previously shown that TP53, CHEK1 and ATM have three separate roles in initiating the G_2/M checkpoint after ionizing radiation in lymphoid cancer cell lines, and ATM and CHEK1 are essential to induce an early and late G_2 arrest respectively[82]. TP53 is essential for induction of the G_1/S DNA damage checkpoint[83,84].

Tumor suppressor and gene regulatory protein TP53 is one of the most important caretakers of genome integrity[85]. CDKN1A (p21), an inhibitor of CDK-CCN complexes, are among the proteins that TP53 can transactivate. TP53 is a regulator of the balance between cell death and repair in response to DNA damage, by either stimulating transcription of pro-apoptotic genes or DNA repair-associated genes[86].

1.2.5 CELL DEATH

The tightly controlled balance of cell division and cell death maintains tissue homeostasis. Several different mechanisms induce cell death. Based on differences in morphology, these are divided into necrosis, apoptosis, autophagy and mitotic catastrophe[87].

Mitotic catastrophe is not established as a separate entity of cell death. It is most commonly described as cell death during or after catastrophic chromosome segregation in mitosis. Morphological features like micronuclei or multiple nuclei[87] are markers of mitotic catastrophe (**figure 1-4**). It is debated whether mitotic catastrophe is a cause of death or a separate cell death mechanism[88], as the cell utilizes either the apoptotic machinery (DNA damage induced caspase 2 activation)[89-91] or become necrotic[92]. Whether or not autophagy is a separate cell death mode is also questioned. Autophagy is the process of intracellular degradation of organelles in enlarged lysosomes or autophagosomes. If this is a process accompanying cell death, a mechanism of cell death or even a damage recovery-pathway is still debated[93].

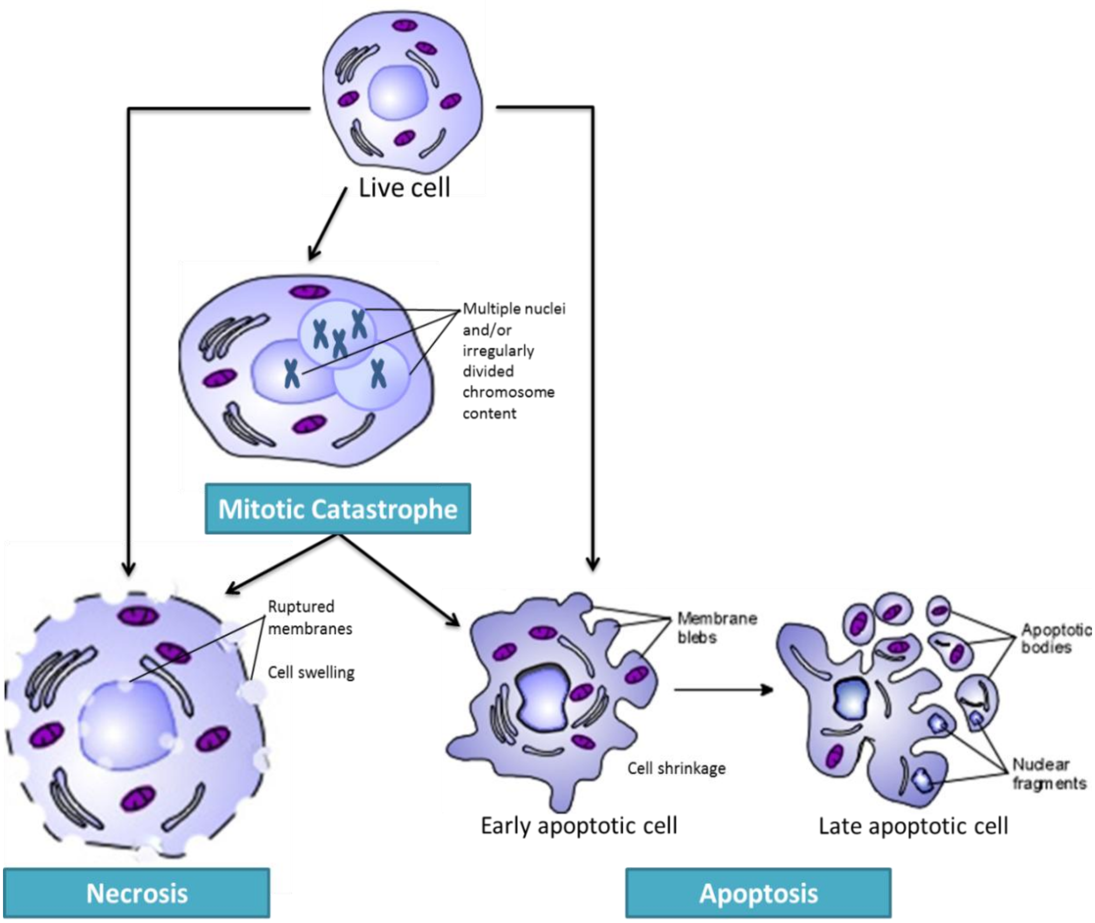

Figure 1-4: Morphological characteristics of cell death by necrosis and apoptosis, as well as a preceding cause of cell death induction, mitotic catastrophe.

Necrosis is a cell death mode characterized by cell swelling, loss of membrane integrity and subsequent leakage of the intracellular fluid into the surroundings (**figure 1-4**). Cytotoxic enzymes (mainly released from disintegrated lysosomes) degrade internal cell structures. When these are released into the extracellular matrix, they can trigger cell death of neighboring cells as well as severe inflammation. In contrast to apoptosis, necrosis is considered an uncontrolled mode of cell death in response to massive injury or energy depletion. New findings indicate that this may not be the case for all necrotic events, as induction of necrosis through death receptor signaling is reported to be activated by FAS ligands[94-96].

Apoptosis or programmed cell death is an active enzymatic process. Proper initiation of apoptosis is crucial to prevent accumulation of damaged or excessive cells. Apoptosis is morphologically characterized by cell shrinkage, chromatin condensation, membrane blebbing, DNA fragmentation and formation of apoptotic bodies (**figure 1-4**). Apoptosis is induced by both internal and external signaling and the two separate pathways are respectively denoted: The intrinsic and extrinsic apoptotic pathway. Intercellular signaling predominantly from the immune response activates the extrinsic pathway, while genotoxic stress primarily activates the intrinsic pathway. Both pathways utilize members of the caspase family of cysteine proteases to initiate and execute apoptosis. A balance of the relative levels of pro- and anti-apoptotic proteins controls induction of the intrinsic pathway. Anti-apoptotic proteins (e.g. MCL1 and BCL2) inhibit cytochrome c release into the cytoplasm from channels of the outer mitochondrial membrane, while the pro-apoptotic proteins (e.g. BAX, BAD and BAK) have the opposite function. Release of cytochrome c or death factor signaling (from ligands like FASL, TNFα and TRAIL) will lead to activation of the "executioner" caspases -3 and -7 through large complexes called the apoptosome and DISC (death inducing signaling complex) respectively. The effector caspases cleave multiple regulatory (e.g. PARP and TP53) and structural proteins (e.g lamins and actins). Finally, the apoptotic cell will present phosphatidyl serine residues on its cell surface to initiate phagocytosis by neighboring cells.

1.2.6 PARP

The Poly(ADP-ribose) polymerase (PARP) family of proteins and PARP like proteins is identified in many entities, from dsDNA viruses and bacteria to a variety of eukaryotes, yet not in the yeasts S. pombe and S. cervisiae[97,98]. PARP proteins require NAD^+ molecules to generate a polymer of ADP-ribose (PAR) and concomitantly release the by-product nicotinamid. PAR is negatively charged and may exist as a free polymer or be a post-translational modification of other proteins. PAR polymers can become several kDa in size and may be linear or branched (bound by glycosylic ribose-ribose links)[99]. PARPs (17 human members, although 10 putative[100]) are capable of <u>either</u> mono- or poly-ADP-ribosylation (PARylation).

Hence, a new name is suggested, the ADP-ribose transferases (ARTs) [97]. The most extensively studied PARP is its founding member PARP1, responsible for 90% of all PARylation[99].

Parp1 knockout mice are viable[101], display increased sensitivity to genotoxic stress[102], and show resistance towards inflammation[103-105]. Although the phenotype of *Parp1*$^{-/-}$ mice is quite mild, depletion of the only PARP-like gene in Drosophila causes larval lethality[106-108]. Additionally, *Parp1* and *2* double knockout in mice was shown to be embryonically lethal[109], indicating that PARP activity is essential in mammals as well. So far, exclusively PARP1 and PARP2 have been found to be activated by DNA breaks and have a DNA-binding domain (zinc finger binding domain)[110,111]. Although PARP1 PARylates many targets, it mostly PARylates itself[112], and DNA damage enhances this activity[113]. The autoPARylation is suggested to cause PARP1 to be repelled from the DNA lesions, as the PAR-polymer and DNA are both negatively charged[114].

Among the many targets for PARylation by PARP1 are transcription factors such as TP53[115,116] and NF-κB[117], histones[99] and enzymes such as AURKB (Aurora kinase B)[76]. The dramatic increase of PAR polymer levels after induction of DNA damage is transient (half-life of seconds to minutes), as the polymers are rapidly catabolized by PAR glycohydrolase (PARG) [118,119]. The removal of PAR from PARP allows new DNA binding[120] . Although PARP1 is abundantly expressed (≈0.5 million copies per cell[121]), the basal level of PARG activity is much higher than that of PARP. Removal of toxic amounts of PAR by PARG is essential as PARG$^{-/-}$ mice die early in embryogenesis[122] PARG was until recently the only known PAR-degrading enzyme, when mithocondrial PAR was found to be degraded by ARH3[123].

Since the discovery of the caspase 3 target PARP1[124], there has been extensive research efforts into the functions of PARPs. Although numerous and diverse functions of PARPs have been discovered, the underlying mechanistic explanations are in some cases conflicting. The established role of PARP1 as a BER/SSBR protein[102,125,126], have been challenged by further studies demonstrating that PARP1 depletion only slow down BER initiation[14,127] or does not affect BER efficiency at all[128]. Moreover, BER is an essential process and knockout of either *Xrcc1*[129] or *Apex1*[130] is lethal early in embryogenesis, while *Parp1* knockouts are viable[131]. Inhibition of PARylation and subsequent PAR-degradation has been reported to retard efficient repair of SSBs[14,132-134], possibly because of PARP1s role in attracting the scaffold protein XRCC1 to the site of damage[135]. PARP1 has also been shown to PARylate ATM in response to DNA damage[6,136]. PARP1 aggregation at DNA DSBs[137] is required for rapid accumulation of MRN-complex proteins NBS1 and MRE11[138]. All of which further establishes PARP1 as a DDR involved protein.

The massive effort put in to development of PARP inhibitors, have resulted in an array of small molecules with different actions. The first generation of NAD^+ analogs (nicotinamide and 3-aminobenzamide) was not very specific. However, the 2nd generation of competitive inhibitors of the enzymatic site e.g. veliparib (ABT-888), PJ34 and olaparib[139] and the 3rd generation of covalent irreversible inhibition of the DNA binding domain (iniparib)[140] have evolved to be highly specific and potent. Most PARP inhibitors inhibits both PARP1 and PARP2, yet they have low adverse effects on normal tissue[141-145]. In fact, the side effects are so mild that patients can be exposed to PARP inhibitors over several months without additional toxicity (olaparib was continuously administered for 168 days in two phase II-studies[146,147]). Several of these inhibitors have undergone more or less successful clinical trials [141,142,146-150]. The clinical trials and preceding development of PARP inhibitors were a result of two promising studies by Bryant et al.[2] and Farmer et al.[1] in 2005 demonstrating synthetic lethality by inhibition of PARP in BRCA1/2-defective cells. Depletion of other DDR proteins such as ATM, ATR and CHEK1 were identified in a siRNA screen searching for kinases that increased sensitivity to PARP inhibitors[151]. PARP inhibitors are promising anti-cancer agents, especially since PARP expression have been shown to be upregulated in several cancer types; hepatocellular carcinoma[152], malignant lymphoma[153] and early stages of colorectal carcinogenesis[154], as well as known HRR-deficient malignancies[13]. The latter has been shown to be HRR deficiency-dependent, as the upregulation is reverted in response to BRCA2 reconstitution *in vitro*[13].

1.2.7 SYNTHETIC LETHALITY: PARP INHIBITION AND HRR DEFECTS

The term synthetic lethality describes the fatal combined loss of two genes/proteins, even though loss of either of the two is compatible with life. First described in Drosophila over 60 years ago[155], synthetic lethality have long been proposed as a cancer treatment strategy[156], yet only one synthetic lethal treatment approach have reached the clinic so far.

Although the initial *in vitro* studies[1,2] seemed very promising, phase II studies of PARP inhibitor (olaparib) treatment of BRCA1/2-defective breast and ovarian cancer have not had the expected effect, with 41[146] and 33%[147] objective response rate (ORR), respectively. A phase II study of metastatic TNBC (without regard to BRCA-status) increased the overall response rate from 32% to 52% by addition of iniparib to gemcitabine and carboplatin (GC) treatment (without increasing normal tissue-toxity of GC)[148]. However, the following phase III studies using PARP inhibitor iniparib in combination with GC as first line-treatment of triple negative breast cancer (TNBC) and non-small cell lung carcinoma, have been reported (both at ASCO 2011, and from the manufacturer Sanofi) to fail their primary goal of increased overall survival. The lack of patient selection by BRCA-status makes it harder to demonstrate synthetic lethality in clinical studies. Additionally, the PARP inhibitory effect of iniparib has recently been disproven[157,158]. Elevated PARP expression has been suggested as a biomarker for response to PARP inhibitor treatment, as this is shown *in vitro* to be correlated to PARP inhibitor response[13]. On a whole, it has now become clear that the failure to demonstrate an equal response in clinical trials as in *in vitro*/*vivo* studies is due to a poor understanding of the consequences of PARP inhibition on the molecular level. Future studies on the underlying mechanisms behind the synthetic lethality of PARP inhibition and defective homologous recombination repair (HRR) are therefore warranted.

When synthetic lethality of PARP inhibition in HRR-deficient cells first was discovered[1,2], the role of PARP in BER/SSBR was the proposed explanation. Cell death was until recently thought to be caused by accumulation of unrepaired DNA SSBs due to PARP inhibition. These were converted into DSBs during replication, and the subsequent failure to repair these by HRR would be incompatible with life (**figure 1-5 A**). This was the leading functional model until considerable amounts of experimental results accumulated to contradict or complicate this explanation[10-14]. Most importantly, the amount of SSBs was not increased after PARP inhibition, shown both by the alkaline DNA unwinding assay[14] and the alkaline comet assay[13]. Moreover, XRCC1 depletion of HRR-defective cells did not cause synthetic lethality[12], and combining XRCC1 depletion with PARP inhibitors actually created an unexpected synthetic lethal effect[10,14]. These data clearly demonstrated that the role of PARP1 in attracting XRCC1 to SSB repair[135] could not be responsible for the phenotype induced by PARP inhibition.

Professor Thomas Helleday has lately proposed two new models of PARP inhibition in HRR-deficient cells, rejecting the formerly accepted hypothesis[159]. The first is termed "PARP trapping model" (**figure 1-5 B**) and is based on a suggested difference in sensitivity to PARP inhibitors and PARP depletion (RNAi techniques). Indicating that catalytically inactive PARP is not inhibited from DNA binding, but the lack of subsequent auto-PARylation prevents PARP from being repelled from DNA. Some results support this theory[2], while others have not found a profound difference between depletion and inhibition[1,12]. A possible explanation for this discrepancy may be that the effect of RNAi-mediated knockdown does not last for many cycles, and PARP inhibitor induced kill of HRR-deficient cells is normally analyzed after 7-12 days. The model further postulates that inhibited PARP is trapped onto DNA lesions, thereby becoming an obstacle for passing replication forks, much like the action of topoisomerase I inhibitors[160]. The subsequent replication fork collapse will produce a one-sided DSB (the Okazaki fragment in process). These DSBs will not be repaired or be incorrectly repaired by NHEJ in the absence of functional HRR.

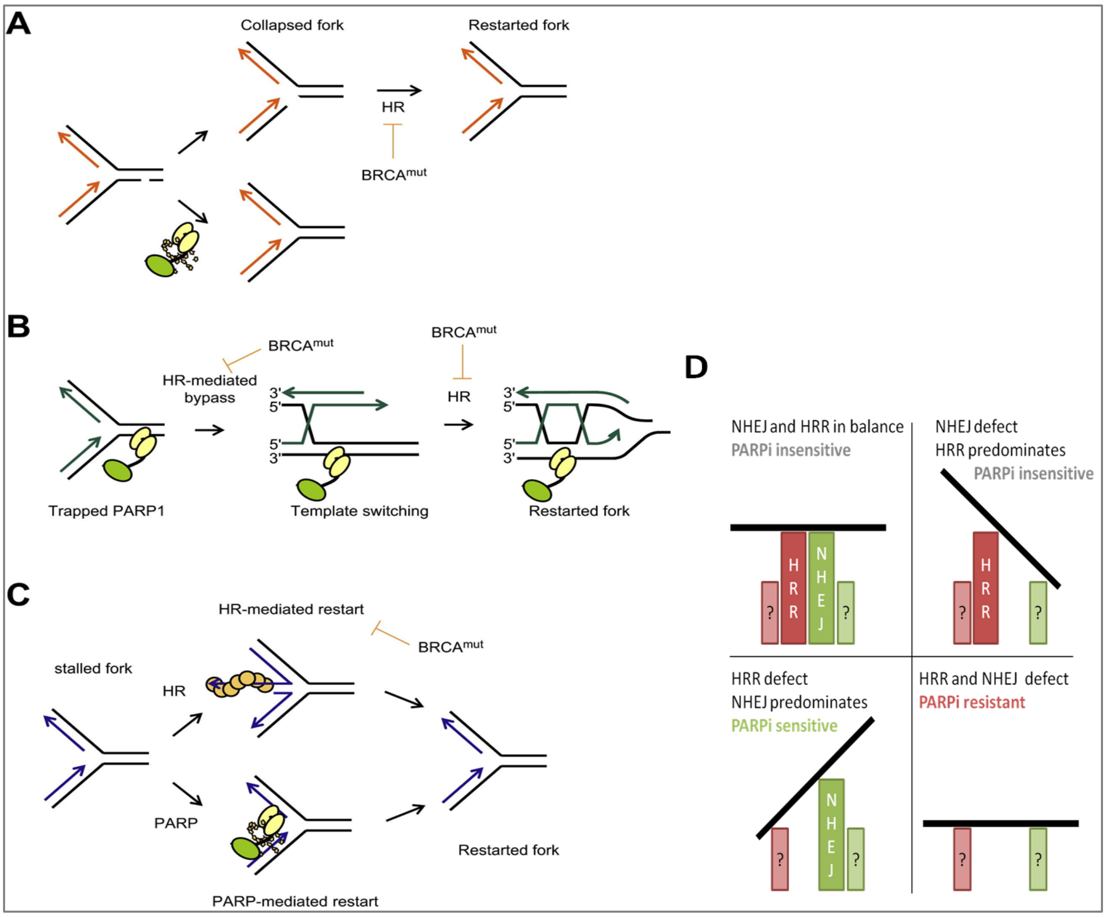

Figure 1-5: Models of PARP inhibition in HRR defect background. Presentations of the original model (A), PARP-trapping model (B) and Replication restart model (C) are from Thomas Helleday's article: "The underlying mechanism for the PARP and BRCA synthetic lethality: Clearing up the misunderstandings" (2011)[159] . PAR-polymers are depicted around PARP1-protein in A and C. "The balance of DSB repair mechanisms" model (D) is adapted from a figure in a review article by Amal Aly and Shridar Ganesan (2011)[161].

The second model called "Replication restart model" (**figure 1-5 C**) is based on the involvement of BRCA2[162] and RAD51[163] in replication fork stabilization/restart, and the reported affiliation of PARP1 at replication forks[11,164]. The model suggests that lethality is caused by abolishing both BRCA-mediated and PARP-dependent replication restart. However, PARylation was not found to colocalize with γH2AX and RPA foci in BRCA2-deficient cells, indicating that the PARP overexpression in these cells is not affiliated with stalled replication forks[13]. Recently, PARP1 and BRCA2 was found to prevent Mre11 dependent degradation of stalled replication forks, and acquired resistance towards PARP inhibition was correlated with reduced Mre11 foci[165].

Several studies have demonstrated an unexpected rescue of the PARP inhibitor induced synthetic lethality in HRR defective cells after additionally inhibiting NHEJ[9,12,166,167]. PARP1 may compete with Ku70/80 for DNA ends[131,167-169], or Ku70/80-affinity to DSBs could be decreased by PARylation of Ku70/80[170]. This suggests a third model of PARP inhibition in HRR-defective cells; tilting the balance of DSB repair mechanisms, towards the error-prone NHEJ (**figure 1-5 D**). Disturbing NHEJ-proteins *in vitro* by DNA-PK_{cs} inhibition or depletion (by RNAi) of DNA-PK_{cs}, Ku80, Artemis or DNA ligase IV all alleviate the synthetic lethal phenotype induced by PARP inhibition in HRR-defective cells [9,12,167]. Additionally, the severe immunodeficiency of *DNA-PK_{cs}*$^{-/-}$ mice was abolished after additional *Parp1*$^{-/-}$ knockout[166]. Other unexpected results of PARP inhibition are the rescue of PARP inhibitor-sensitivity in BRCA1-defective cells by loss of *53BP1*[171]. 53BP1 is a TP53 activating and DSB-binding protein[172], and is found to guide DSB repair towards NHEJ in the absence of BRCA1[171]. Severe structural chromosome aberrations have also been reported in BRCA1/2-defective cell lines after PARP inhibition[1], indicating high activity of low fidelity repair. Radial chromosomes have been reported in *BRCA1* mutants rescued by *TP53* or *53BP1* knockout[171]. A recent study of the requirement of 53BP1 and γH2AX in *Parp1*$^{-/-}$ mice, reported that additional *H2AX* knockout induced synthetic lethality and proposed NHEJ associated repair to be 53BP1-dependent[173]. The DSB repair balance model still does not give an explanation as to how repair is facilitated in the combined absence of HRR, NHEJ and PARP (**figure 1-5 D**, lower right quadrant), although a reconstitution NHEJ and HRR have been proposed[161].

Efforts have also been put into researching synthetic lethality induced by depletion of other HRR proteins combined with PARP inhibition[4-9,13]. Several studies have established that loss of function of ATM is synthetically lethal when combined with PARP inhibitor treatment[4,6-9]. Although, *Atm* and *Parp1* double knockouts were found to die at gastrulation[5]. The *in vitro* and *in vivo* studies revealed that synthetic lethality of ATM and PARP loss is somewhat less potent than that of PARP and

BRCA1/2[4,6-9]. However, most of these studies have solely focused on the potency of PARP inhibitors on cell death-induction. The study by Aguilar-Quesada et al. reported that ATM is activated by PARP inhibitor-induced DNA DSBs[6]. Moreover, Williamson et al. found that DNA-PK inhibition rescued synthetic lethality of PARP inhibition in ATM-deficient cells, and that additional synthetic lethality by PARP inhibition was observed in ATM- and TP53-defective cells[9]. Thus, inhibition of PARP in an ATM-deficient setting requires further study to elucidate its full potential and mechanism.

2 MATERIALS AND METHODS

Supplier information (including product numbers) regarding all materials used in this study is listed in the appendix. Detailed recipes for the different solutions needed to perform the methods described in this chapter, can also be found in the appendix. The specifications and dilutions of antibodies used are listed in a separate section in the appendix. Supplier and product information of instruments and software are listed continuously in the text.

2.1 CELL CULTURE AND TREATMENT

2.1.1 CELL LINES

Reh is derived from a pre-B cell acute lymphoid leukemia (ALL) patient[174]. U698 is derived from a diffuse large cell lymphoma[175]. JVM-2 is an Epstein-Bar virus (EBV)-transformed B-lymphocytic leukemia (B-CLL) cell line[176] which was acquired from the Deutsche Sammlung von Mikroorganismen und Zellkulturen (DSMZ, Braunschweig, Germany). There are several studies indicating that B-CLL s carrying the t(11,14) translocation may correspond to blastoid MCL variants[177], and use of the JVM-2 cell line as a model system for MCL is well established. Granta-519 is an EBV-transformed cell line from a high-grade MCL relapse patient with t(11,14) translocation. Granta-519 was also purchased from DSMZ[178]. Granta-519 is ATM-deficient with one *ATM* allele deleted[179], and the other allele containing a missense mutation R2832C in the ATM kinase domain[180]. All cell lines were confirmed free of mycoplasma infection before use.

2.1.2 CULTURE CONDITIONS

All cell lines were incubated at 37 °C with 5 % CO_2 and H_2O-saturated air in a Nu-5510/E/G incubator (NuAire, Plymouth, MN). Reh, U698 and JVM-2 cells were grown in RPMI 1640 containing 10%(v/v) fetal bovine serum and 1%(v/v) penicillin-streptomycin and 2mM L-glutamine. Granta-519 cells were first grown in Dulbecco's Modified Eagle Medium (DMEM) as recommended by DSMZ with the same supplements.

Comparison of growth rates of Granta-519 in DMEM and RPMI 1640 over 4 weeks indicated that there was a growth advantage in the RPMI 1640-medium and this medium was later used for all experiments involving Granta-519 cells. Cells were split and reseeded every Monday, Wednesday and Friday at a density of $3.0 \cdot 10^5$ cells/ml for U698 and Reh and $1.5 \cdot 10^5$ cells/ml for JVM-2 and Granta-519. Cells were grown and handled in a sterile environment, to prevent infections from bacteria and fungi.

2.1.3 CELL TREATMENT

All cells treated with the PARP inhibitor olaparib/AZD2281 [139] were seeded in their normal culture medium containing 0.3 – 10µM PARP inhibitor (PARPi) for the duration of the experiment. Stock solutions of both 1 and 10mM olaparib in DMSO were prepared from dry state. Initial experiments with 1.0, 3.0 or 10µM PARPi alone in ATM proficient cells treatment for 48h revealed equally severe cell cycle arrests induced by both 3 and 10µM, therefore 3µM was selected as the highest concentration to be used in further experiments. Patients that received 200mg or 400mg of olaparib twice each day were reported to have blood plasma concentrations of olaparib ranging from 1.38 to 20.0µM[145]. All cells treated with the ATM inhibitor KU-55933[181] were seeded in their normal culture medium containing 10µM ATM inhibitor (ATMi) for the duration of the experiment. The stock of ATMi was prepared from dry state into a 10mM solution in DMSO.

Reh, U698, Granta-519 and JVM-2 cells were all treated for 72h with three different concentrations of the PARPi alone or in the presence of 10µM ATMi. Untreated control (receiving vehicle alone) and ATMi alone control were also included for each cell line in every experiment. Chosen experimental and clinically relevant concentrations of PARPi were 0.3µM, 1µM and 3µM. The experimental layout is illustrated in **figure 2-1**. The cultures not treated with ATMi were all given equivalent amounts of DMSO, the final DMSO concentration in the cultures ranged from 0.10-0.13%. In order to keep the cells growing at an exponential rate for the duration of the experiment, an appropriate starting density of each cell line was chosen. The experiments started at following cell densities: Reh at 250.000cells/ml, U698 cells at 200.000cells/ml, JVM-2 at 100.000cells /ml and Granta-519 at 120.000cells/ml. Reh and U698 cells were treated in 25cm^2 culture flasks, with a starting volume of 10ml. JVM-2 and Granta-519 were treated in 75 cm^2 culture flasks and, with a starting volume of 20ml.

Cells were harvested from each culture at 24, 48 and 72h after treatment. 2ml (Reh and U698) or 4ml (JVM-2 and Granta-519) of the culture was washed once in phosphate buffered saline (PBS) and then fixed in 1ml -20°C, 100% methanol, and kept at -20°C until staining. 0.5ml (Reh and U698) or 1ml (JVM-2 and Granta-519) of the harvested cells was immediately counted on a Coulter Counter. 0.5ml (Reh and U698) or 1ml (JVM-2 and Granta-519) of each culture was also harvested for immediate live cell staining.

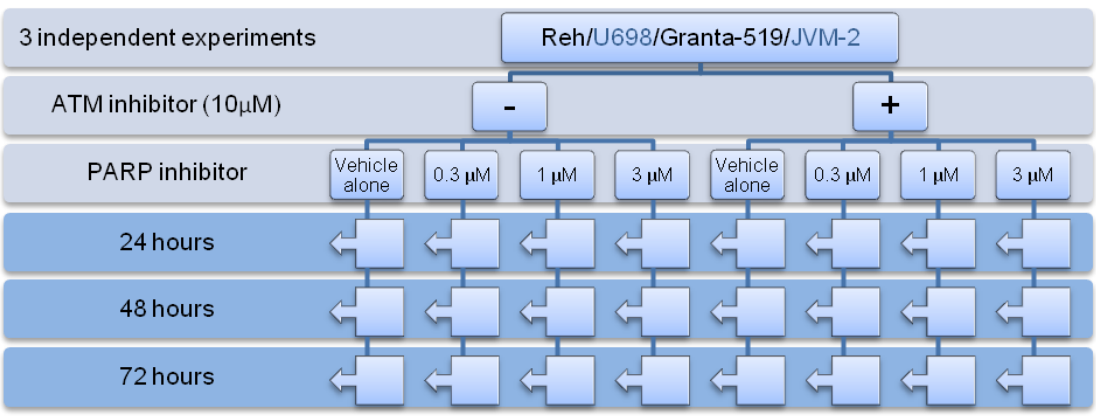

Figure 2-1: Experimental layout of 72h PARP inhibition in each cell line with or without ATM inhibition.

The flux of cells into mitosis for all the cell lines was monitored by adding 1µg/ml of the microtubule-polymerization inhibitor nocodazole[182] for 6h prior to cell harvest. In cells with proficient spindle assembly checkpoint, nocodazole treatment causes MAD2 binding of all kinetochores, resulting in a cell cycle arrest in metaphase[183,184]. The cells were first treated with vehicle alone (DMSO), 3µM PARP inhibitor and/or 10µM ATMi, and harvested at 24h and 72h. A control of each sample (not treated with nocodazole) was also harvested at the same time. Cells were fixed at the time of harvest as described above.

A 144h continuous exposure of U698 cells with vehicle alone or 3µM PARP inhibitor with/without ATMi was replicated twice. Nutrient depletion of the medium was avoided by medium substitution after 72h treatment. The cells were spun at 500g for 4 minutes, before 85% of the old medium was substituted with fresh medium containing the same concentrations of PARPi and/or ATMi. Cell growth measured by Coulter Counter and fixed samples after 72h for these experiments were similar to the previous three replicates of 72h treatment.

Cells with or without 10µM ATMi was irradiated with 4Gy for protein expression analysis. X-irradiation was executed at a dose rate of 1Gy/min in a CP160 X-ray generator (Faxitron, Tucson, AZ) at 160kV and 6.3mA. One hour after irradiation, the cells were washed once in ice cold PBS.

2.2 CELL STAINING

The appendix contains detailed recipes, as well as specifications and suppliers of all primary and secondary antibodies used in this section.

2.2.1 FIXED CELL STAINING

An automated cell staining procedure for fixed cell samples was developed using the microplate washer ELx405 Select (BioTek, Winooski, VT) and the microplate sample processor Precision XS (BioTek). The spatial properties of all vessels and tips had to be defined for the microplate processor by a procedure called "stepping". This procedure determines the travel margins for the microplate processor, in x-, y-, and z-direction, for instance making sure the tips reaches the desired depth in a defined sample volume and preventing crashes of the mobile parts. BD Falcon 5 ml polystyrene tubes can be used directly on all the flow cytometers available in the lab. These tubes have good pellet visibility and electrostatic properties. The supplied 48 tubes-rack allowed these tubes an unacceptable margin of motion within each tube position, which could potentially be damaging for the precise movement of the instrument. A new 48 tubes-rack specifically fitted for the smaller diameter of the 5ml BD Falcon tubes was therefore made at our instrument workshop.

Version 2.0 of the software Precision Power (BioTek) was used to create a sample processing and cell-staining program for the Precision XS microplate sample processor. The program contained the following steps:

1. Transferring samples from 5ml tubes to 96 well microplates
2. Performing a TUNEL-assay with biotinylated dUTPs
3. Primary antibody staining of phosphorylated proteins, Histone H3 and Histone H2AX.
4. Addition of fluorescently labeled secondary antibodies and fluorescence-labeled streptavidin.
5. DNA-staining with Hoechst 33258
6. Returning the stained samples from the microplate to 5 ml tubes

The fixed cell samples were manually washed in 3ml PBS. Afterwards, the samples were transferred with the microplate sample processors single channel pipette from 5ml BD Falcon tubes onto a Nunclon 96 round well plate. The microplate washer was used for washing and supernatant aspiration between the steps in the Precision XS program. The ELx405 Select is equipped with the *Dual Action* manifold that consists of independent 8x12 dispenser and 8x12 aspiration tubes. Each sample wash was performed by a protocol administrating 200µl PBS through the dispensing manifold simultaneously on the walls of all wells. A suitable aspiration protocol for aspirating supernatant after centrifugation was designed to minimize residual fluid in each well while keeping cell loss at a low level. The final aspiration protocol left 15µl of fluid when used on a plate filled with water.

It is necessary that the cell pellets are sufficiently firm, as to allow aspiration. On the other hand, they must also be loose enough for dissolving into single cell suspensions upon plate vortexing or mixing by the microplate processor. Thus, centrifugation speed and time used was optimized for fixed suspension cells. The microplates were all centrifuged at 700g for 5 minutes in a GS-15R centrifuge (Beckman Coulter). The program for the microplate sample processor was defined to pre-mix and dispense all staining solutions and mix (by pipetting) the staining solution and cell pellet.

The Terminal deoxynucleotidyl transferase (TdT) dUTP nick end labelling (TUNEL) assay was used to detect cells with fragmented DNA, which is associated with apoptosis. TdT can be used to catalyze the polymerization of dUTPs (biotin-labelled) to the free ends of DNA strand breaks. Although TdT has the ability to label blunt ended DSBs and 5'-overhang ends, it has strongest affinity for 3'ends. TUNEL assays were performed using the microplate sample processor in a volume of 20µl per well. The TUNEL-assay reaction solution from the Recombinant Terminal Transferase kit had previously been optimized for minimal reagent use (appendix), and using microplates instead of tubes further reduced the total volume used for each sample by 43%. 0.1mM DTT (a reducing agent) was added to the reaction solution (0.2M potassium cacodylate, 25mMTris-HCl, 25mg/ml BSA, 1.6U/µl TdT enzyme, 1.5mM $CoCl_2$, 10µM biotin-16-dUTP). DTT relaxes the chromatin and frees more DNA-strand breaks[185], increasing the sensitivity of the assay. The samples were incubated for 30 minutes at 37°C. To stop the reaction, the samples were washed using the microplate washer.

The phosphorylation of Histone H3 at serine 10 (pHistone H3) is involved in chromatin condensation in the G_2 to prophase transition, and it is widely used as a marker of the onset of mitosis[186-188]. Anti-pHistone H3 (Ser10), diluted 1:500, was administered by the microplate sample processor to the sample wells in a blocking buffer of 5%(w/v) non-fat dry milk in PBS and incubated for 30 minutes on a microplate shaker in room temperature.

Staining of phosphorylated serine 139 on Histone H2AX (γH2AX) was used to detect DNA double strand breaks. The antibody was administered in a dilution of 1:500 in a blocking buffer of 5%(w/v) non-fat dry milk in PBS together with the anti-pHistone H3 antibody.

Nuclear envelope breakdown is essential for the onset of mitosis, and reassembly happens during anaphase and telophase. The nuclear envelope consists mainly of the intermediate filaments lamins, where laminB is a major component[189]. To inspect possible multinucleation or deformed nuclei, an antibody against the nuclear envelope protein, LMNB2 (Lamin B2), was deployed to stain JVM-2 and U698 cells. The antibody was diluted 1:200 in PBS containing 5% dry milk, and incubated for 30 minutes at room temperature.

All samples were washed twice in PBS after primary antibody incubation. Secondary antibodies against pHistone H3 (PE-conjugated) and γH2AX or LaminB2 (both FITC-conjugated) were diluted 1:50 in PBS supplemented with 5% dry milk. The staining for apoptosis (Cy5-conjugated streptavidin) was also added to this solution of secondary antibodies, in a 1:400 dilution. Incubation for 30 minutes was performed at room temperature, before the samples were washed once in PBS.

Hoechst 33258 is a non-permeable nucleic acid binding fluorescent dye, with high affinity to adenine and thymine rich areas, efficiently excluding RNA binding. When the molecule binds non-covalently to areas of double stranded-DNA, the fluorescence is 60-fold enhanced, which is important as DNA-bound and -unbound Hoechst stain is at equilibrium in cells which are suspended in a Hoechst solution. As a final step in the staining procedure, 1.5µg/ml Hoechst 33258 in PBS was added for DNA staining, and incubated for at least 20 minutes.

2.2.2 LIVE CELL STAINING

The BD Cell Viability Kit was used to quantify the amount of dead cells in the cultures treated with molecular inhibitors. It contains two nucleic acid dyes with different membrane permeable properties, which were used simultaneously to distinguish cells with permeable membranes. Thiazole Orange (TO) and Propidium Iodide (PI) was added directly to culture samples. TO is a permeant dye that stains the nucleic acids (preferably RNA) of the whole cell population, effectively excluding debris from the analysis. PI, on the other hand, stains only nucleic acids of cells with compromised membranes, i.e. dead cells. 84nM TO was added 5 minutes prior to flow cytometry analysis, and 4.3µM PI was added to each sample at the time of analysis.

Hoechst 33528 (non-permeable) was added to a final concentration of 1.5 µg/ml to stain dead cells immediately prior to cell sorting of live and dead cells.

2.3 FLOW CYTOMETRY

Data acquired during flow cytometry measurements was processed using the FACS Diva Software (BD Biosciences), version 4.1.3 or newer. Cell sorting into 5ml tubes or directly on microscopy slides was performed in a FACS Vantage SE (BD Biosciences, San Jose, CA) equipped with a 50mW 351 and 355nm krypton laser, a 200mW 488nm argon laser (both Coherent, Santa Clara, CA) and a 20mW 633nm laser (Spectra Physics, Santa Clara, CA). The flow cytometry analysis was performed on either of two BD LSRIIs equipped with the following laser combinations:

- 60mW 355nm (JDSU, Milpitas, CA), 20mW 407nm, 50mW 488nm and 20mW 633nm (all Coherent)
- 100mW 405nm, 50mW 488nm, 40mW 561nm and 40mW 639nm (all Coherent)

Flow cytometry is fluorescence and light scatter analysis and counting of single microscopic particles in suspension. A hydrodynamically focused stream of particle suspension is passed through one or more lasers, one particle at the time. The particles will be excited and scatter light when passing through each laser focus. Fluorescence emission and scattered light from each particle is collected by detectors, e.g. photomultiplier tubes (PMT), and converted into electric pulses (signal intensity over time) (**figure 2-2 A-D**). A threshold value for pulse signals in one of the detectors (either scatter or fluorescence) (**figure 2-2 A**) is set to exclude noise (electronic and optical) and analyze solely on particles of interest. The intensity of the detected signal must generate a pulse height above the threshold value to be analyzed and counted. The detected emission intensity signal is directly proportional to the expression of each stained target molecule.

Emission originating from each excitation source (laser) is directed into several emission detectors, enabling the simultaneous use of multiple fluorescent markers in the same sample. Emission is partitioned by wavelength through dichroic mirrors and optical filtration. Moreover, overlap of multiple emission spectra as well as excitation spectra may require additional fluorescence spillover-compensation of detected signal. The forward light scatter (1-10˚ angle from the laser) is nearly proportional to the size of the particle, while side scatter (around 90˚ angle) is mainly caused by internal structures in the cell or particle. The power of flow cytometry is the ability to separately analyze multiple parameters of each cell rapidly and combine the information from the single cell level into a detailed picture of the whole population.

One signal originating from two cells (doublet) (**figure 2-2 D**) is a major confounding factor. The problem may be reduced by filtering the cell suspension, but post-processing the data by gating strategies is still essential (**figure 2-2**). Gating of single cells requires combining the pulse width and the pulse area of one parameter. The parameter must be universal for the population of interest.

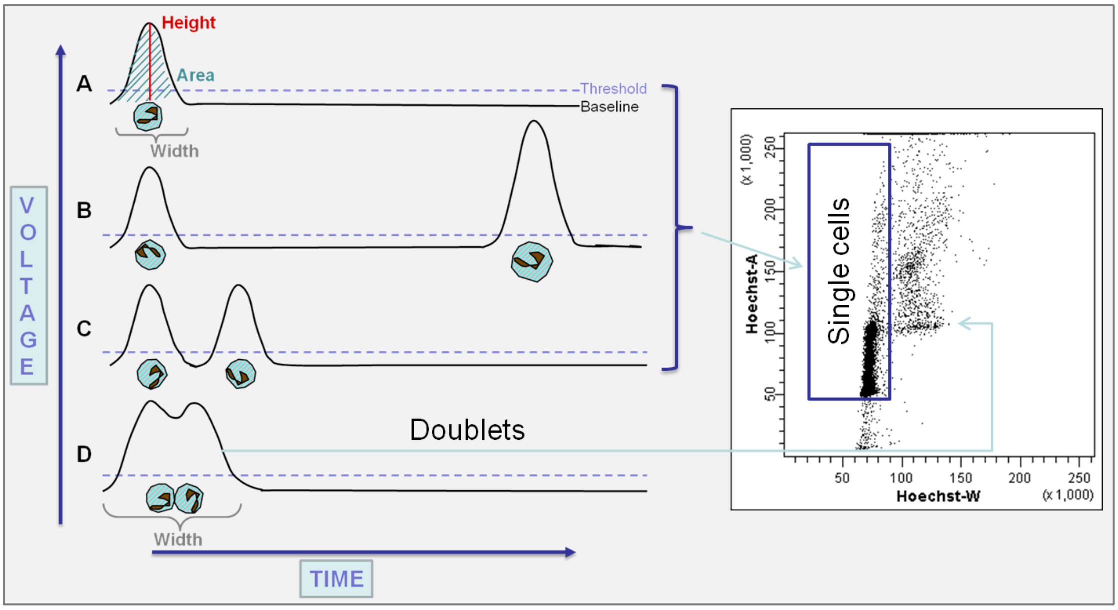

Figure 2-2: Doublet discrimination: A. One cell gives rise to an electrical pulse. Parameters measured of each pulse are height, width and area. B. Two differently sized cells generously separated in time, giving rise to proportionately sized pulses. The width of the pulse from the bigger cell is not increased in the same magnitude as the pulse height and area. C. Two cells closely separated in time. The signal reaches below the threshold value between the two pulses, the cells are separately analyzed. D. Two cells are attached or in immediate proximity and the generated single pulse is bimodal. Both pulse area and width are less than the sum of the pulses generated by each of the two cells, separately. A, B and C will be gated as single cells in a Hoechst width against area dot plot, shown on the right, while the cells analyzed as doublets will be gated out.

A forward scatter (FSC) signal threshold was applied to all unfixed cell samples at a constant FSC detector voltage for each cell line. A Hoechst 33258 fluorescence threshold, of 5.000 (arbitrary units) was used for fixed cells and PMT voltage was individually set for each sample so the peak for G_1 phase cells was placed at 50.000 (arbitrary units). Unless it is stated otherwise, 30.000 events (signals above threshold) were recorded for each cell sample.

Single cell gating, for all flow cytometry analysis in this thesis, was either done on Hoechst staining or on side scatter, using the area and width of each signal as illustrated in **figure 2-2**. The discrimination of doublets was done prior to all other analysis.

2.3.1 DETERMINATION OF CULTURE VIABILITY

The BD Viability kit was employed to determine the amount of live cells in each cell culture sample. Each sample was directly stained with Thiazole Orange (TO) and Propidium Iodide (PI) before flow cytometry analysis, as described in chapter 2.2.2. The absolute concentration of cells was determined by adding a fixed volume of fluorescent microspheres (BD Liquid Counting Beads), further described in chapter 2.5.2. TO fluorescence (510-540nm) was measured with excitation at 488nm. PI fluorescence (663-677nm) was measured with excitation at 561nm. There was no spectral overlap under these conditions. Beads and debris were excluded (**figure 2-3 A**) before gating live cells from dead and injured as shown in **figure 2-3 B and C**. A stopping gate of 5000 beads was employed and the total number of recorded cells varied from 10.000-100.000 cells.

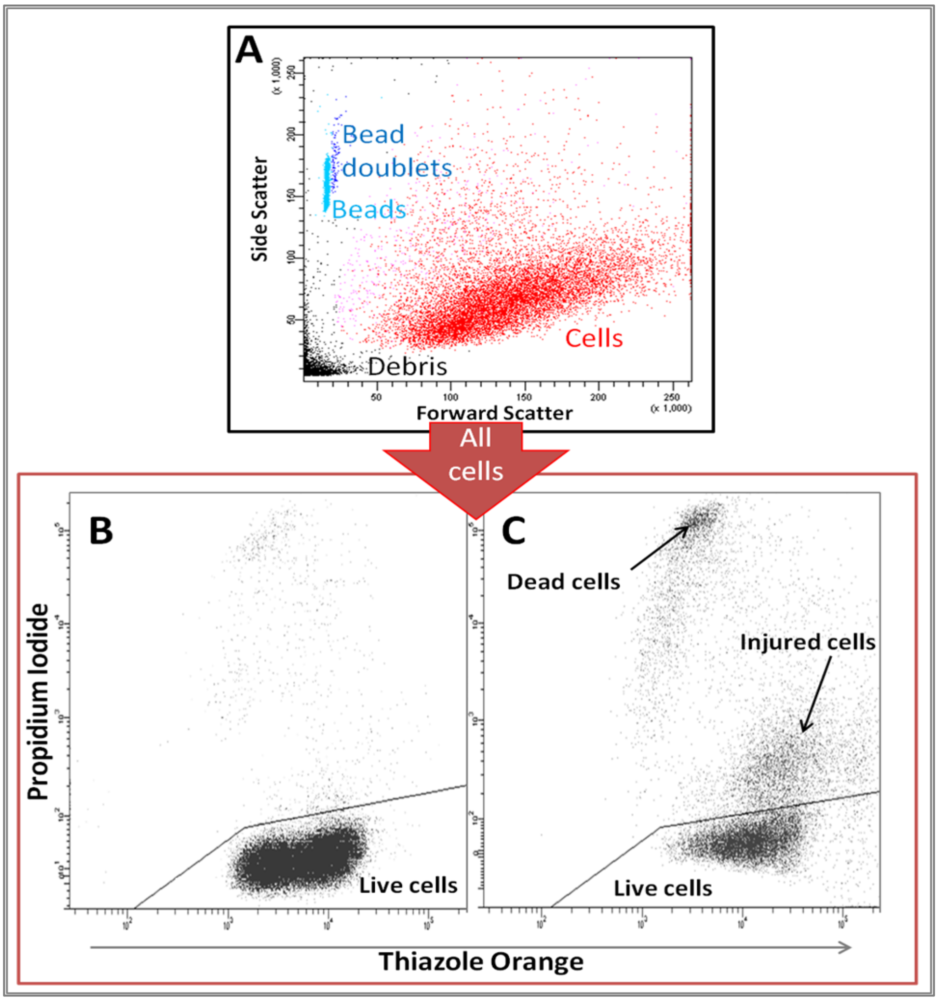

Figure 2-3: Flow cytometry analysis of live and dead Reh cells stained with propidium iodide and thiazole orange, after gating away debris and beads based on forward and side scatter (A). The untreated control (B) and cells treated with 10µM ATM inhibitor and 3µM PARP inhibitor (C) after 72h incubation.

2.3.2 DETERMINATION OF CELL CYCLE FRACTIONS AFTER DNA STAINING

DNA content of each cell was indirectly measured by the signal intensity of Hoechst 33258 emission. As each cell's DNA content is measured, the total distribution of the varying DNA content in the cells analyzed yields a cell cycle distribution for each sample. Hoechst 33258 fluorescence (425-475nm) was measured with excitation at either 405nm or 355nm for analysis (LSRIIs), and with 351/355nm for cell sorting (FACS Vantage SE). Analysis of the cell cycle distributions obtained by flow cytometry was all analyzed by version 7.2.4 of the FlowJo software (TreeStar, Ashland, OR).

Doublet and fragment discrimination of each sample as well as removal of apoptotic cells (further described in section 2.3.3) was done prior to this cell cycle analysis. The FlowJo software computed an automatically fit cell cycle model. Cell cycle fractions for 282 of 288 samples were computed by the Watson Pragmatic model[190] whiles the 6 samples which were Watson-incompatible (no easily definable G_1 peak) was calculated by the Dean-Jett-Fox model[191]. Both models fit G_1 and G_2/M distributions with Gaussian curves. However, the Dean-Jett-Fox model fits the S phase-distribution with a 2nd degree polynomial curve, while the Watson model fits the acquired shape exactly and without theoretical assumptions. A total Root Mean Squared (RMS) value of the fit of the model is calculated from the RMS of each cell cycle phase model fit. In the cases where the automatic model clearly fitted the actual distribution incorrectly, e.g. giving negative values for the sub G_1-fraction, the model was manually adjusted. The adjustments were guided by reduction of the RMS value, thereby minimizing the difference between the model and the actual distribution. The mean RMS value for the 288 samples was 2.4, with a standard deviation of 0.7.

2.3.3 ANALYSIS OF pHISTONE H3, γH2AX AND TUNEL-ASSAY

Hoechst 33258 fluorescence (425-475nm, DNA content) was measured with excitation at either 405nm or 355nm. Cy5 fluorescence (664-677nm, DNA fragmentation/apoptosis) was measured with excitation at either 633nm or 639nm. Thirty thousand events were recorded for each cell sample. Following doublet discrimination employing area and pulse width of the DNA signal, the fraction of apoptotic cells were estimated, and gated out for the further analysis of non-apoptotic cells, in a plot of DNA content versus apoptosis. The lower boundary of the region defining the apoptotic cells (Cy5 positive) was set at 50% of the intensity of G_1 cells along the Hoechst 33258 fluorescence axis and just above the viable cells along the Cy5 axis (**figure 2-4 A**). This was done to avoid that fragmented apoptotic bodies originating from one cell were counted more than once, but may result in an underestimation of the apoptotic fraction when extensive fragmentation has occurred. No upper border in DNA content or Cy5 intensity was employed for this gate.

PE fluorescence (570-600 nm, mitosis) was measured with excitation at either 561nm or 488nm. FITC fluorescence (525-575nm, γH2AX) was measured with excitation at 488nm. Only when the LSRII without a 561nm laser line was used, there was a need for spectral overlap compensation. In the case of 488nm excitation for both FITC and PE, the FITC emission will spill over into the PE fluorescence detector, and to a small degree from PE into the FITC detector. This was compensated for by subtracting about 20% of the FITC signal in the PE channel, and about 2% of the PE signal in the FITC channel.

The fraction of mitotic cells was determined by setting a region around the pHistone H3 positive population with 4n DNA content (**figure 2-4 B**). Single, non-apoptotic cells were divided into pHistone H3 positive and negative cells. The pHistone H3 negative cells were further subdivided in a cell cycle histogram (**figure 2-4 C**) and the γH2AX intensities of those subgroups and the mitotic cells were then determined (**figure 2-4 D**). Median γH2AX intensity for each subgroup was determined in the cases where the peak was a symmetrical. This was the case for G_1, S and mitotic cells. The distribution of γH2AX in the G_2 fraction was, however, often bimodal, but with insufficient separation of the two populations for separate analysis (**figure 3-9 and figure S4** in the appendix). Thus, the γH2AX intensities of G_2 cells were not calculated.

Cell numbers in each sample varied from 250.000 to $5 \cdot 10^6$ cells. Both specific and background antibody binding increased at low cell numbers. Hoechst fluorescence also increased at low cell numbers, but this was adjusted for by varying the PMT voltage, such that the G_1 peak was positioned with an intensity of about 50.000 (arbitrary units). In the cases where no G_1 peak was suspected to be present, the sample was mixed with control cells to annotate ploidies accurately (see appendix).

The TUNEL- and pHistone H3 positive populations were clearly separated from the negative population, i.e. discrete binary variables (either positive or negative). The position of the regions used for enumeration and gating was therefore adjusted for each sample by eye to compensate for the variation in specific and non-specific binding. The estimation of a continuous variable; γH2AX content, however, required a more objective treatment of the flow cytometry data. Each cell may contain any given number of γH2AX foci, and the strength of the foci varies, yielding a distribution of γH2AX content. As shown in section 3.3 (**figure 3-9 A and B**), background due to the secondary antibody increased with decreasing cell number. We also noted that the γH2AX staining of G_1 cells increased at lower cell numbers, although only a few of these cells contained γH2AX foci by microscopy, even in heavily treated samples (**figure 3-10**). Hence, the staining in G_1 cells was due to non-specific binding of the primary, as well as the secondary antibody. Assuming that background binding increases with DNA content and cell size, the γH2AX intensity in the different cell cycle phases was divided by the γH2AX intensity of G_1 cells multiplied with the amount of DNA in that cell cycle phase. This procedure ensured that fold changes from G_1 should be close to one if expression increases in parallel with DNA content throughout the cell cycle. Mid-S phase γH2AX-intensity was divided by 1.5 times the γH2AX intensity of G_1 cells in the same sample, while intensity in mitosis were divided by 2 times the γH2AX intensity of G_1 cells. Others have previously employed a similar normalization of γH2AX intensity, compensating for the variation in background and normal cell cycle specific differences[37].

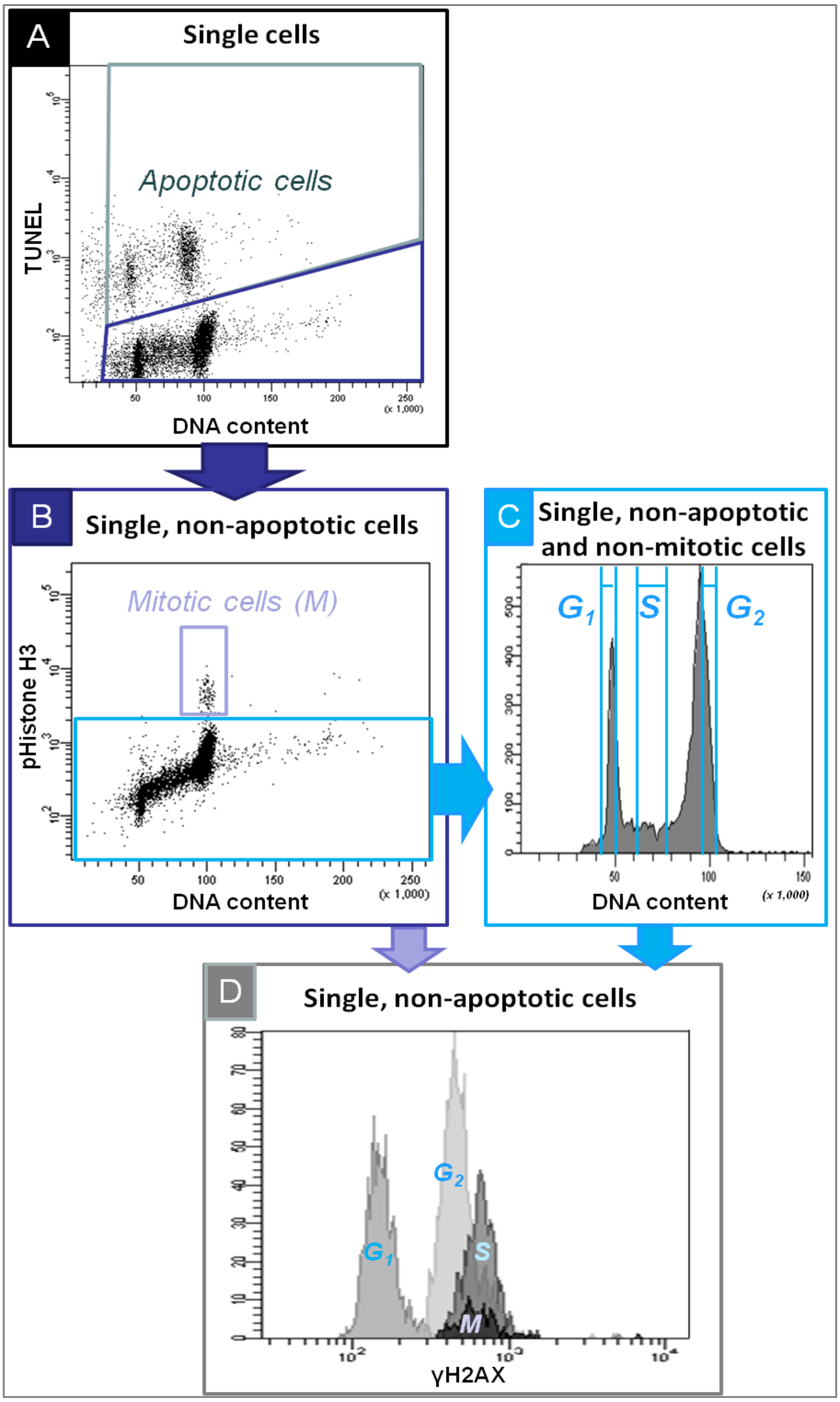

Figure 2-4: Gating strategy used for determining apoptotic and mitotic fraction and γH2AX staining intensity according to cell cycle phase of fixed cells. Reh cells treated with 3µM PARP inhibitor and 10µM ATM inhibitor for 72h is shown as an example.

2.4 STRUCTURED ILLUMINATION FLUORESCENCE MICROSCOPY

Structured illumination microscopy is a method of improving the resolution and out-of-focus rejection in a conventional microscope. Instead of expensive laser-scanning and spinning-disc methods of traditional confocal microscopy, a single-spatial-frequency grid pattern of projected light is used to create high resolution optical sectioning of the specimen[192]. Differential interference contrast (DIC/Nomarski) is a microscopy technique in which the difference in optical path length between two states of polarized light is used to enhance the contrasts of a transparent specimen.

Cells from fixed or unfixed samples were either sorted by FACS directly onto a glass slide, or samples were spun at 1500g for 4 minutes before supernatant removal and they were transferred onto glass slides. All samples were mounted immediately after fluid condensation by ProLong Gold Mounting media. Coverslips of 0.17mm was used to avoid spherical aberrations. Tables of specifications of all primary and secondary antibodies used in this section can be found in the appendix.

An Axio Z1 Imager microscope was used for immunofluorescence imaging and DIC microscopy of cells. This microscope was equipped with an ApoTome (enabling structured illumination) and a 120W Hg metal halide lamp (all Carl Zeiss, Oberkochen, Germany). DNA was detected using Hoechst 33258 fluorescence. Antibodies towards the nuclear envelope (LaminB2) and DNA DSBs (γH2AX) were both detected by FITC fluorescence, and these two parameters were not stained for simultaneously. Mitotic cells were stained for by an antibody against pHistone H3, and detected by PE fluorescence. Apoptotic cells were stained with a streptavidin linked Cy5 fluorochrome for biotin-dUTP incorporation after the TUNEL assay. To avoid photobleaching during imaging, the cells were illuminated with decreasing wavelengths, e.g. the last parameter to be imaged was DNA (UV light for Hoechst excitation). The filter sets used during microscopy are listed in table 2-1.

Table 2-1: Fluorescence microscopy filter set specifications. HE abbreviates High Efficiency and BP abbreviates Band Pass filter.

Fluorochrome	Filter set	Exitasion filter (nm)	Beam splitter (nm)	Emission filter (nm)
Cy5	50	BP 640/30	>660	BP 690/50
PE	43 HE	BP 550/25	>570	BP 605/70
FITC	38 HE	BP 470/40	>495	BP 525/50
Hoechst 33258	49	BP 365/5	>395	BP 445/50

A 63x oil immersion-objective with numerical aperture of 1.4 (0.2µm resolution) was used for all microscopy of fixed cells. For unfixed cells, a 40x air immersion-objective with a numerical aperture of 0.95 (0.3µm resolution) was employed. For visualizing multinucleated cells (LaminB2) each image field was optically sectioned into five 1.5 µm thick slices, for counting γH2AX foci each field was sectioned into seven slices of 1.0µm. AxioVision LE software (Carl Zeiss), version 4.5, was used to process the microscopy images.

2.5 CELL COUNTING

2.5.1 COULTER COUNTER

Coulter counting is an efficient way of calculating the cell concentration in a cell suspension. The Coulter Counter-principle is based on detecting electrical resistance changes between two electrodes in a conductive fluid on each side of a cylindrical aperture. Each change in resistance is caused by a particle transiently displacing the conductive fluid in the aperture, as a fixed volume of particles is brought through. In a dilute solution of particles, each particle changes the impedance between the two electrodes and this generates an electrical pulse [193]. The height of the pulse is proportional to the volume of the particle [193-195]. The exact relation between pulse height and actual particle volume is calibrated using a uniform bead solution of known bead volume.

A Z2 Coulter Counter (Beckman Coulter, Brea, CA) was utilized for growth assessment and reseeding calculations, both during routine cell culturing and during all the experiments with molecular inhibitors. An amount of thoroughly mixed cell culture was diluted to appropriate counting concentration in physiological saline solution (NaCl 0.9%). The range for appropriate counting concentration was determined by the noise threshold and the highest tolerable chance of *coincidence*. The noise threshold was determined by five replicates of counting a solution of pure media diluted in the same manner as each sample. The threshold value average was 114 counts with a standard deviation of 10, whereas the lowest cell count measured in a sample was 6500 counts. The term coincidence refers to event of two particles entering the aperture at the same time. In that case, two discrete particles will be measured as one particle with the combined size of the two particles. The chance of coincidence was calculated from the concentration of the particle solution and automatically corrected for in the Coulter Counter.

2.5.2 BD LIQUID COUNTING BEADS

A liquid suspension of fluorescent microspheres, BD Liquid Counting Beads (an addition to the BD viability kit) enables cell counting. The principle of these beads is that a relative concentration of cells can be determined in a solution with a known bead concentration using flow cytometry. To test the reliability of the method, all Coulter counted cell samples was also analyzed with this counting method. The BD Liquid Counting Beads solution has an accurate bead concentration, and cell samples with unknown cell density was added a fixed volume of 50µl BD Liquid Counting beads. The sample volume was 0.5ml for all Reh and U698 samples and 1.0ml for JVM-2 and Granta-519 samples due to the differences in initial cell concentrations. To acquire reliable data for all samples, a stopping gate of 5.000beads was chosen. This ensured a minimum cell count of 10.000cells for the samples with the lowest cell concentrations. The beads and bead doublets was clearly distinguishable from cells in a plot of side scatter against forward scatter. **Figure 2-3 A**, in section 2.3.1, illustrates a typical example of the population of beads and cells.

The concentration of cells in the sample was calculated using equation [1].

$$[\mathrm{Cell}]_{\mathrm{sample}} = \frac{\#\mathrm{Cells}}{\#\mathrm{Beads}+\#\mathrm{Bead\ Doublets}} \times \frac{\#\mathrm{Liquid\ Counting\ Beads/test}}{\mathrm{Test\ volume}} \times \mathrm{dilution\ factor} \qquad [1]$$

An ordinary linear regression was performed to establish the correlation between the Liquid Counting Beads and Coulter counting (**figure 2-5**).

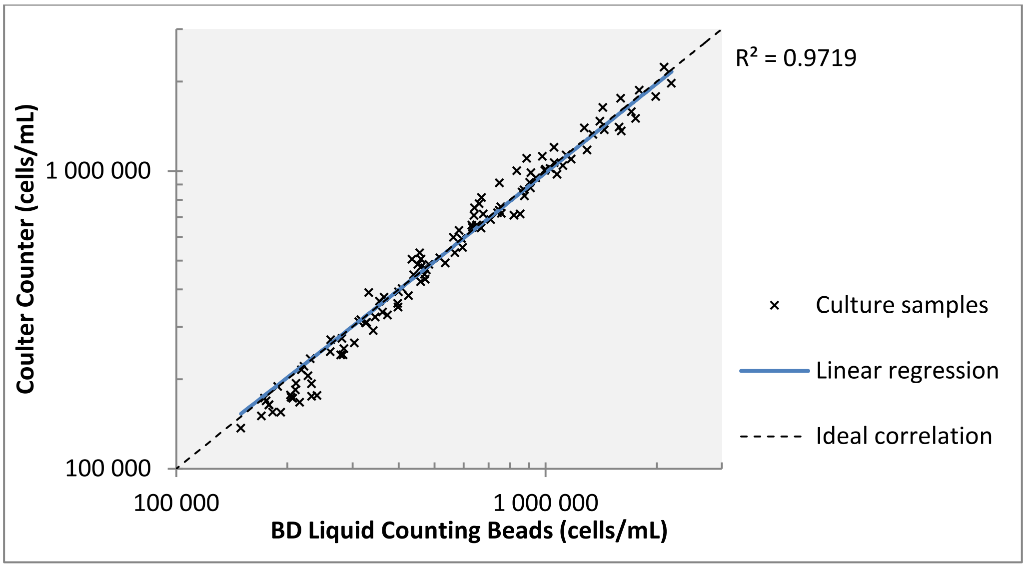

Figure 2-5: Ordinary linear regression of cell concentration assessment in the same samples with Coulter Counter and BD Liquid Counting Beads

2.6 WESTERN BLOTTING

For detailed specifications of all primary and secondary antibodies, as well as recipes used this section, see appendix.

Protein lysates for western blotting were prepared by adding 100µl 2x loading buffer (0.125M Tris-HCl, 5mM DTT) directly to cell pellets consisting of 500.000 cells. The loading buffer contains 4% Sodium dodecyl sulfate (SDS). The negatively charged SDS molecules will coat the denatured proteins according to size. A glycerol content of 20% and 0.1% Bromophenol Blue in the loading buffer, will ensure eased and more secure loading into running buffer-submerged wells. 5-10 U/ml Benzonase, 0.025-0.05 TIU/ml Aproteinin and 0.1% of phosphatase inhibitor cocktail II and III were added to the loading buffer to reduce sample viscosity, proteolysis and phosphatase activity respectively.

The cells were both chemically lysed by the detergents in the loading buffer (mainly SDS and DTT) and mechanically lysed by pipetting on ice, vortexing for 5 minutes and, finally, by heat denaturation at 95°C for 7 minutes. Samples were stored at -20°C and used within a two-week period.

SDS-Polyacrylamide Gel Electrophoresis (PAGE) was used to separate the SDS-coated proteins in the lysates by size. First, an 8% polyacrylamide gel with a standard Tris/Hepes-running buffer was employed, but the phospho-ATM protein band at 370kDa was barely visible and blurred. Separation and blotting of this large protein was successfully improved by using a 7.5% polyacrylamide TGX-gel from Bio-Rad with the supplied Tris/Glycine/SDS-running buffer. SDS-PAGE was performed at 150V for 1h. When an electric current is applied to the gel, the negatively charged SDS-coated proteins will be trapped and concentrated between the chlorides and the glycine in the first part of the gel (stacking gel), before the pH changes in the separating part of the gel and the zwitterion glycine shifts charge to positive. To assess the size of the proteins after SDS-PAGE, a dual colored protein standard of known size (kDa) was applied to at least two separate wells of each gel.

The negatively charged, separated proteins were transferred from the gel to a methanol activated polyvinyldifluoride (PVDF)-membrane (pore size 0.45 µm), during an overnight electro-blotting procedure at 15V in transfer buffer (20%methanol, 0.02M Tris-HCl, 0.2M Glycine) at 4°C. The PVDF-membrane was preblocked in a 5% dry milk solution of TBS (Tris-buffered saline) with 0.05% Tween 20 (TBS-T) for 1h, before incubation with primary antibodies diluted in TBS-T. The membrane was cut horizontally between the 75 and 100kDa protein standard bands, the upper part was incubated with 1:1000 anti-phospho-ATM (Ser1981), the lower part was incubated with 1:1000 anti-phospho-CHEK2 (Thr68) and 1:5000 anti-TUBG2 (γTubulin). Incubation of the membrane with primary antibodies was done overnight at 4°C, before the excess antibodies were washed from the membrane in three times TBS-T for 5 minutes. Species-specific secondary antibodies conjugated with horseradish-peroxidase (HRP) were incubated 1:10.000 in 5% dry milk TBS-T for 1h before the same wash procedure was performed.

To detect the protein bands on the membrane, enhanced chemiluminescence (ECL)-detection was used. Photons are released by oxidization of luminol, as hydrogenperoxide is reduced by the HRP-enzyme. The HRP-linked antibody is again bound to the proteins of interest. Light emitting from the chemiluminescent substrate stained a photosensitive Amersham Hyperfilm ECL (GE Healthcare, Little Chalfont, UK). The film was developed in a Curix 60 automatic developer (Agfa, Greenville, SC), and scanned using a GS800 scanner (Bio-Rad, Hercules, CA).

2.7 CALCULATION OF CELL CYCLE PHASE DURATIONS

The age distribution in the mitotic cell cycle is not uniform because one cell at cell cycle completion always divides into two newborn daughter cells. Consequently, the proportion of the duration of one cell cycle phase is not equal to the proportion of cells in that particular phase. The relative proportion of cells of any cell cycle age decreases exponentially with increasing cell cycle age. To calculate the duration of each cell cycle phase in a population, a function of cell cycle age frequency was derived. Relative frequency of cells at different cell cycle time points in an exponentially growing population can be defined by the function [2]:

$$\boxed{N(t) = N(0)e^{-k\frac{t}{T_c}}} \qquad [2]$$

$N(t)$: Relative frequency of cells at time, t

t: Time (h)

T_c: Total cell cycle duration (h)

A normalized time parameter was defined to make the function as universal as possible, excluding differences in total cell cycle duration between different cell systems:

$$t' = \frac{t}{T_c} \xrightarrow{yields} N(t') = N(0)e^{-kt'} \ [0 < t' < 1]$$

Under the assumption of an ideal, asynchronous population during exponential growth, the frequency of cells at time zero will always be twice the frequency of cells at cell cycle completion. To ensure this premise, the negative constant k must satisfy:

$$\frac{N(t'=0)}{N(t'=1)} = \frac{e^0}{e^{-k}} = 2 \Rightarrow e^{-k} = \frac{1}{2} \Leftrightarrow$$

$$\underline{k = -\ln 2}$$

Integration of the relative frequency of cells as a function of t' yields the fraction of cells between given time points in the cell cycle. To ensure a total cell fraction of one in the definite integral from time=0 until time=T_c, a normalization of N(0) is required:

$$\int_0^1 N(t')\,dt' = 1 \Leftrightarrow N(0)\int_0^1 e^{-\ln(2)t'}\,dt' = 1 \Rightarrow$$

$$\underline{N(0) = 2\ln 2}$$

The final equation [3] describing cell cycle time and cell frequency is illustrated in **figure 2-6**:

$$\boxed{N(t') = 2\ln(2)\,e^{-\ln(2)t'}, [0 < t' < 1]} \qquad [3]$$

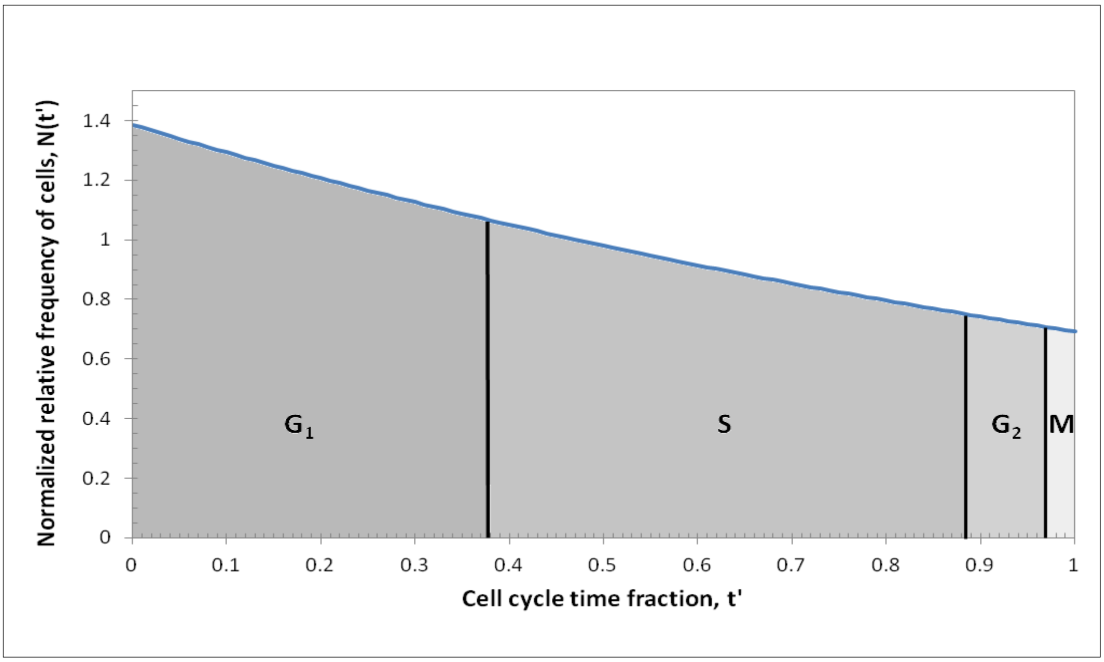

Figure 2-6: Distribution of cells in an ideal, asynchronous population of proliferating cells. Cell cycle phase areas defined by 47% cells in G_1, 42% in S, 6% in G_2 and 2% in mitosis (M). The shape of the distribution is given by function [3].

The total cell cycle duration was assumed equal to the doubling time, and was calculated by the mean cell counts. Thereafter, function [3] was used to calculate the lengths of the cell cycle phases from the mean cell cycle fractions after three replicates of 24h incubation with PARPi and ATMi.

2.8 CALCULATION OF ADDITIVE EFFECT

Determination of additive effect of combining two drugs in the same cell system requires advanced calculation if both drugs have an effect on the system. Simple calculation of potentiation and enhancement can be used if one drug does not have an effect by itself, but increases the effect of the other drug. According to the Chou-Talalay method, calculation of whether the combination of two drugs has a synergistic (more than additive), additive or antagonistic (less than additive) effect, requires testing of at least three appropriate concentrations of each drug alone and in combination[196]. However, the combined effect (E_{1+2}) of two mutually non-exclusive drugs (1 and 2), as expected for ATMi and PARPi, can be described by the simple function [4]:

$$E_{1+2} = E_1 + E_2 - (E_1 \cdot E_2) \qquad [4]$$

The equation can be rewritten as:

$$\frac{(1 - E_1)}{(1 - E_{1+2})} = \frac{1}{(1 - E_2)}$$

This equation shows that the combination curve and the dose response curve of the single drug are in parallel in a logarithmic plot. In the case of this study, the total effect of PARPi and ATMi is additive if this curve is in parallel with the PARPi curve in a logarithmic dose response plot.

2.9 STATISTICAL METHODS

Standard Error of the Mean (SEM) has been used throughout this thesis to describe the variation in the expected mean of repeated measurement-series. Standard deviation (SD) was only used to describe the variation between measurements using a particular method. Ordinary linear regression was performed with version 18.0 of SPSS (IBM, Armonk, NY).

3 RESULTS

3.1 CELL DEATH AND PROLIFERATION AFTER PARP AND/OR ATM INHIBITION

Cell death and total cell numbers were measured during a 72h-period after addition of PARP inhibitor (PARPi) and/or ATM inhibitor (ATMi). Before proceeding with these experiments, we first wanted to determine the functionality of ATM in these cell lines. If present and functional, ATM is autophosphorylated at serine 1981 after e.g. X-irradiation[44]. Immunoblotting showed that ATM became strongly phosphorylated in Reh, U698 and JVM-2 cells 1h after irradiation with 4Gy (**figure 3-1**). However, some phospho-ATM (pATM) was also induced in Granta-519 cells, although these cells have been reported to have defective ATM function[179,180]. If cells were irradiated in the presence of ATMi, phosphorylation was reduced, but not entirely back to control levels. The downstream ATM-target CHEK2 was also analyzed, and the phosphorylation of threonine 68 of CHEK2 (pCHEK2) levels varied in the same manner.

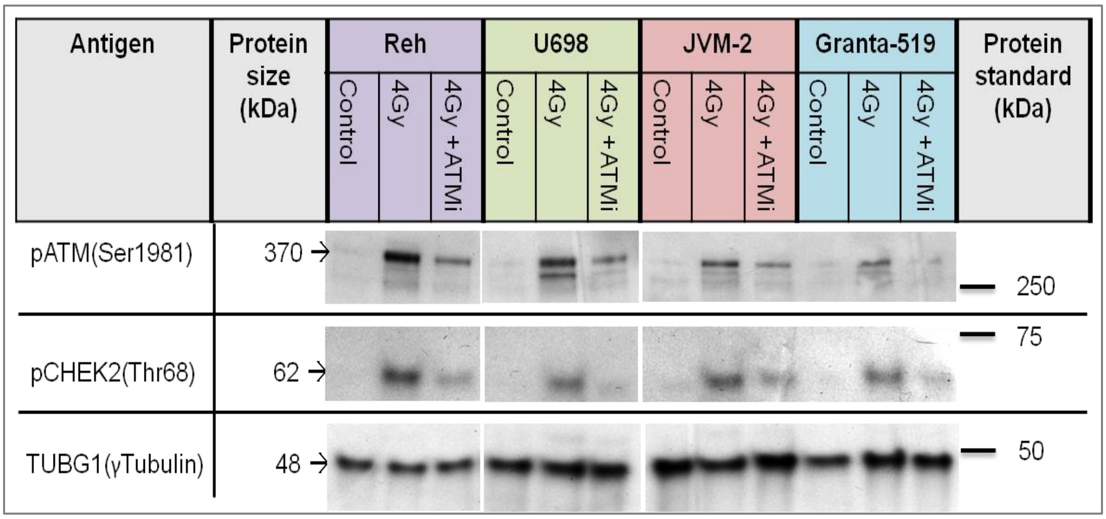

Figure 3-1: ATM autophosphorylation and phosphorylation of downstream ATM target CHEK2 in unirradiated, irradiated and ATM inhibited and irradiated Reh, U698, JVM-2 and Granta-519 cells. Samples were lysed 1h post-4Gy, and an irradiated sample of each cell was added 10μM ATM inhibitor 15 minutes prior to irradiation. Loading control was TUBG1 protein amount displayed in the last row.

The fraction of dead cells was assessed by the PI/TO assay and was below 5% in control Reh and U698 cells, and 8-13% in control JVM-2 and Granta-519 cells during the time course of the experiment (**figure 3-2**). Treatment with ATMi alone did not induce more cell death than in the control.

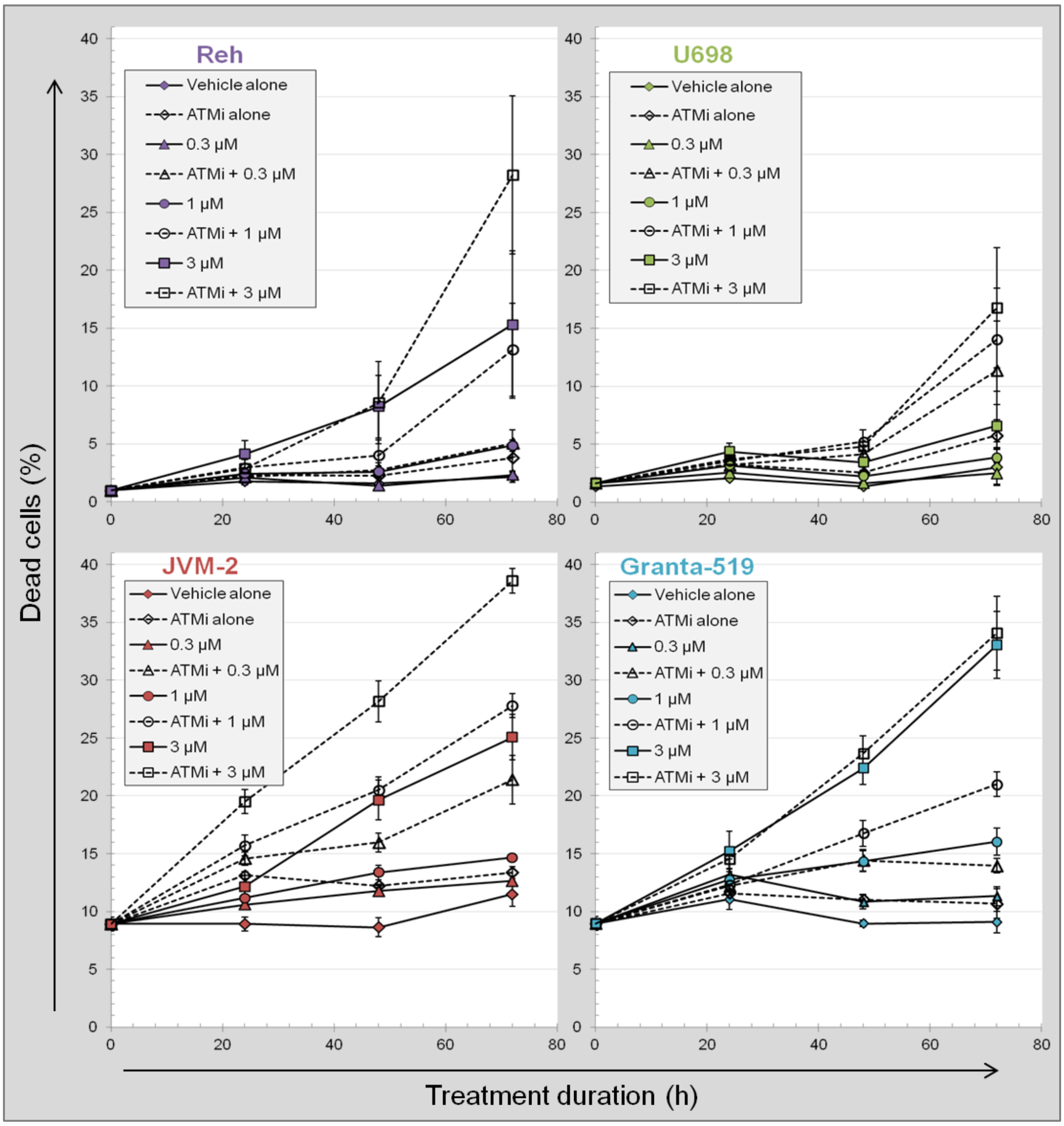

Figure 3-2: Fraction of dead cells as a function of PARP and/or ATM inhibitor treatment duration for Reh, U698, JVM-2 and Granta-519 cells. Mean value from three independent experiments ±SEM.

Treatment with PARPi alone at varying concentrations did not increase the fraction of dead cells, the exception being for the highest concentration (3µM) in Reh, JVM-2 and Granta-519, and a slight increase for Granta-519 after incubation with 1µM.

However, cell death caused by inhibition of PARP by the three different concentrations of PARPi was increased from control levels in the presence of ATMi, indicating enhancement of the effect of PARP inhibition by inhibition of ATM (synthetic lethality). The exception was Reh cells treated with 0.3µM PARPi and ATMi (**figure 3-2**).

The dose response curves for cell death at 72h as a function of PARPi concentration are shown in **figure 3-3**. Inhibition of ATM caused an increase in cell death for Reh, U698 and JVM-2 cells for all concentrations of PARPi. This effect was much less pronounced for Granta-519, which only showed a small increase in cell death caused by ATM inhibition at 0.3 and 1.0µM PARPi.

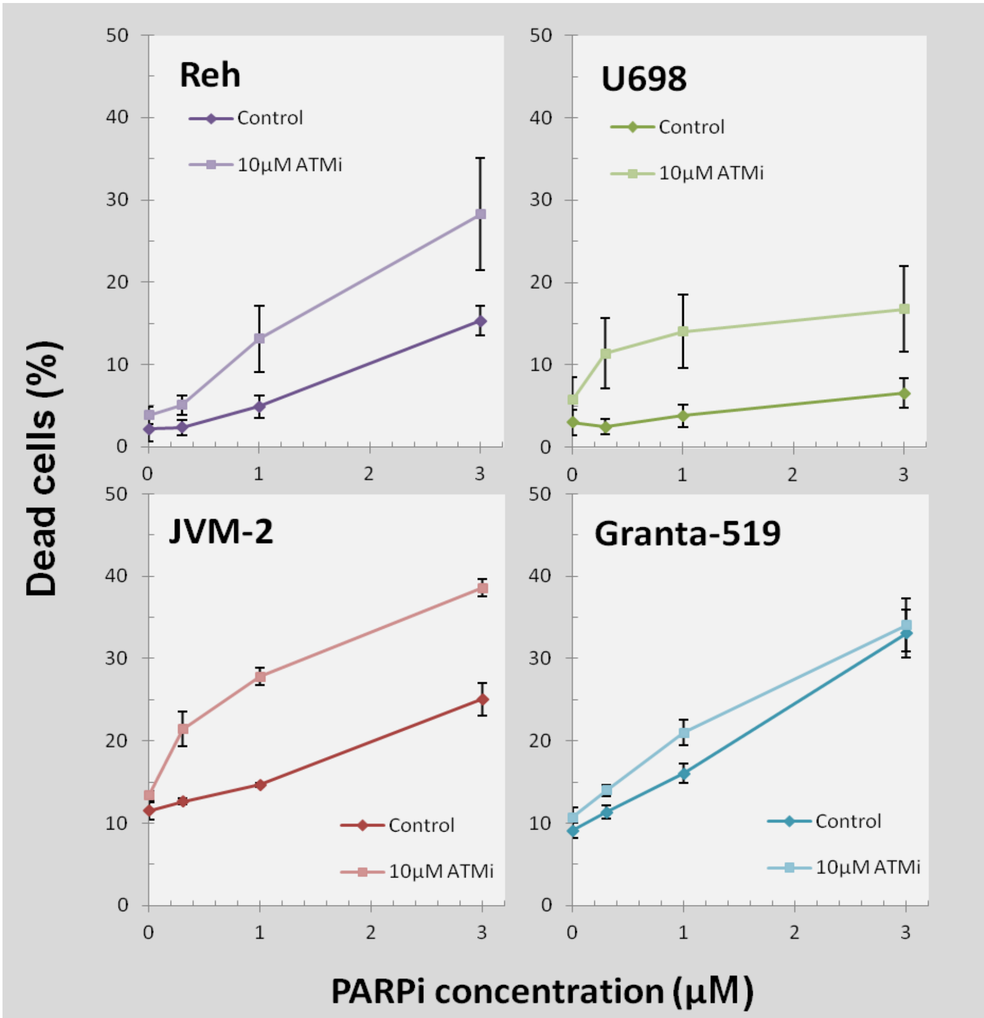

Figure 3-3: Dose response curves of cell death in Reh, U698, Granta-519 and JVM-2 as a function of PARP inhibitor concentration after 72h treatment with/without 10µM ATM inhibitor. Mean value from three independent experiments ±SEM.

Total cell numbers were assessed by Coulter counting. The number of viable cells was calculated from the raw data after subtraction of the number of dead cells (**figure 3-4**). Growth was close to exponential in control cultures. Although treatment with ATMi alone did not increase the fraction of dead cells (**figure 3-2**), a decrease in live cell numbers was observed at all time points in all cell lines, indicating that the ATM inhibition caused an increased cell cycle time.

Inhibition of PARP in the absence of ATMi decreased the number of cells at 48-72h in a dose-dependent manner (**figure 3-4**). At 0.3µM, this reduction was only significant for JVM-2. Additionally, the growth curves after treatment with 3µM PARPi were not exponential at the later time points. This is to be expected if cell death becomes more extensive, which was observed for Reh, JVM-2 and Granta-519 (**figure 3-2**).

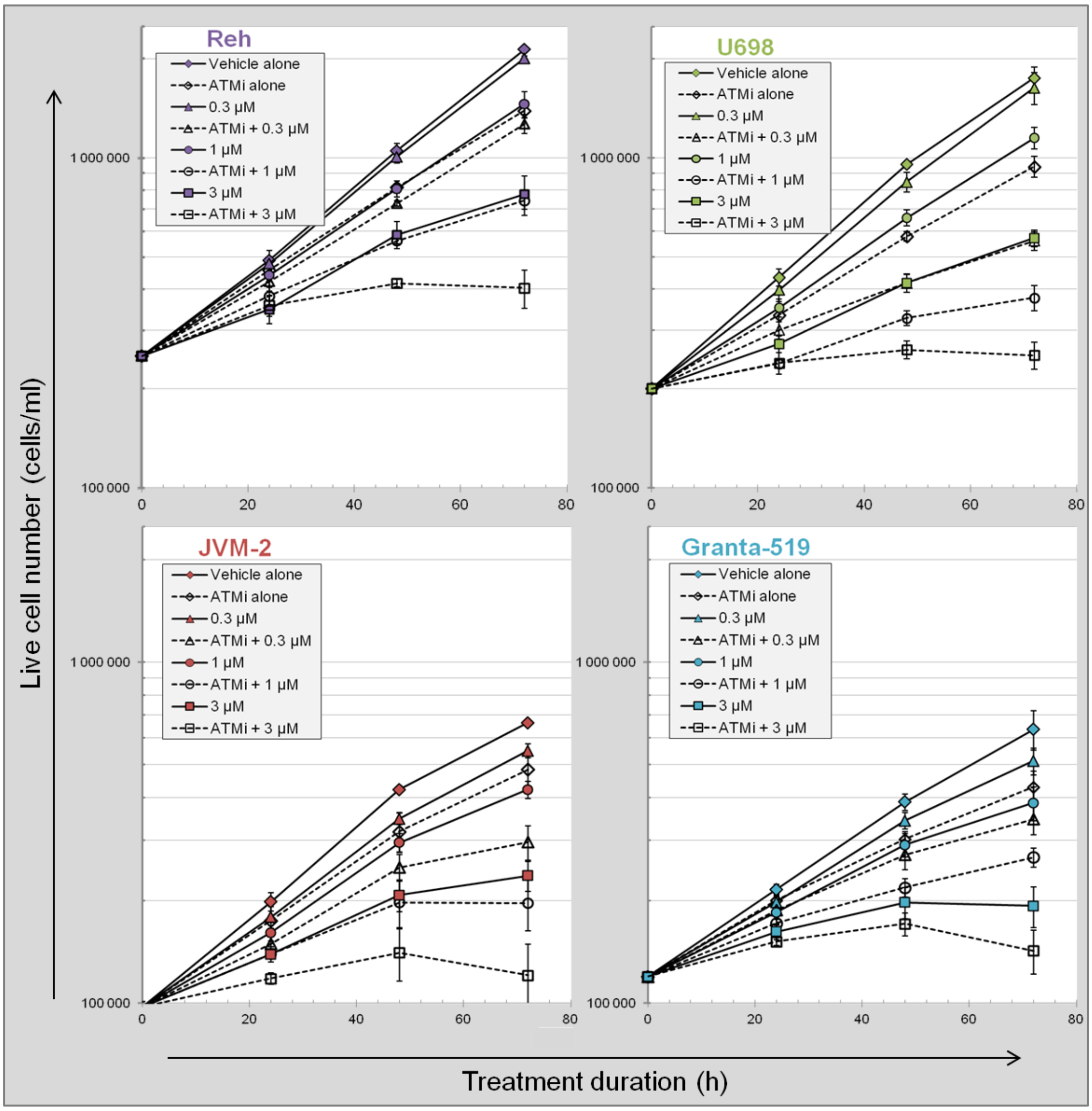

Figure 3-4: Cell growth during PARP and/or ATM inhibitor treatment in Reh, U698, JVM-2 and Granta-519 cells. Live cell number is plotted as a function of treatment duration. Mean value from three independent experiments ±SEM.

When cells were treated with ATMi in addition to PARPi, the cell numbers decreased further, but this reduction was not significant for Granta-519 at 3µM PARPi. The cell numbers tended to decrease from 48 to 72h after treatment with ATMi and 3µM PARPi (**figure 3-4**); at this time, there was pronounced cell death for all cell lines (**figure 3-2**). If a simple model for additive effect is applied (see section 2.8), the dose-response curves in the absence and presence of ATMi should be parallel (**figure 3-5**). This was the case for Granta-519. However, for the other cell lines, and particularly for U698, the diverging curves indicated that the total effect of the two inhibitors was larger than the sum of the individual treatments, i.e. the effect was synergistic.

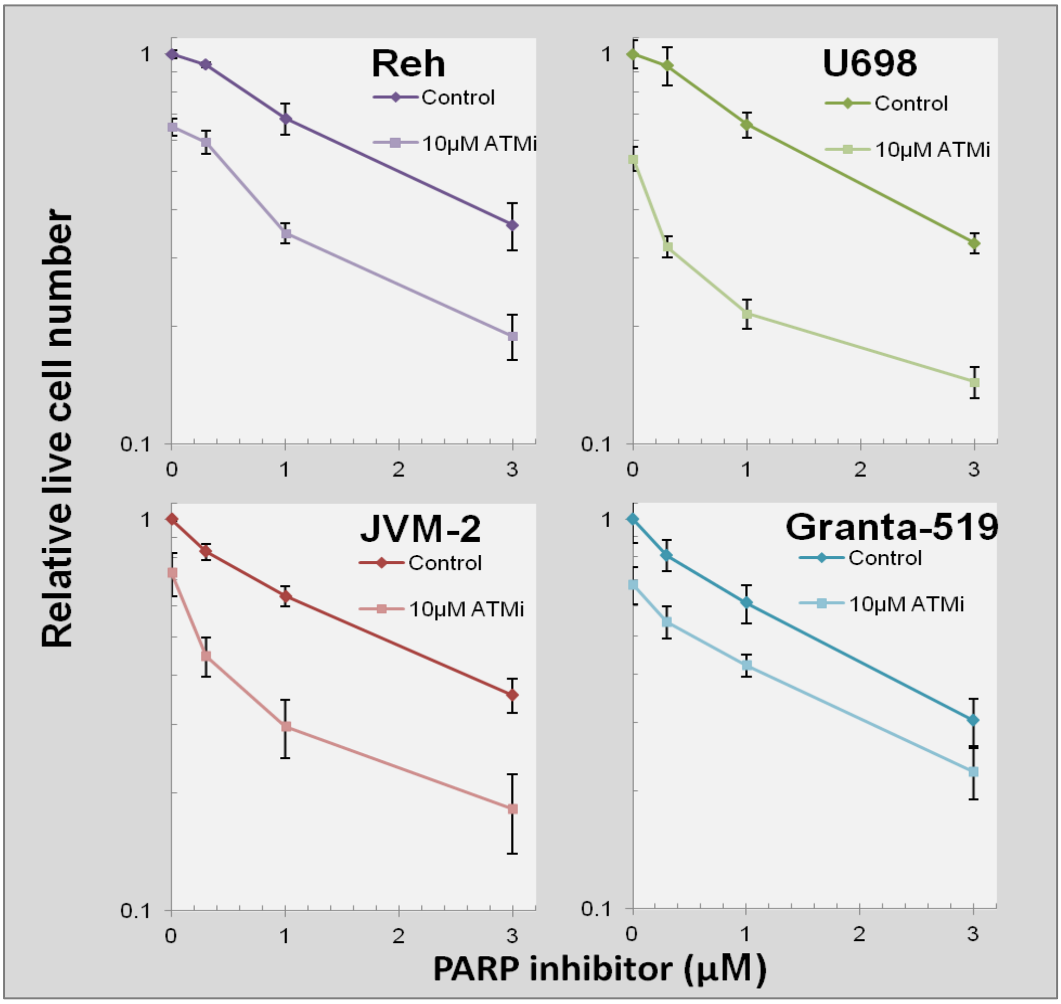

Figure 3-5: Dose response curves of relative live cell numbers in Reh, U698, Granta-519 and JVM-2 as a function of PARP inhibitor concentration after 72h treatment with/without 10µM ATM inhibitor. Mean value from three independent experiments ±SEM.

3.2 PARP AND ATM INHIBITED GRANTA-519 AND REH CELLS DIE BY APOPTOSIS

Apoptosis was measured by TUNEL-assay (DNA fragmentation), but also confirmed during fluorescence microscopy as all the observed TUNEL-positive cells had typical morphological characteristics associated with apoptosis. Cells which were TUNEL positive were in general smaller than average, some had undergone membrane blebbing, and apoptotic bodies were observed. It is difficult to determine by microscopy whether an apoptotic cell originates from an interphase cell or a mitotic cell. However, a distinct peak of apoptotic cells likely to be tetraploid, strongly suggested that the cells initiated apoptosis from G_2 or mitosis.

Apoptotic fraction in the mock-treated cell samples was below 1.5% in Reh and U698 cells, below 4% in JVM-2 cells and below 6% in Granta-519 cells (**figure 3-6**). Treatment with PARPi alone induced no increase in apoptosis in U698 cells compared to control. However, a slow increase, most pronounced at 48h and 72h, was observed in 3µM PARPi treated Reh and JVM-2 cells. ATM inhibition alone did not cause significant increases in apoptosis in Reh and U698 cells, but a slight elevation in JVM-2 and up to 3% increase in Granta-519. A rapid increase in apoptotic levels was observed in Granta-519 cells at all three PARPi concentrations. The combined PARPi/ATMi treatment increased the apoptotic fractions compared to PARP inhibition alone. However, the apoptotic fractions were below 4% and 11% for U698 and JVM-2, respectively. There was a large, but again delayed, increase in apoptosis in Reh cells caused by the additional treatment with ATMi. The apoptotic fractions of Granta-519 cells also increased in the presence of ATMi, but the effect was not as pronounced, and not significant at 3µM PARP inhibition for 72h.

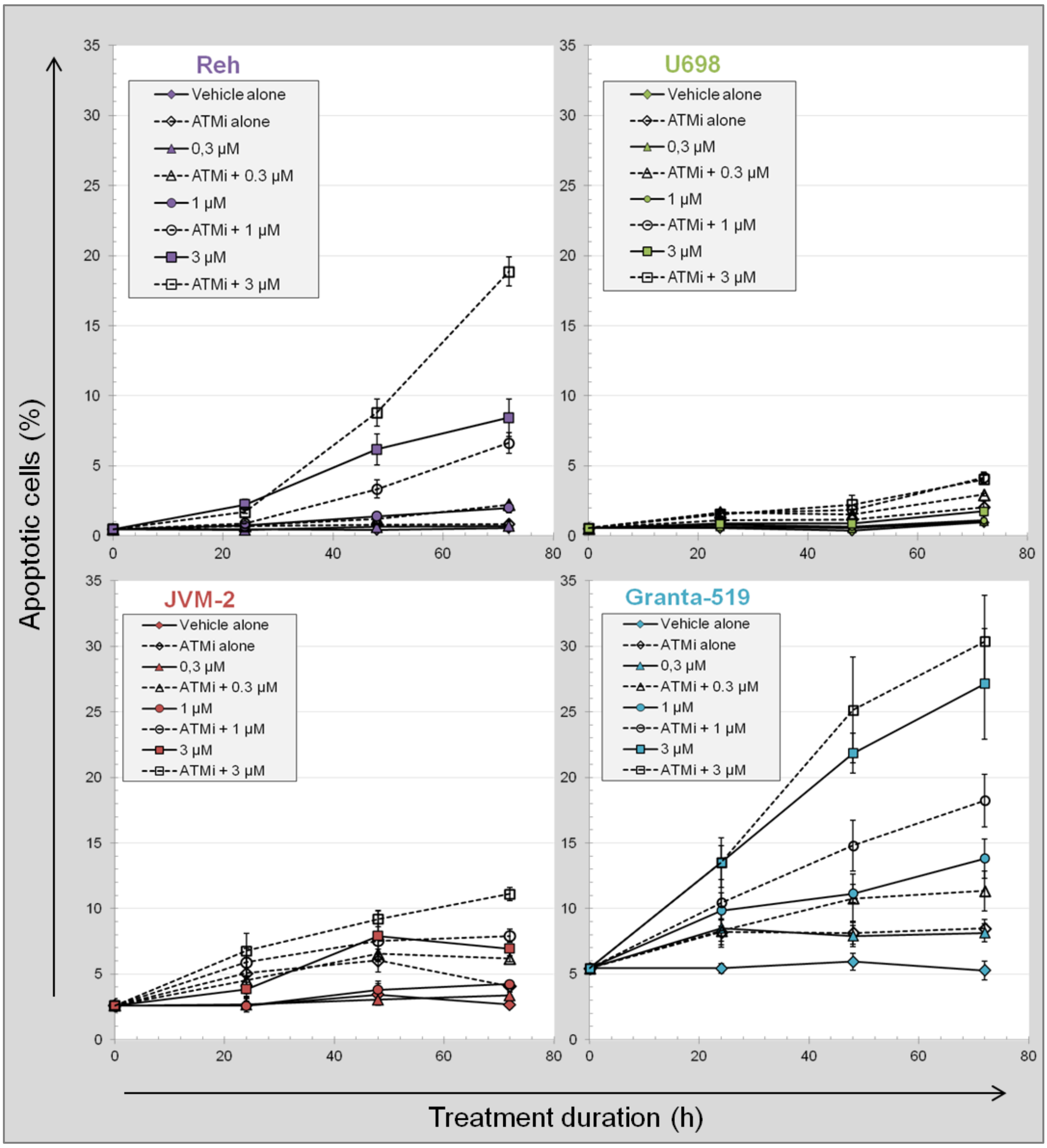

Figure 3-6: Apoptosis measured by TUNEL assay in Reh, U698, JVM-2 and Granta-519 cells during 72h treatment with PARP and/or ATM inhibition. Apoptotic fraction is plotted as a function of treatment duration. Mean value from three independent experiments ±SEM.

The dose-response curves for apoptosis after 72h treatment revealed an enhancement of approximately threefold in Reh cells (**figure 3-7**). A synthetic lethal interaction between the two drugs was seen in Reh cells, since there was no effect of ATMi alone. In contrast, the apoptotic fractions of the presumably ATM-deficient Granta-519 cells (**figure 3-1**) were only 50% enhanced by ATMi (at 0.3µM PARPi). This increase was also observed with ATMi alone, resulting in almost parallel dose-response curves in the absence and presence of ATMi. The dose-response curves for

U698 and JVM-2 suggested some enhancement by ATMi, but the effects of treatment on apoptosis were far less pronounced than on cell death (**figure 3-3**).

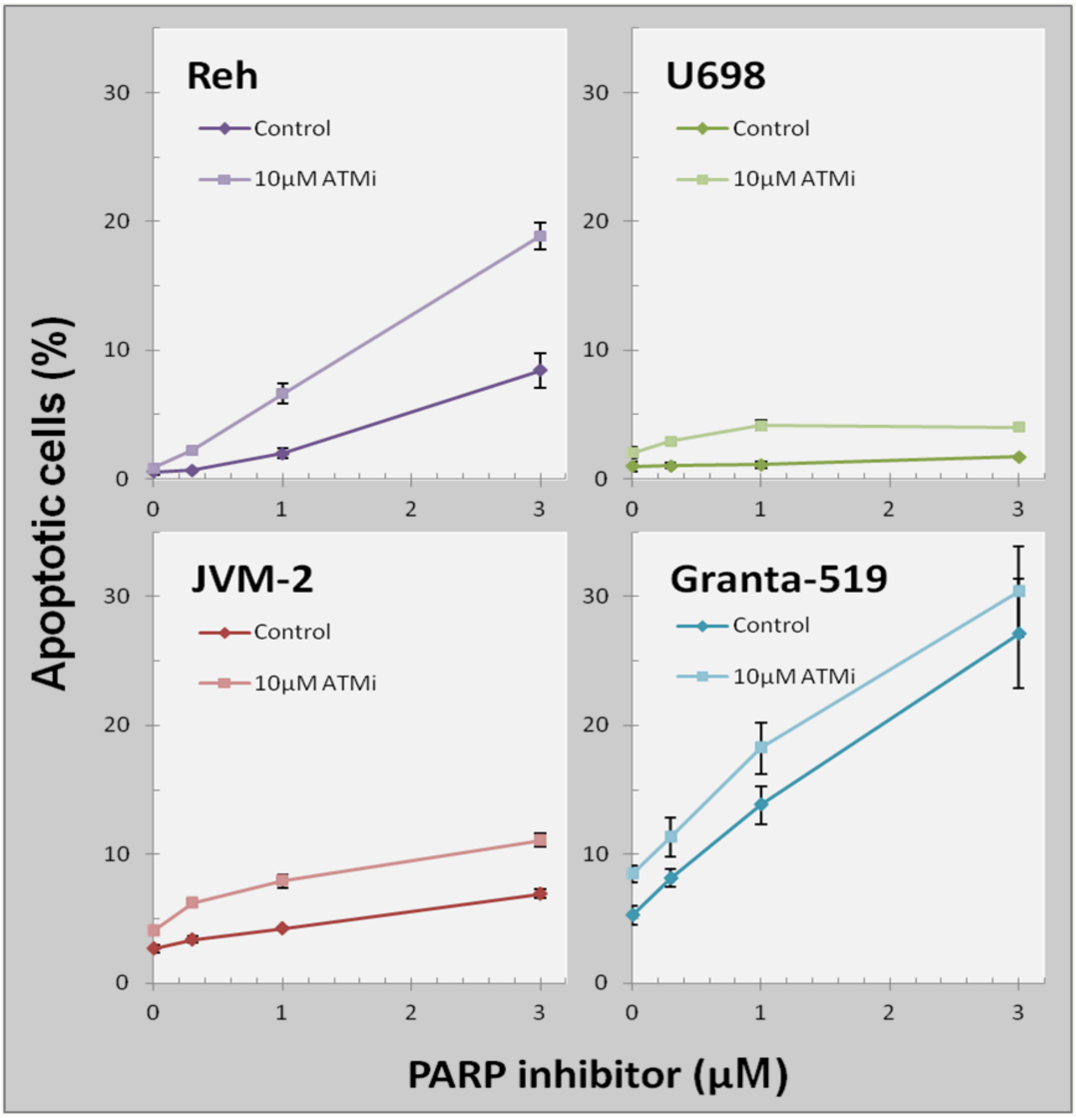

Figure 3-7: Dose response curves of 72h treatment with PARP inhibitor and/or 10 µM ATM inhibitor on induction of apoptosis. Mean value of single, TUNEL positive cells ±SEM.

Ordinary Linear Regression (OLR) of cell death as a function of apoptosis for all treatments at all time points for the four cell lines (**figure 3-8**), revealed that the dead cell fractions were almost three times (slope of regression lines/regression coefficients) higher than the apoptotic fraction in the same samples of U698 and JVM-2 cells. The regression coefficient in Granta-519 cells was not significantly different from 1.0.

Reh cells showed the same trend as Granta-519, but the slope of 1.39 was significantly different from 1.0 (95% CI of 1.23-1.54). Since there are few data points at the high levels of apoptosis and cell death for Reh, the regression is heavily influenced by those points without regard for the insecurity of the measurement. More observations of severe cell death and apoptosis in Reh cells (e.g. new experiments with expanded treatment duration) could be performed to test the validity of the current slope. OLR results for each cell line are attached in the "Calculations" section in the appendix.

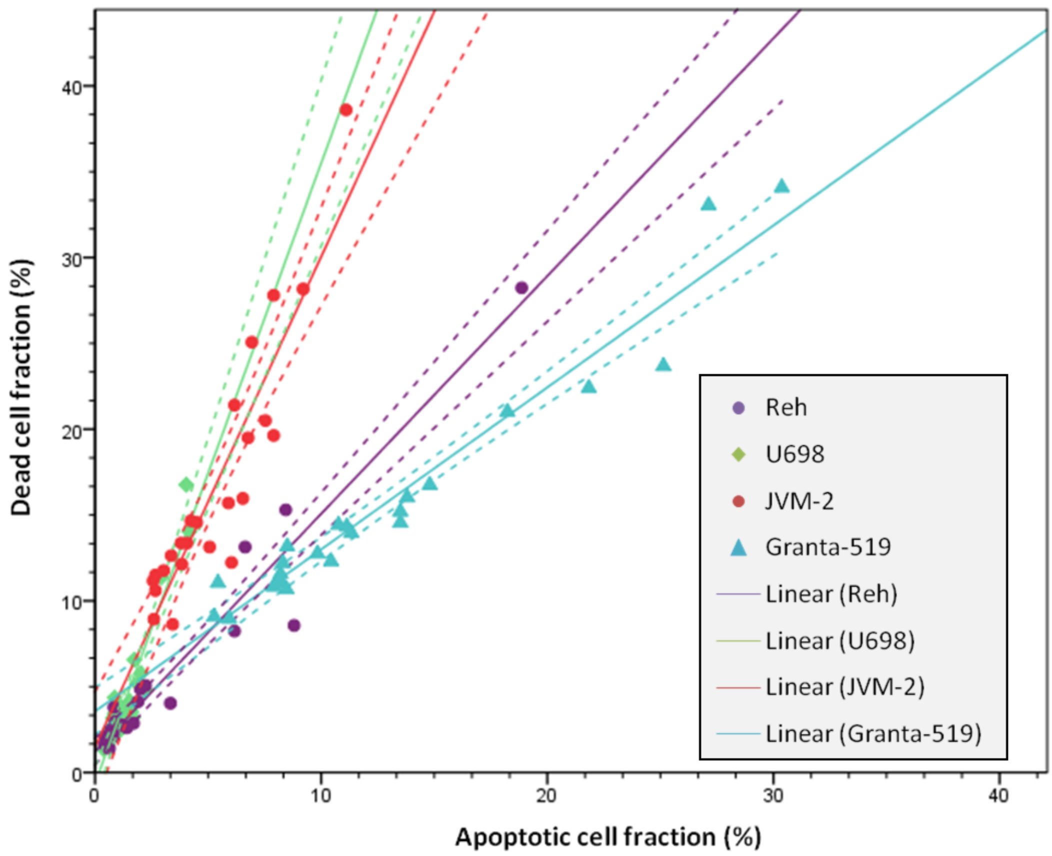

Figure 3-8: Ordinary linear regressions of dead cell fraction as a function of apoptotic cell fraction in the 24 differentially treated samples of PARP and/or ATM inhibited Reh, U698, JVM-2 and Granta-519 (mean values from three independent experiments). The dotted lines represent the 95% confidence interval of the regression coefficient.

Hence, Reh and Granta-519 cells died by apoptosis after PARP inhibition, while JVM-2 and U698 cells mainly died by necrosis (further evaluated in sections 3.6 and 3.7).

3.3 DNA DAMAGE IN S PHASE INCREASE BY PARP INHIBITION

To assess the amount of DNA double strand breaks occurring as a result of PARP inhibition, we measured the closely correlated intensity of phosphorylated Serine 139 on histone H2AX (γH2AX) by flow cytometry[197]. However, antibody binding varied with cell number, and normalization of the data was required. It was observed that secondary antibody background was highly dependent on cell number as shown in **figure 3-9 A** (approx. 1.5 million stained cells) and B (approx. 300.000 stained cells). This background increased linearly with increasing DNA content. Untreated cells have been shown to have a bimodal γH2AX-distribution due to cell cycle specific DSBs and subsequent repair[37,39]. PARP inhibition induced phosphorylation of γH2AX in a cell cycle specific manner, and the γH2AX levels increased during S and partially in the G_2 phase (**figure 3-9 A and B**). There were no local variations in intensity during S phase, and we therefore assessed γH2AX content in mid-S to avoid contributions from G_1 and G_2/M. In contrast, X-irradiated cells will acquire DSBs independently of position in the cell cycle. As the DNA content in mid S is 1.5 times that of G_1, this is consistent with the observed 1.5-fold increase in γH2AX intensity in mid-S phase compared to G_1 in the irradiated sample (**figure 3-9 C**)

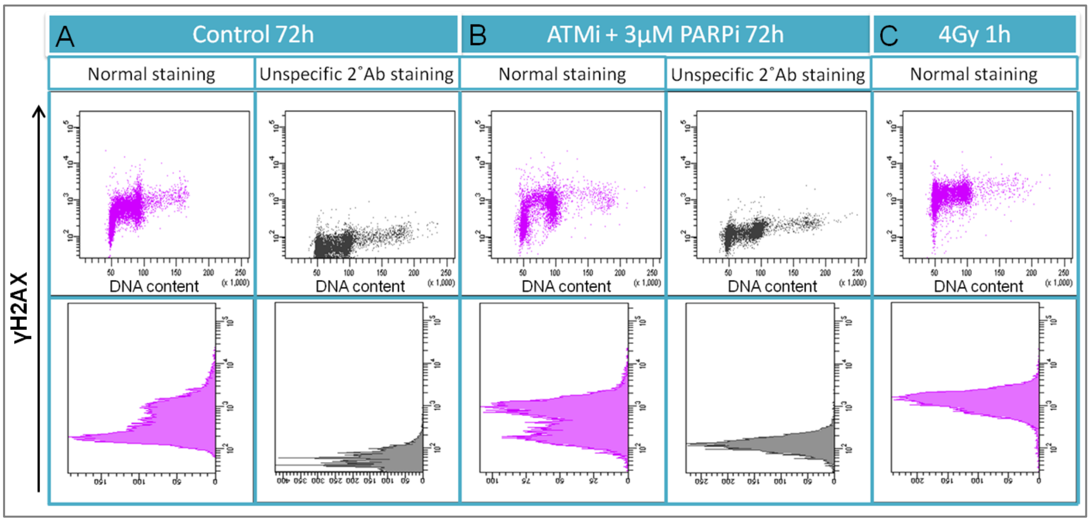

Figure 3-9: Flow cytometry analysis of γH2AX staining intensity in Granta-519 cells exposed to vehicle alone (A) or 10µM ATM inhibitor and 3µM PARP inhibitor (B) for 72h or 1h post-irradiation of 4Gy (C). Staining with secondary antibody (2˚Ab) alone is shown in black/white for A and B. Upper row shows two parameter dot plots of γH2AX against DNA content, while the lower row shows the γH2AX intensity histograms for the same samples.

The bimodal γH2AX distributions suggest that the fluorescence of the G_1 cells was due to non-specific staining. We sorted cells according to DNA and pHistone H3 content by flow cytometry and inspected them by fluorescence microscopy for the characteristic γH2AX foci in cells with DSBs[198]. Most G_1 cells had no foci; some had one γH2AX focus, and a few had two foci (**figure 3-10**). The γH2AX intensity of G_1 cells by flow cytometry should thus reflect background staining. Assuming that the background of the primary antibody varied in the same manner as the secondary, we normalized the flow cytometry data for S and M phase cells to the G_1 intensity as described in 2.3.3. S phase cells had multiple foci both in treated and untreated samples, although the variation in number of foci was higher in the untreated samples, and the mean focus number was higher in the treated samples. This was in agreement with the internally varying intensities of γH2AX in control S phase cells (**figure 3-9 and figure S4** in the appendix) and the higher intensity of treated S phase cells by flow cytometry, respectively (**figure 3-11** and **figure S4** in the appendix). G_2 cells showed a bimodal γH2AX distribution, which was most pronounced for JVM-2 and Granta-519 (**figure S4** in the appendix). The bright G_2 cells are probably the ones that most recently left S phase and have not yet repaired the damage inflicted in S phase. Most of the G_2 cells with low γH2AX content had no foci, with some cells having one or two foci (**figure 3-10**), reminding of the distribution seen in G_1 cells. Mitotic cells showed strong and diffuse staining, although they rarely contained foci.

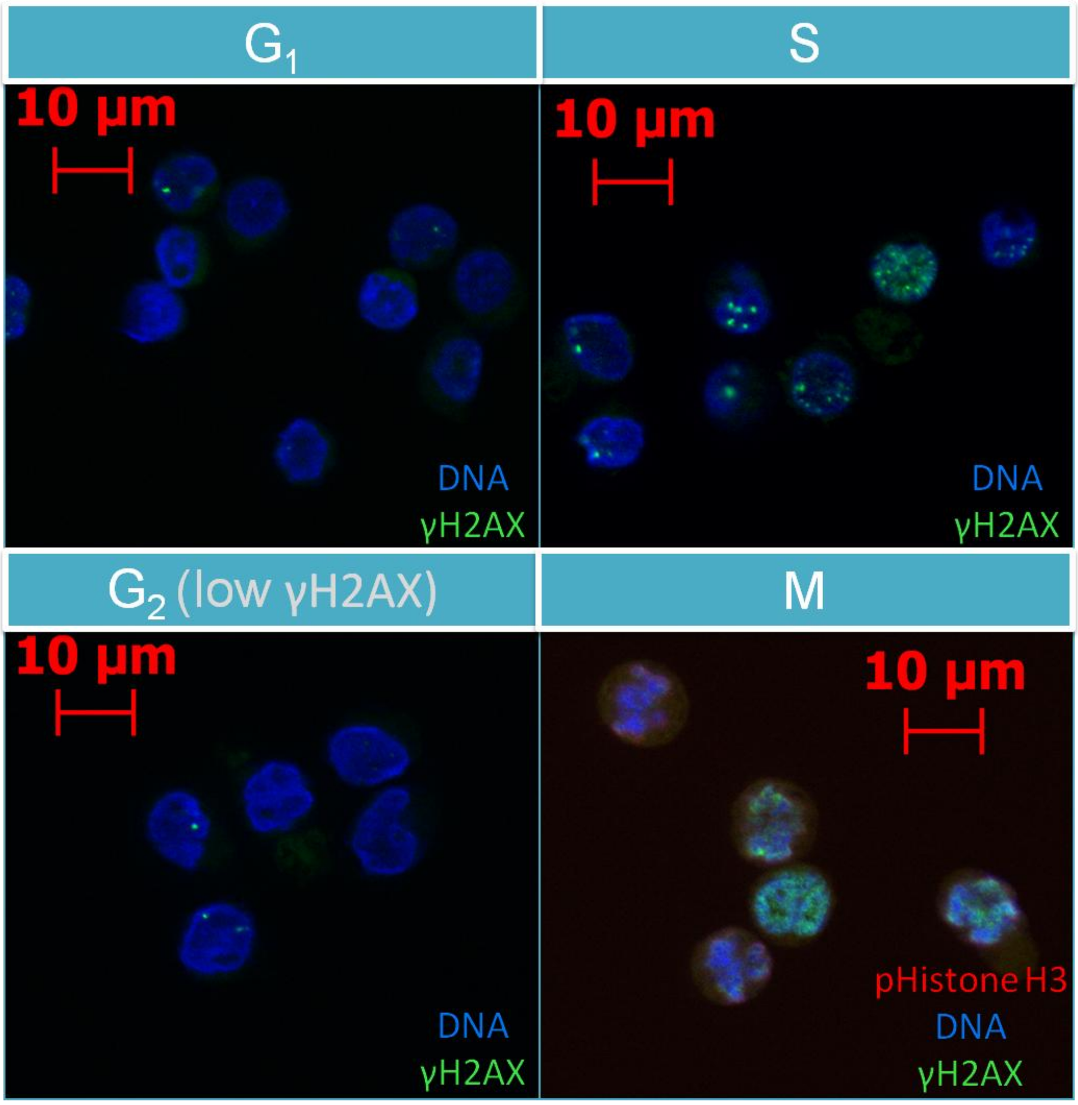

Figure 3-10: Fluorescence microscopy images of Granta-519 cells treated with 10µM ATM inhibitor and 1µM PARP inhibitor for 48h. The cells were sorted on DNA content and pHistone H3 status prior to microscopy.

The normalized γH2AX level in mid-S phase of the untreated samples was found to be 1.5-3.5 times the amount in G_1 (**figure 3-11**), which is in agreement with previous studies[37]. In contrast to this, the normalized γH2AX level in mid-S phase cells after IR was close to 1.0 (**figure 3-9**). PARPi alone increased the amount of DNA DSBs in S phase in a dose dependent manner for all cell lines. ATMi had no significant effect alone in Reh or Granta-519 cells, but increased γH2AX for JVM-2 and U698 cells. Combined PARP and ATM inhibition did not enhance or alter the effect of PARP inhibitor treatment in Reh and Granta-519, and the trend for U698 cells is actually a decrease in induction of γH2AX with increasing PARPi concentration, while JVM-2 cells had less systematic changes.

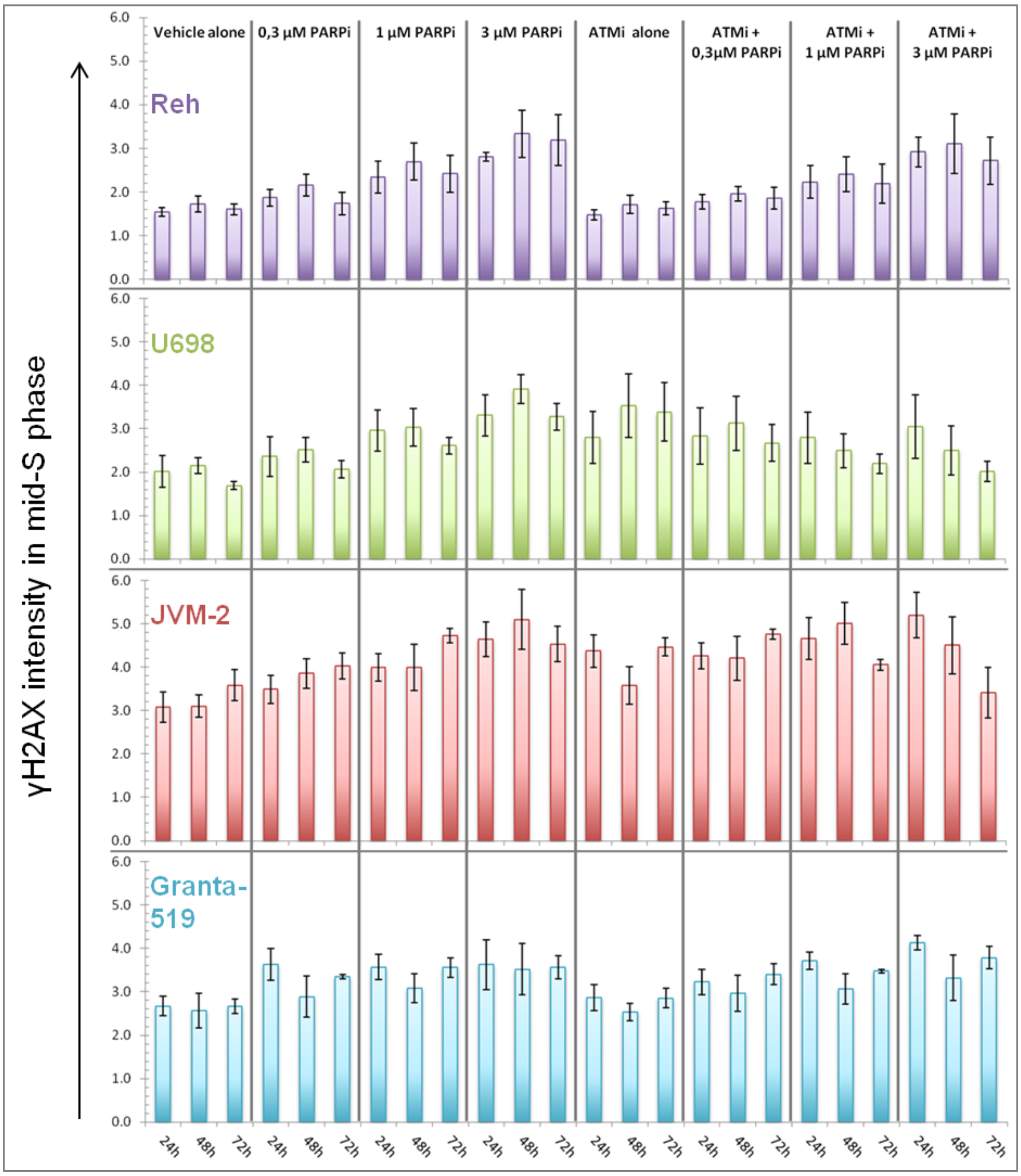

Figure 3-11: γH2AX intensity in mid-S phase cells during 72h PARP and/or ATM inhibitor treatment. The fold change of γH2AX intensity in mid S phase was normalized by DNA content (1.5) and the intensity of G_1 phase in the same sample (three experiments, ±SEM).

Mitotic cells in this cell line panel displayed high γH2AX intensity even in the untreated samples (**figure 3-12**). This was in good agreement with the results from fluorescence microscopy (**figure 3-10**), showing that the pHistone H3 (Ser10) positive cells had diffuse and strong γH2AX staining. DNA DSBs should cause focal staining, and such foci have been observed in cells that enter mitosis after ionizing radiation[38]. Additionally, substantial and non-focal γH2AX induction in mitosis have previously been found to be independent of DNA damage[199]. The relative γH2AX content in mitotic cells did not increase after treatment with either of the inhibitors alone or in combination (**figure 3-12**). In contrast to the S phase results, the mitotic cells displayed a trend of decreasing intensity with increasing PARPi concentration.

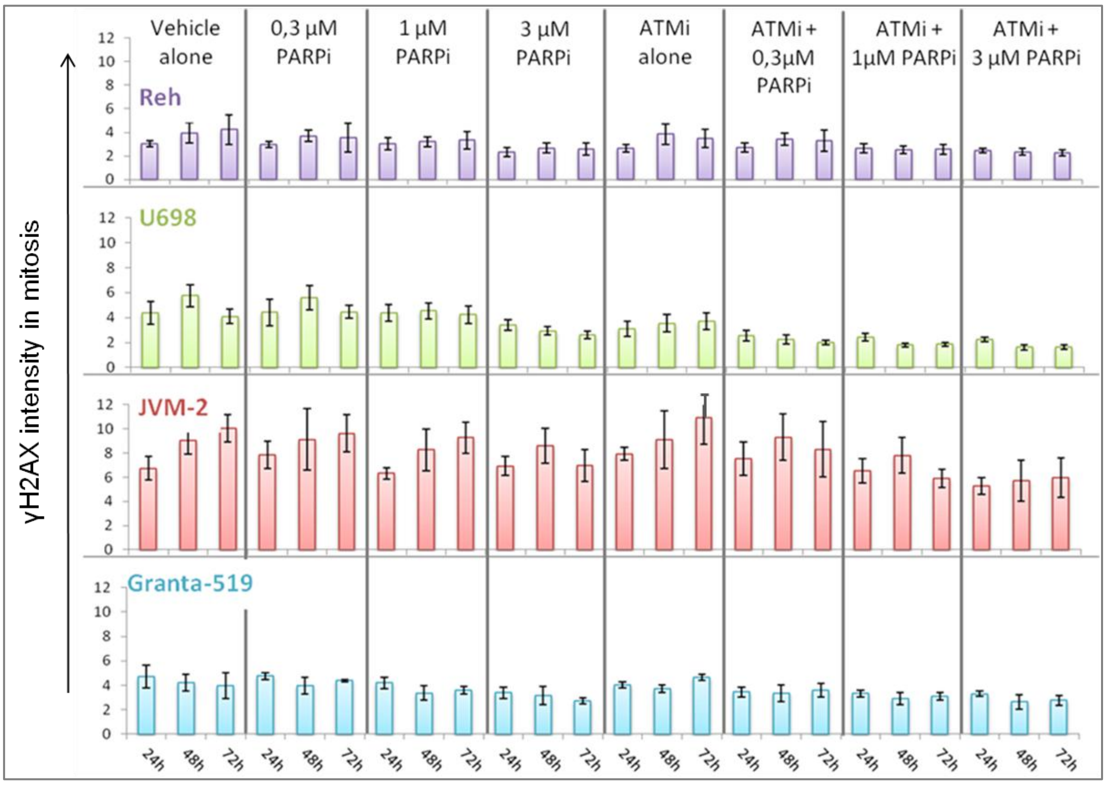

Figure 3-12: γH2AX intensity in pHistone H3 positive cells during 72h PARP and/or ATM inhibitor treatment. The fold change of γH2AX intensity in mitotic cells was normalized by DNA content (2.0) and the intensity of G_1 cells in the same sample (three experiments, ±SEM).

PARP inhibition induced about half the amount of DNA damage as 4Gy of ionizing radiation induced in Granta-519 cells (**figure 3-9**).

3.4 ATM INHIBITION INDUCES MITOTIC DELAY IN U698 AND GRANTA-519

The mitotic fraction was assessed by immunostaining of pHistone H3 (Ser10). In U698 and to some degree in Granta-519 the ATMi alone caused an increase in the mitotic fraction (**figure 3-13**). We have previously observed that the ATMi (KU-55933) is able to create this phenotype in U698 cells[82]. PARP inhibition reversed this effect in a dose dependent manner for U698 and Granta-519 cells. The doubling time increased somewhat in the presence of ATMi (**figure 3-4**), and the transition time through mitosis thus increased even more. Although the mechanism for this delay is unclear, it may contribute to the growth inhibiting effect of ATMi alone in these cell lines. With only a few significant changes in mitotic fraction, PARP and/or ATM inhibition had no systematic effect on the mitotic of Reh and JVM-2 cells (**figure 3-13**).

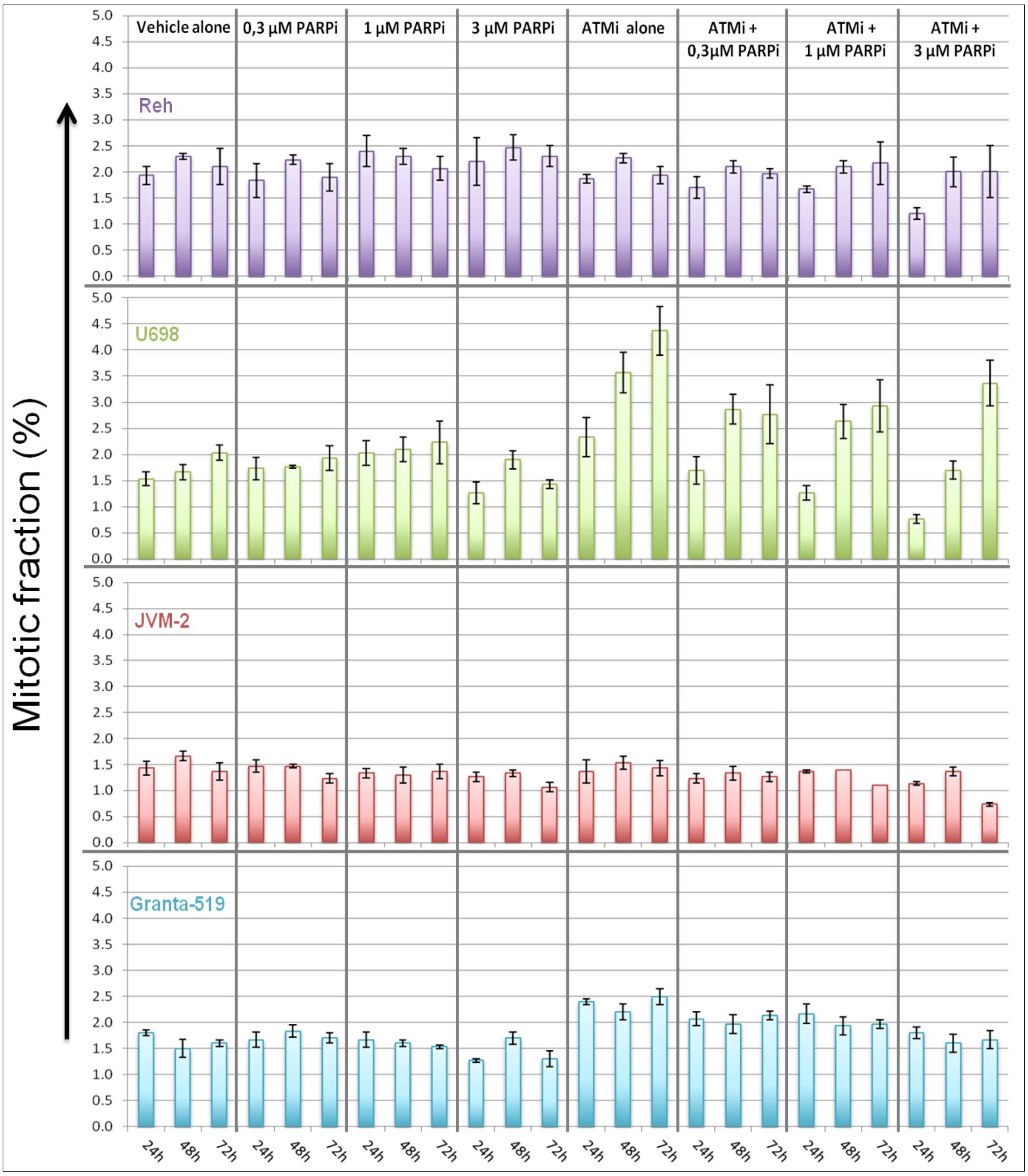

Figure 3-13: pHistone H3 (Ser10) positive fraction of single non-apoptotic Reh, U698, JVM-2 and Granta-519 cells during 72h treatment with PARP inhibitor and/or 10µM ATM inhibitor. Mean value is derived from three independent experiments ±SEM.

3.5 PARP AND ATM INHIBITION CAUSES G_2-PHASE DELAY

Cell cycle distribution analysis is a static snapshot of a dynamic process. The distribution does not give information about the duration of the cell cycle. Moreover, it will not be altered in the event of simultaneous arrest/delay of the whole population. As PARP and ATM inhibition caused low and in some cases negative cell growth rates (**figure 3-4**), we needed to address whether or not the cells were actually cycling. The mitotic fraction was not changed significantly by PARP inhibition alone (**figure 3-13**), indicating that this treatment did not cause a disproportional increase in mitotic transition time. The flux of cells into mitosis was monitored by adding the microtubule polymerization-inhibitor nocodazole 6h prior to harvest after 24h and 72h (**figure 3-14**) incubation with 3 µM PARPi and/or ATMi. This stathmokinetic experiment demonstrated that cells were passing through mitosis in all the samples. The amount of cells trapped in mitosis by nocodazole was reduced by PARP inhibition, consistent with an increased doubling time at 24h (**figure 3-4**).

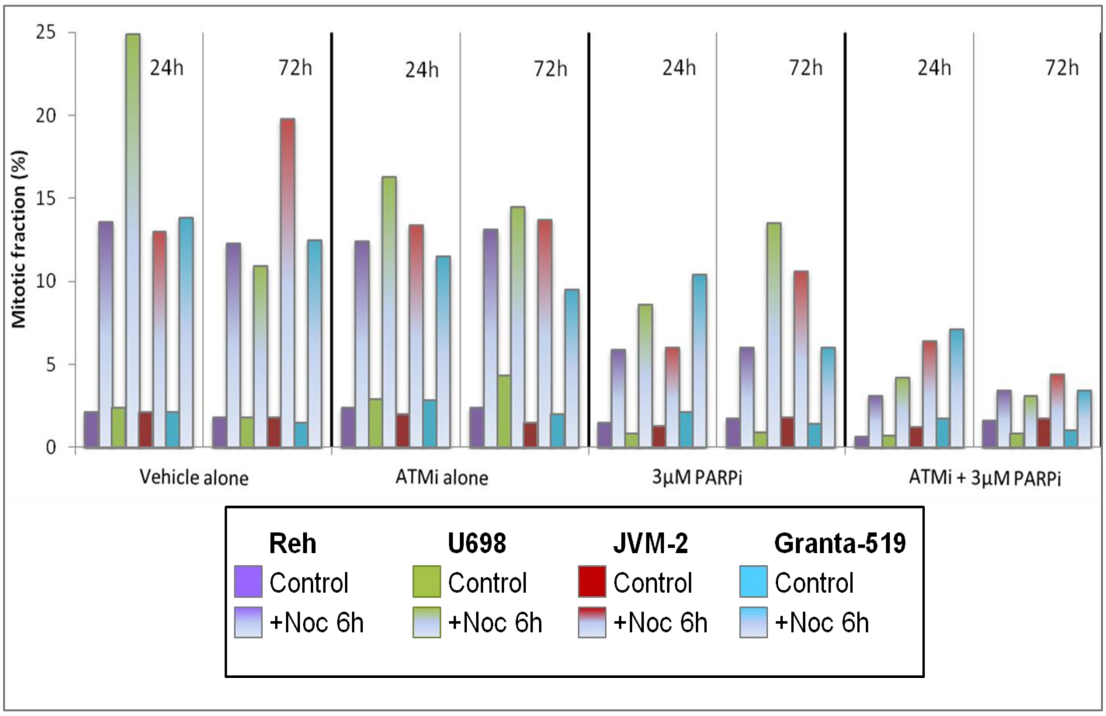

Figure 3-14: Nocodazole induced mitotic arrest during 18-24h and 66-72h of PARP and/or 10µM ATM inhibition. The controls were harvested at 24h and 72h.

Cell cycle analysis by flow cytometry revealed that the cell cycle distributions in control samples varied somewhat between the cell lines (**figure 3-15**). Most notably, Reh cells differed from the three other cell lines by having a lower G_2 fraction and no cells with >4n DNA content.

Only small changes in cell cycle distribution were observed after ATM inhibition, notably an increase in mitotic fraction (in U698 and Granta-519) discussed in section 3.4. Inhibition of PARP resulted in a dose-dependent increase in the G_2 fraction, except for JVM-2 cells. Additional treatment with ATMi increased the G_2 fraction compared to PARP inhibition alone, but not for Granta-519 cells. The fraction of U698 cells with >4n DNA content also increased upon PARPi treatment (in a dose- and time-dependent manner), and this effect was further enhanced in the presence of ATMi. In Granta-519 and JVM-2 cells the fraction of cells with >4n DNA content did not increase with PARP and/or ATM inhibition. The treatment-induced decrease in G_1 fractions is only relative, as it will be shown later that the G_1 transition time (at 24h) was almost constant (**figure 3-17**).

The dose-response curves revealed that ATMi-enhancement of PARPi effect on G_2 fractions was most pronounced in Reh followed by U698 cells (**figure 3-16**). PARPi was tenfold potentiated by the ATMi in Reh cells, as 3µM PARPi alone created the same effect as 0.3 µM PARPi combined with ATMi. While the y-fold enhancement increased with PARPi concentration for Reh cells (up to threefold), maximum enhancement was achieved in U698 cells at 0.3µM PARPi. In JVM-2 cells, the enhancement was less pronounced, and only significant after incubation with 1 and 3µM PARPi. The ATMi alone caused a small enhancement of the effect of PARPi in the Granta-519 cell line.

Reh
Vehicle alone
0,3 µM PARPi
1 µM PARPi
3 µM PARPi
ATMi alone
ATMi + 0,3µM PARPi
ATMi + 1 µM PARPi
ATMi + 3 µMPARPi
Cell cycle fractions (%)
100%
90%
80%
70%
60%
50%
40%
30%
20%
10%
0%
M
G2
S
G1
24h
48h
72h
U698
Vehicle alone
0,3 µM PARPi
1 µM PARPi
3 µM PARPi
ATMi alone
ATMi + 0,3µM PARPi
ATMi + 1µM PARPi
ATMi + 3µM PARPi
Cell cycle fractions (%)
>4n
M
G2
S
G1
24h
48h
72h

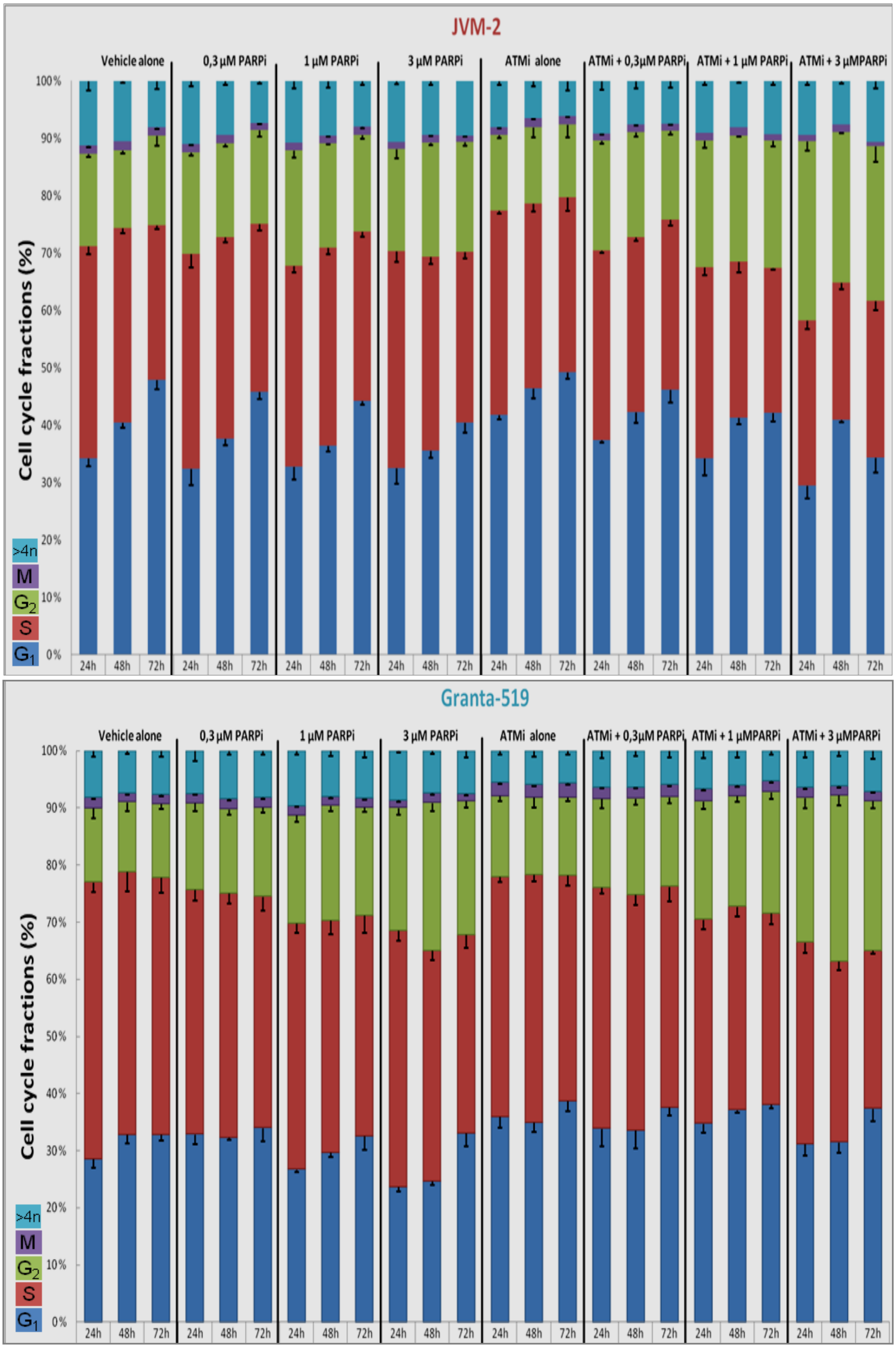

Figure 3-15: Cell cycle analysis of single non-apoptotic Reh, U698, JVM-2 and Granta-519 cells during 72h treatment with PARP- and/or 10µM ATM inhibition. Mean values from three independent experiments ±SEM.

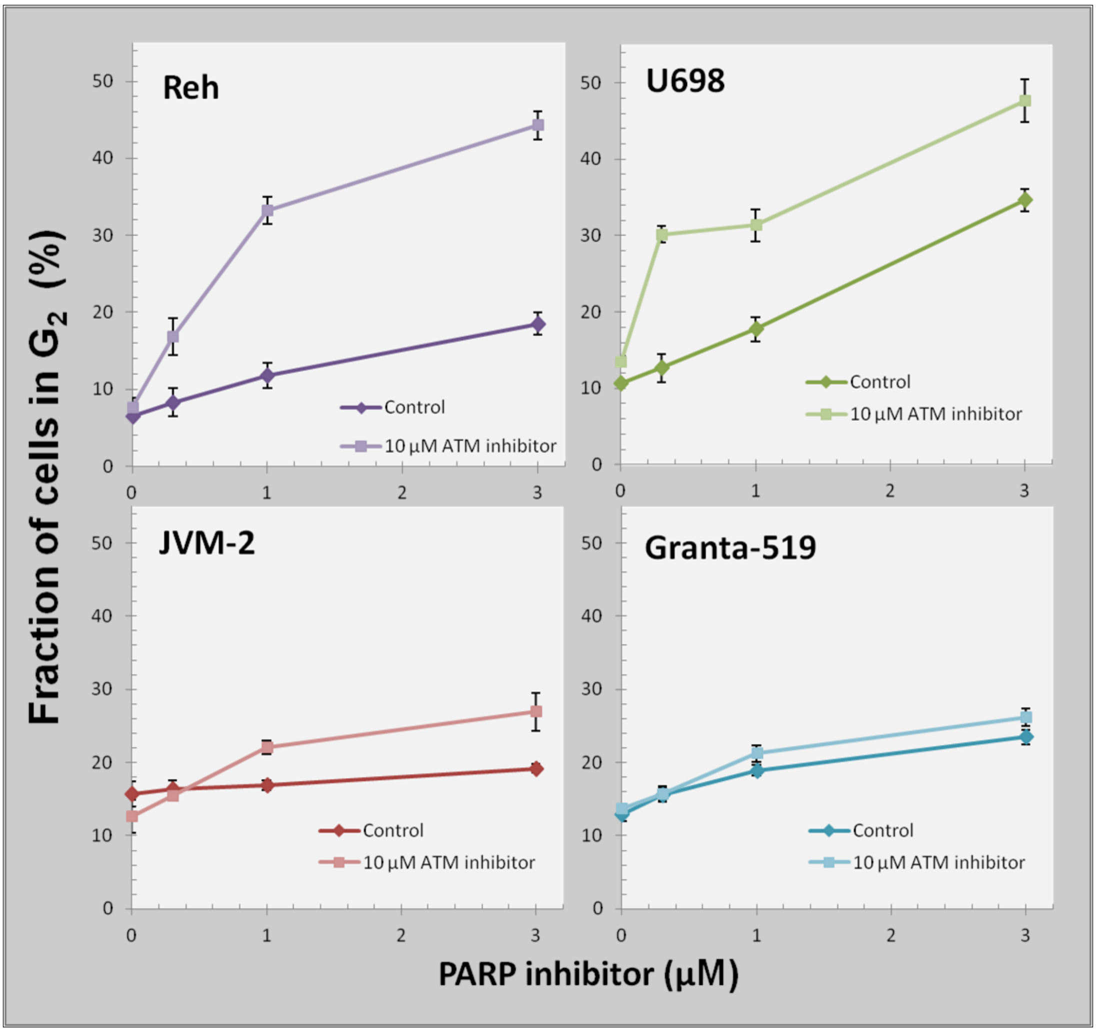

Figure 3-16: Dose response curves of the effect of 72h treatment with PARP and/or ATM inhibition on accumulation of cells in G_2 phase. Mean value from three independent experiments ±SEM.

Cell cycle phase durations were calculated from the increases in cell numbers and the cell cycle distributions at 24h (**figure 3-17**). Later time points had to be excluded as cell death and endoreduplication (further discussed in 3.6 and 3.7) became so pronounced that cell cycle durations would have been overestimated. The cell cycle duration is close to 24h for all control samples. ATMi alone increased the doubling time with 2-9h, and delayed G_1 for all cell lenes. The increase in G_2 phase duration after PARP inhibition was striking for Reh and U698, but less so for JVM-2 and Granta-519 cells. This effect was further increased with additional treatment with ATMi. S phase was also prolonged in all cell lines. Especially PARPi increased the duration of S phase. There were only small changes in the length of G_1 and mitosis.

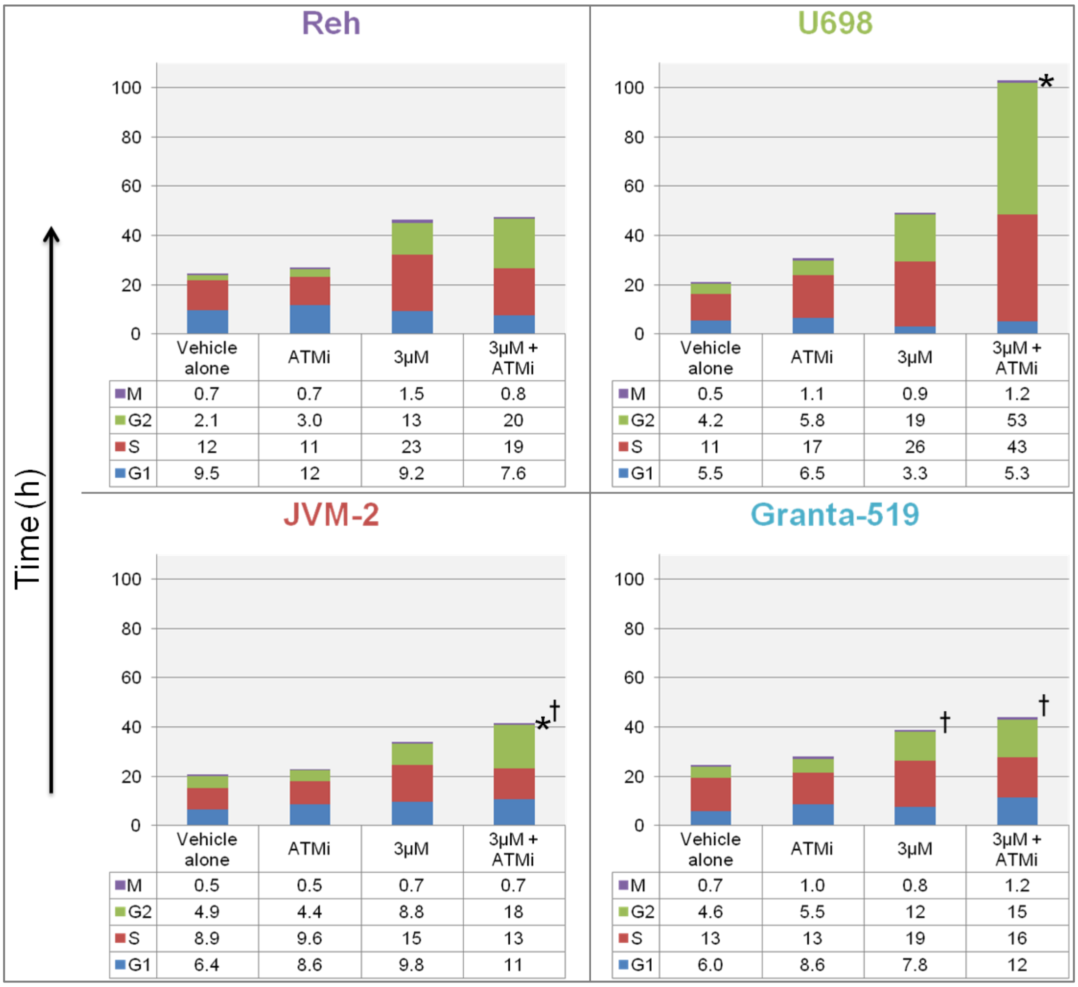

Figure 3-17: Cell cycle durations (h) for Reh, U698, JVM-2 and Granta-519 after 24h PARP inhibitor and/or 10µM ATM inhibitor treatment. Mean cell cycle phase durations (h) are listed in the table below the column chart of each cell line. The G_2 fraction and the calculated cell cycle phase durations could have been overestimated for the samples in which failed cytokinesis was observed at later treatment times (marked with an asterix). Moreover, extensive cell death may lead to overestimation of the lengths of cell cycle phases, as dead cells are not part of the growth fraction. Samples with significant increase in apoptosis and/or necrosis at 24 hours are marked with a cross.

3.6 U698 CELLS DIE BY NECROSIS AFTER EXTENSIVE ENDOREDUPLICATION

U698 cells displayed low levels of cell death and apoptosis after 72h (**figures 3-2 and 3-6**). However, the highly pronounced effect on cell growth and especially the increase in cells with DNA content exceeding 4n (**figure 3-15**), indicated that U698 cells may respond to the treatment in a different manner. To reveal the fate of these cells, we extended the treatment of U698 cells to 144h.

Cell cycle analysis of U698 cells after 144h inhibition of PARP and ATM confirmed that endoreduplication was extensive, and 62±6% of the cells had DNA content above 4n (**figure 3-18**; the peak annotations were confirmed by a mixture with diploid control cells, see **figure S2** in the appendix). Diploid cells only accounted for 4.5±2.8% of the single non-apoptotic cells. Thus, almost all treated cells eventually fail to complete cytokinesis. A cell with DNA content of 4n can represent either a tetraploid G_2 cell or a binucleated post-mitotic cell. This makes calculation of the length of the cell cycle phases at these times more complicated. However, the shift in ploidies from 72 to 144h (**figure 3-18**) in the combined ATM and PARP inhibited sample indicated a duration of the endoreduplication cycle of the same magnitude as the perturbed cell cycle from 0-24h (**figure 3-17**). Flow cytometry analysis of the sample treated with both inhibitors for 144h revealed pHistone H3 positive cells with 8n and 16n DNA content, and pHistone H3 positive cells about 15-20µm in size were also observed during fluorescence microscopy of this sample (see appendix, **figure S3**).

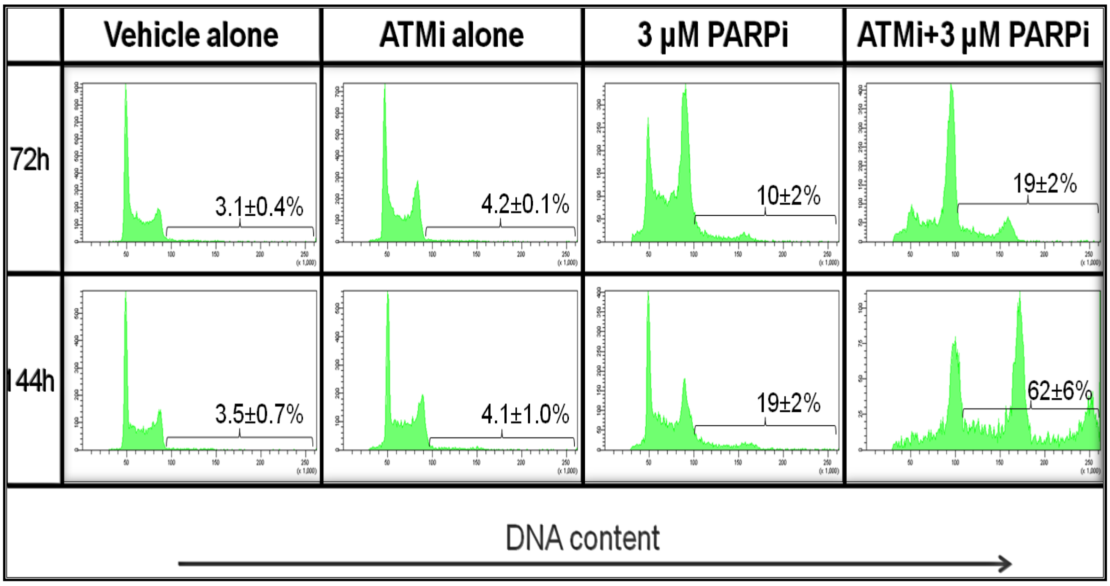

Figure 3-18: DNA histograms of single, non-apoptotic U698 cells treated for 72h or 144h with 3µM PARP inhibitor and/or 10µM ATM inhibitor. Fraction of cells with more than 4n DNA content (inset in each histogram) is represented in the 144h time point by the mean value of two replicate experiments ±range, and for the 72h time point the mean value is given by three independent replicates ±SEM.

The cell numbers did not increase from 72h to 144h in the presence of ATMi/PARPi (**figure 3-19 A**), which is expected if the bulk of the cells endoreduplicate. More than 60% of the cells had DNA content above 4n at this time (**figure 3-19 B**). Cell death also increased from 17% at 72h to 26% at 144h (**figure 3-19 C**). Quantification of apoptotic cells by the TUNEL-assay in endoreduplicating cells is not straightforward. Fragmented apoptotic bodies from one cell that died with 8n DNA content is undistinguishable from intact apoptotic cells with 4n or 2n DNA content. Nevertheless, TUNEL-positive cells with DNA content of 16n were present, indicating that at least some of the endoreduplicating U698 cells died by apoptosis, such cells were also observed during microscopy (**figure S3** in the appendix). Both cell death (>25%) and the number of cells endoreduplicating (instead of dividing) explained the lack of increase in cell number in U698 after treatment with PARPi and ATMi (**figure 3-19**).

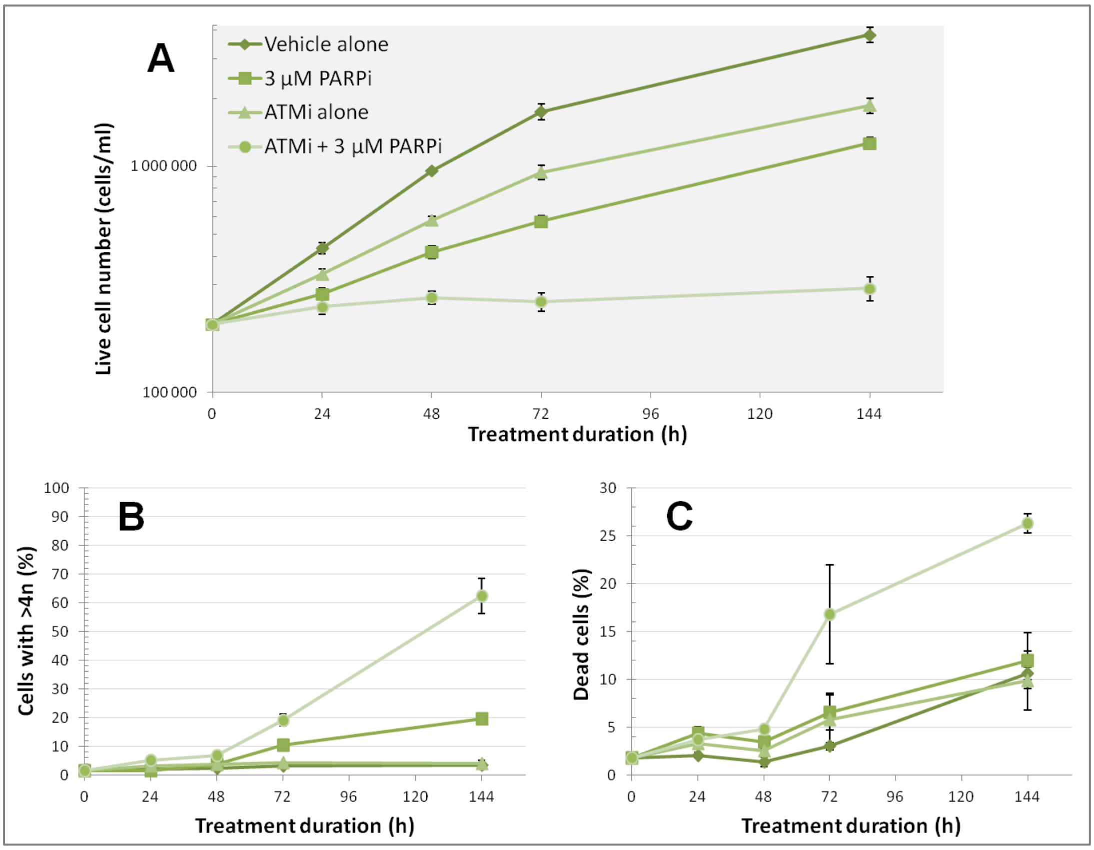

Figure 3-19: Live cell numbers (A), fraction of single, non-apoptotic U698 cells with DNA content above 4n (B) and dead cell fraction of U698 cells during 144h incubation with 3µM PARP inhibitor and/or 10 µM ATM inhibitor (C). The time point at 144h is the mean of two replicate experiments ±range, for the 0-72h time points the mean value is given by three other independent replicates ±SEM.

Fluorescence microscopy of U698 cells treated for 144h with both PARPi and ATMi revealed that they had been going through several aberrant mitoses without cytokinesis, as they were mostly multinucleated (**figure 3-20**). These cells were also larger, approximately 20µm, compared to control cells which were about 10µm. Some multinucleated cells were also observed in the samples treated with 3µM PARPi alone, consistent with the increase of cells with more than 4n DNA content of about 20% after 144h.

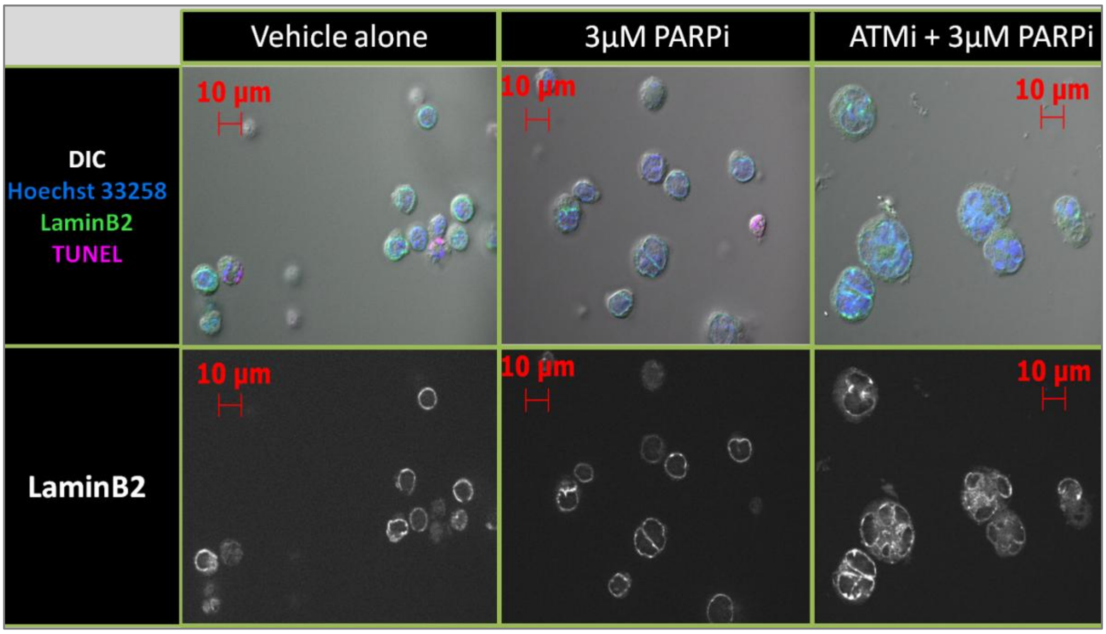

Figure 3-20: Fluorescence and DIC microscopy images of U698 cells treated for 144h with PARP inhibitor and 10µM ATM inhibitor.

A few PARP and ATM inhibited U698 cells died by apoptosis, but the main death mechanism, after extensive endoreduplication, was necrosis. The heavily treated cells displayed phenotypes typical of mitotic catastrophe: Multiple nuclei and micronuclei.

3.7 JVM-2 CELLS DIE BY NECROSIS AFTER MITOTIC CATASTROPHE

JVM-2 cells showed significant decreases in cell viability after 72h PARP and ATM inhibition (**figure 3-2**), yet the level of apoptosis could not account for the cell death caused by the treatment (**figures 3-4 and 3-6**). Cell sorting on JVM-2 cells were based on the same criteria as when measuring cell death, namely uptake of a non-permeable dye (in this case, Hoechst 33258). DIC and fluorescence microscopy (**figure 3-21**) was performed on the sorted JVM-2 cells after 48h inhibitor treatment. The dead cells had the appearance of necrotic cells. The cytoplasmic and nuclear membranes had ruptured, and DNA was no longer confined to the nucleus or even the cell.

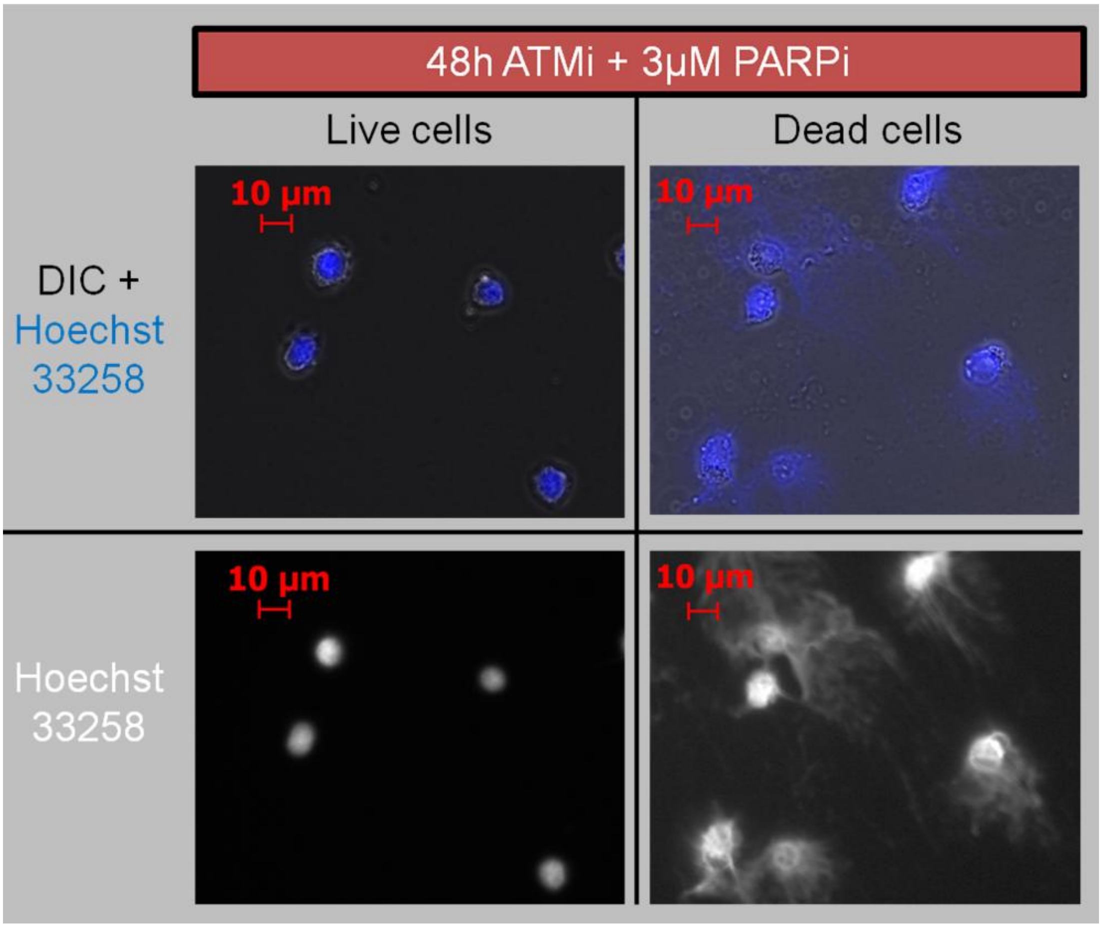

Figure 3-21: Microscopy images of Hoechst 33258 fluorescence and combined fluorescence and DIC microscopy of mounted, unfixed JVM-2 cells. After 48h treatment with 3µM PARP inhibitor and 10µM ATM inhibitor, live (Hoechst 33258 negative) and dead (Hoechst 33258 positive) cells were sorted prior to microscopy.

Immunostaining of the nuclear envelope component Lamin B2 revealed that many of the PARP and ATM inhibited JVM-2 cells were multinucleated, compared to the untreated control cells (**figure 3-22**). The increase in number of nuclei and cell size were not as extreme as for the endoreduplicating U698 cells (**figure 3-20**). The fraction of cells with DNA content above 4n did not increase with treatment in JVM-2; they were therefore not able to enter a new S phase after having failed to complete cytokinesis.

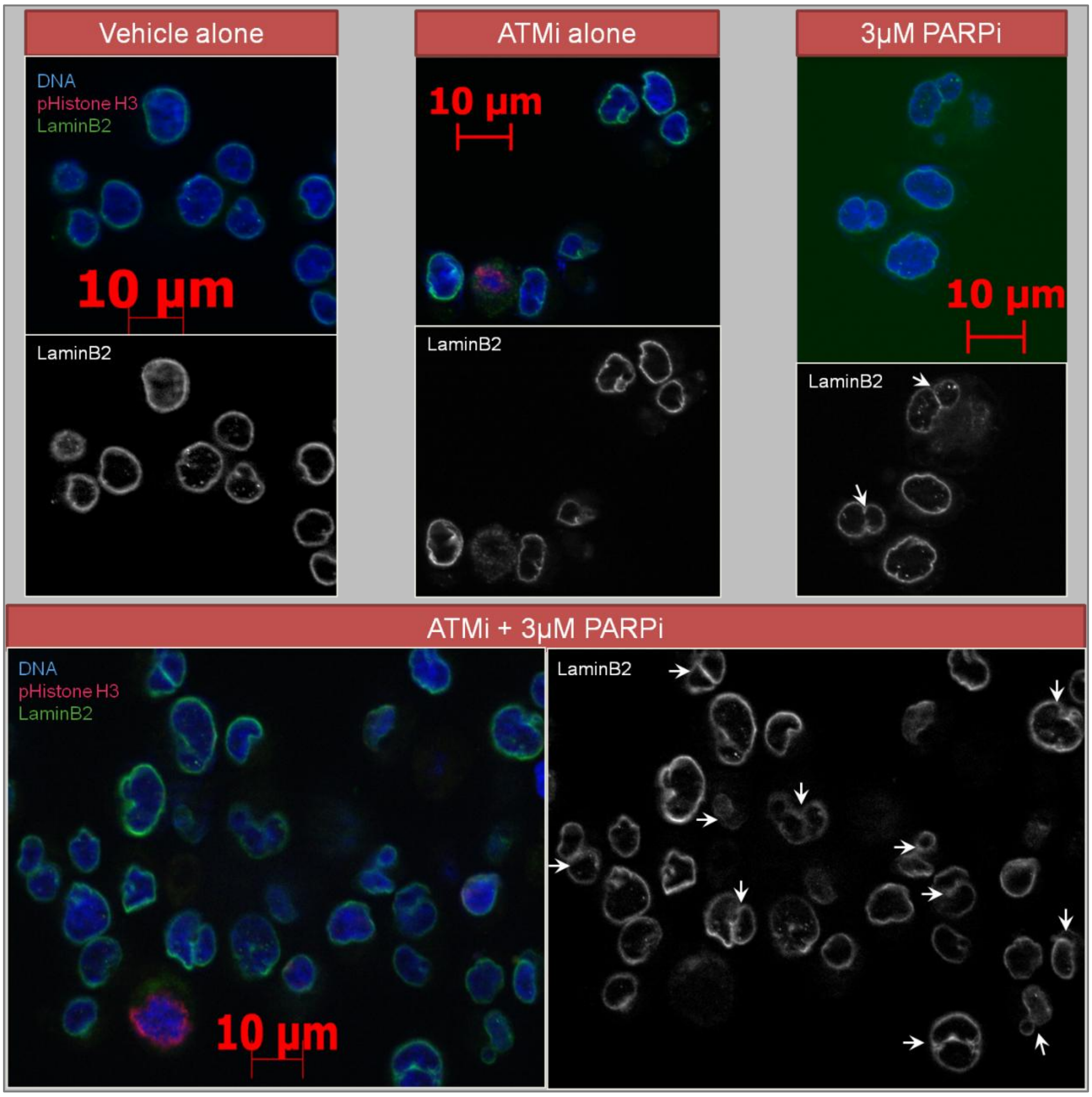

Figure 3-22: Fluorescence microscopy images of JVM-2 cells treated for 48h with 3µM PARP inhibitor and/or 10µM ATM inhibitor. Each multinucleated cell is indicated by an arrow.

4 DISCUSSION

The discovery of synthetic lethality[3] in cells with homologous recombination repair (HRR)-defects after treatment with PARP inhibitors[1,2] spurred a rapid implementation of PARP inhibitors in cancer treatment. Originally, it was suspected that PARP inhibition led to impared repair of SSBs, which were converted into DSBs during replication. These DSBs was tought not be repaired by the HRR-deficient cells, and thereby cause cell death. However, the amount of SSBs has not been found to increase in response to PARP inhibition[13,14]. Hence, the proposed mechanism of synthetic lethality was recently acknowledged to be inaccurate[159]. In this study we have demonstrated some of the phenotypes induced by combined loss of activity of PARP and the HRR-initiating protein ATM. An automated staining procedure for combined assesment of γH2AX, DNA content, mitosis and apoptosis by flow cytometry was developed. Severe cell death, cell cycle progression delay and dose-dependent induction of DNA DSBs was observed during the three day continuous exposure to PARP and ATM inhibitors.

Development of an automatic staining procedure by use of a microplate sample processor and microplate washer reduced the sample preparation time by 30-40%. The procedure minimized the strenuous and labor-intensive pipetting, supernatant removal and relocation of each tube both in and out of the centrifuge. This procedure could possibly reduce occupational injuries (due to pipetting). In addition, hands-on time was lowered and the reagent-volumes could be minimized, thereby experiment-costs were reduced as well.

We wanted to investigate PARP inhibition in ATM-deficient lymphoid cancer cells, as ATM deficiency is common in both MCLs[16] and B-CLLs[17]. Chemically induced ATM deficiency was obtained with the ATM inhibitor KU-55933, and combined with the PARP inhibitor olaparib in the cancer cell lines Reh, U698, JVM-2 and Granta-519. The Granta 519 cell line was reported to be ATM-deficient[179,180]. Previous studies have shown a lack of functional ATM activity in this cell line based on the ATM autophosphorylation site Serine 1981[4,7,8]. However, our immunoblotting of pATM (Ser1981) indicated some residual autophosphorylation of ATM in irradiated Granta-

519 cells, yet less than for the other cell lines (**figure 3-1**). The phosphorylation of ATMs downstream target CHEK2 (Thr68) was consistant with the pATM results. All of the Granta-519 dose response curves in the presence of ATM inhibitor are in parallel or overlapping with the corresponding control curves (**figures 3-3, 3-5, 3-7 and 3-16**). Thereby, Granta-519 cells deviates from the three ATM proficient cell lines, indicating low effect of inhibiting the residual ATM function in Granta-519 cells.

We anticipated no severe effect by ATM inhibitor alone on the measured parameters in this study, based on our previous work with this inhibitor[82]. Our assumption was valid for cell death, apoptosis and cell cycle distribution in general. Cell line specific ATM inhibitor induced changes were observed in γH2AX S phase intensity (increased in JVM-2 and U698) and mitotic fraction (increased in U698 and Granta-519). Additionally, a marked increase in doubling time after ATM inhibitor treatment were seen in all cell lines (**figure 3-2**). Although, we have previously observered the effect of ATM inhibition on progression of mitosis[82], our previous experiments were not carried out for enough time to observe the growth inhibiting effect. Another group have reported that the antiproliferative effect of ATM inhibitor was phenocopied by siRNA-mediated knockdown of ATM, suggesting that the effect is ATM specific[200]. ATM has lately been shown to activate Akt in response to insulin-signalling[201], DSBs[202] and ionizing radiation[201]. Akt/PKB is known for inhibition of apototisis and promoting cell cycle progression, and A*kt1* knockout mice display increased apoptosis and cell growth retardation[203]. The ATM inhibitor KU-55933 generates the same phenotype in cancer cells[204]. This may explain the results in this study and the fact that insulin resistance have been reported for 30 years in ataxia telangiestacia-patients[205,206]. Further investigations of the Akt pathway could demonstrate whether this is the cause of the growth inhibiting effect of ATM inhibition in our study.

The durations og S and G_2 was prolonged due to the treatment with PARP inhibitor and/or ATM inhibitor (**figure 3-17**). The stathmokinetic experiment with nocadazole (**figure 3-14**) confirmed that the cells were not arrested. As the length of G_1 was relatively unchanged, while S phase was delayed by PARP inhibition, a likely cause would be an increased number of DNA DSBs caused by the treatment (**figure 3-11**).

Additional loss of ATM activity dramtically prolonged G_2, consistant with the hypothesis that cells acquire problems repairing these DSBs in the absence of HRR. The range of γH2AX intensity in G_2 for untreated and treated are more pronounced in JVM-2 and Granta-519 (bimodal distributions) than in Reh and U698 cells (**figure S4** in the appendix). In addition, the most extreme G_2 delay was seen in Reh and U698 cells (**figure 3-16**). The coinciding results of delay and γH2AX distribution in G_2 may reflect differences in the repair kinetics of these cell lines. While Granta-519 and JVM-2 cells may repair the damage rapidly, U698 and Reh cells may require more time to resolve the same amount of DNA damage. Thus, Granta-519 and JVM-2 spend a larger fraction of their G_2 phase in a γH2AX-negative state. Reh and U698, on the other hand, spend more time on repairing DNA and may be released into mitosis almost immediately after becoming γH2AX negative. The lack of focal γH2AX staining in PARP inhibited mitotic cells was treament independent (**figure 3-10**), supporting the view that the cells must repair the damage associated with γH2AX foci in G_2 before mitotic entry. ATM and DNA-PK function redundantly to phosphorylate H2AX (Ser139) in response to DNA damage[207]. Non-damage related γH2AX induction in mitosis have previously been proposed to be ATM dependent as ATM-reconstituting a A-T cell line caused mitotic γH2AX expression, while DNA-PK-deficient cells displayed normal mitotic γH2AX-phenotype[199]. In contrast, our data showed high γH2AX levels in mitosis independent of ATM inhibition (**figure 3-12**). This inconsistency may be clarified by dual inhibition of DNA-PK and ATM in our cell lines.

In this study, Reh and Granta-519 cells were found to die by apoptosis after PARP inhibition (**figures 3-2 and 3-6**). We have previously shown that U698 cells are resistant to irradiation-induced apoptosis, while Reh cells are not[208]. However, U698 cells become apoptotic in response to being nutrient depleted in dense growing culture and to prolonged nocodazole treatment[208]. Thus, U698 cells have intact apoptotic machinery and the error must be in the upstream apoptosis-inducing part of the DDR signaling. Both the untreated and irradiated TP53-deficient U698 cells have elevated expression of anti-apoptotic protein *MCL1*[209], and several studies show that apoptosis is avoided in TP53-deficient cells because of failure to degrade MCL1[210,211]. Our results of induction of apoptosis after PARP inhibition in Granta-519 cells are in agreement with studies by Williamson et al. (TUNEL , Annexin V and Western blots)[4,9]. Weston et al.[7] reported negative results of Annexin V-staining and proposed mitotic catastrophe as main death mechanism of PARP inhibited Granta-519 cells. Weston et al. argued that a mitotic catastrophe was pHistone H3 negative cells with loss of nuclear membrane integrity with Lamin B1-staining and multiple nuclei.

Continuous ATM and PARP inhibition for 144h in U698 cells revealed that over 60% of the cells were multinucleated (**figure 3-19**) and endoreduplicating, while only about 4% were in diploid G_1 (**figure 3-18**). Microscopy of PARP and ATM inhibited JVM-2 cells revealed that they were largely multinucleated (**figure 3-22**), but they did not endoreduplicate (**figure 3-15**). Mitotic catastrophe followed by necrosis was the main death mechanism in U698 and JVM-2, as the number of apoptotic cells (**figure 3-6**) was clearly outnumbered by dead cells (**figure 3-2**). Even though some of the multinucleated U698 and JVM-2 cells still were viable at the end of the experiments, they did not seem able to resume proliferation (i.e. they are not potentially malignant).

In contrast to U698 cells, JVM-2 cells do not endoreduplicate in response to PARP and ATM inhibition. We have previously shown that U698 cells lack a functional G_1/S checkpoint in response to IR[208], and proposed that this is caused by loss of *TP53*. The role of TP53 in prevention of polyploidy and endoreduplication has previously been reported[90]. JVM-2 cells have wildtype *TP53*[212] and *RB1*[213] and are assumed to have retained the integrity of the G_1/S checkpoint. Checkpoint activation after a mitotic catastrophe may inhibit new rounds of DNA replication. Endoreduplication have previously been shown in staurosporine treated U698 cells, but this treatment abolished mitosis and resulted in mononucleated cells[214]. Hence, another mechanism is the cause of PARP inhibitor induced endoreduplication with failed cytokinesis after mitosis. The possibility of uncoupling the order of cell cycle phases has been seen in normal, although specialized cells, like hepatocytes[215] and during meiosis. Interestingly, PARPs is known to interact at centrosomes[216-218] and PARylation of several important spindle assembly checkpoint-proteins such as AURKB has been reported[76]. In addition, PARP inhibitor PJ34 has recently been shown to kill cancer cells with supernumerary centrosomes selectively by declustering of the centrosomes during mitosis[219]. The mitotic aberrations of JVM-2 and U698 cells might therefore be used as a model system in further studies of the role of PARP in the spindle assembly checkpoint.

The principle of drug-induced synthetic lethality is based the enhancement of the effect(s) of one drug by another drug, which itself has no effect. As the ATM inhibitor alone had impact on growth rates, drug synergy must in principle be determined by using three different concentrations of this drug as well. However, an additive effect can be predicted if the dose response curves of the PARP inhibitor are in parallel with and without ATM inhibitor (assuming non-mutual interactions of these inhibitors). This was the case for Granta-519 (**figure 3-5**), which may indicate that the presence of ATM inhibitor is not related to the DNA repair functions of ATM (discussed above). In contrast, the three other cell lines had diverging dose response curves, and U698 cells showed the most pronounced deviation from additivity. Concerning PARP inhibitor induced cell death (JVM-2 and U698) and apoptosis (Reh), there was a clear enhancement of the effect after additionally inhibiting ATM (ATM inhibitor had no effect alone). Apoptosis was somewhat higher in Granta-519 cells treated with ATM inhibitor alone, but the dose response curves (**figure 3-7**) were in parallel, indicating additive effect of ATM inhibition combined with PARP inhibition on apoptosis as well.

The induced increase in DSBs during S phase (**figure 3-11**) does not distinguish between the “PARP trapping-model”, “replication restart model” [159] or “Balance of DSB repair mechanisms” model (**figure 1-5**). Yet one could speculate that the proposed inability to restart stalled replication forks would cause failure to complete DNA replication, and possibly death from S phase. This is not in agreement with our data, as the cells acquire tetraploid DNA content and G_2 delay is more severe than S phase delay. Farmer et al. revealed complex rearrangements and chromatid breaks by chromosome analysis after PARP inhibition of BRCA1 /2-deficient cells[1]. Thus, the repair of DSBs in these cells has probably not been homology-dependent. The mitotic catastrophe phenotype in U698 and JVM-2 indicates failure of the mitotic machinery or chromosome segregation-trouble due to possible complex chromosomal rearrangements. This may be due to aberrant repair of multiple DSBs by NHEJ, in agreement with the “Balance of DSB repair mechanisms model”.

From our current data, we cannot establish whether Reh and Granta-519 died from G_2 or mitosis. DNA fragmentation is a late event in apoptosis and pHistone H3 (Ser10) positive cells was not observed to be additionally TUNEL-positive. TUNEL may not be a valid assay of apoptosis from mitosis at such a late stage in apoptosis. Further studies of possible chromosomal rearrangements in all cell lines and determination of which cell cycle phase Granta-519 and Reh die from are required. This may determine whether PARP and ATM inhibition causes chromosomal rearrangements, leading to mitotic catastrophe in U698 and JVM-2. Additionally, the duration-dependent increase of PARP inhibitor treatment (**figures 3-2, 3-4 and 3-6**) suggest that damage not associated with γH2AX may accumulate with increasing numbers of cell cycles. The possibility of using PARP inhibitors over a long period of time further emphasizes the importance of this finding, as the effect would be more and more severe throughout the treatment course.

The underlying background for this study was the attractive possibility of using PARP inhibitors in treatment of ATM-deficient cancers. A recent study by Williamson et al.[9] suggested that the ATM inhibitor KU-55933 could be used in combination with PARP inhibitor olaparib in treatment of TP53-deficient malignancies. Our data does not support this proposition, as ATM and PARP inhibited TP53-proficient cell lines (Granta-519, Reh and JVM-2) reveals the substantial amount of damage to the normal tissue this would induce (**figure 3-2**). However, the perspective of additional sensitization to PARP inhibitors in tumors with both *ATM* and *TP53* loss, which is reported in 10% of all MCLs[21], is in agreement with our results. The *TP53* negative cell line (U698) was the most sensitive to combined PARP and ATM inhibition and interestingly the least sensitive to PARP inhibitor alone (**figures 3-4, 3-5, 3-15, 3-16 and 3-19**). This is in agreement with the reported lack of PARP inhibitor response in TP53 deficient cells[9]. Although *TP53* loss might contribute to PARP inhibitor and HRR-defective synthetic lethality, it is not by itself a synthetic lethal combination with PARP inhibitor.

Our results are in agreement with previous studies, stating that the synthetic lethality of PARP inhibition and loss of ATM function[1,4,7,8,220] is less pronounced than the effect of PARP inhibition in BRCA1/2-defective cell *in vitro*[1,2]. Since BRCA1 and 2 are essential for HRR[221,222] and ATM is involved in the upstream signalling of HRR[77], this is not surprising. Yet the possibility of providing patients with ATM-deficient malignancies (e.g. aggressive MCL) with a low side effect-treatment option, such as PARP inhibitors[141,142], is still attractive. Although the PARP inhibitors did not have the desired kill efficiency as a single agent, it is still a possibillity to enhance treatment effect of current DSB inducing-chemotherapy and/or irradiation with PARP inhibitors. Such studies are presently being performed[145,223-225] .

5 CONCLUSION

The findings of this study show that PARP and ATM inhibition will generate DSBs during DNA replication. The DSBs are subsequently repaired/attempted to be repaired during G_2, causing a DNA damage-induced G_2 delay. Cells without fully repaired DNA are not allowed to enter mitosis, and could die by apoptosis directly from G_2 (Granta-519 and Reh). The cumulative nature of the effect of PARP and ATM inhibition suggests that low fidelity DNA repair takes place. The high frequency of failed cytokinesis (mitotic catastrophe) is possibly due to difficulty in separating structurally abnormal chromosomes (JVM-2 and U698). Cell cycle progression is slowed through S and G_2 in response to the DNA damage, but the treatment do not cause cells to stop cycling. Thus, the continuous exposure to the inhibitors ensures that each cycle is likely to cause new DNA damage and erroneous repair. The repeated process will inevitably lead to cell death, as the genome becomes increasingly damaged (**figure 5-1**). The cell line specific differences in treatment induced phenotypes and cell death mode may be due to other aberrations in the DNA damage response system. E.g., the difference between endoreduplication (U698) and post-mitotic arrest (JVM-2) could be attributed to the impaired G_1/S checkpoint in U698 (*TP53* loss).

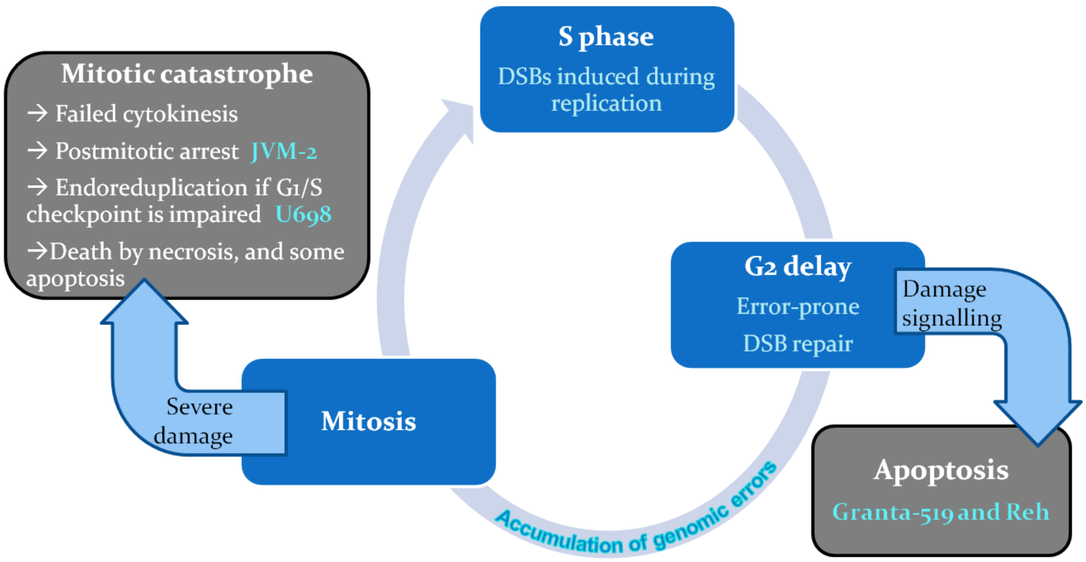

Figure 5-1: Proposed cumulative cycle of damage, repair and eventually synthetic lethality caused by PARP inhibition while ATM activity is suppressed.

6 FUTURE PERSPECTIVES

As this study was time limited, we still have several ideas that we wish to pursue in our further study of the phenotypes induced by PARP and ATM inhibition in lymphoid cells.

The apoptotic cells (measured by DNA fragmentation) in this study was mostly pHistone H3 negative. This could indicate that apoptosis occurred from G_2. However, we must first ensure that this phospho-epitope is not lost before the DNA fragmentation stage of apoptosis. We plan to induce apoptosis from mitotically arrested cells, by long term (24h) nocodazole treatment, as we have previously done in U698 and Reh[208]. Then we will co-stain for both pHistone H3 and DNA-fragmentation (TUNEL-assay). If these apoptotic cells retain pHistone H3, we will be able to conclude that Granta-519 and Reh became apoptotic from G_2.

Secondly, we will perform karyotyping of PARP and ATM inhibited cells. This could determine whether the mitotic abnormalities observed in JVM-2 and U698 cells are caused by structural chromosome damage such as ring-chromosomes, dicentric chromosomes or other complex rearrangements, which is bound to cause failed or catastrophic cytokinesis.

In this study we have not addressed whether PARP inhibition just causes an increase in DNA damage (PARP trapping-model and replication restart model in **figure 1-5 B and C**)[159], or if it is the switch to improper and/or inefficient DNA repair that causes synthetic lethality in HRR-deficient cells (Balance of repair mechanisms-model in **figure 1-5 D**). To test the latter model, we are going to employ a specific inhibitor against DNA-PK (NU-7026). DNA-PK inhibition is reported to rescue cells from synthetic lethality of PARP and ATM inhibition[9]. We wish to further evaluate the phenotypes of DNA damage, proliferation and cell cycle specific delay, after this proposed rescue. NHEJ is suggested to be 53BP1-dependent[171]. Thus, we would like to stain for 53BP1-associated DSB foci in PARP and ATM inhibited cells, as this might reveal whether a shift towards NHEJ is the cause of synthetic lethality. Expression profiling by microarray of DNA-PK, PARP and ATM inhibited cells, compared to all dual inhibitor combinations and single agents, is also something we plan to perform. This might shed more light on the unknown mechanisms of synthetic lethality in DNA repair.

There are conflicting results after PARP knockdown in the literature[1,2,12]. If the correct mechanism of PARP inhibition is the PARP trapping-model, the phenotypes induced by PARP knockdown should be less severe than the PARP inhibition induced phenotypes. We will also elucidate whether this is the mechanism behind synthetic lethality in HRR-defective cells by comparing double knockdown of PARP1 and PARP2 to PARP inhibition.

We wish to confirm that TP53 is responsible for the post-mitotic arrest in JVM-2 cells by shRNA-mediated knockdown of TP53 in JVM-2, by investigating the possible induction of endoreduplication after PARP and ATM inhibition.

It seems likely that the cells entering G_2 phase have γH2AX foci and are positive for γH2AX by flow cytometry. After repair of the DSBs, they may enter a γH2AX negative compartment in G_2 before entry into mitosis (see JVM-2 and Granta-519 in **figure S4** in the appendix). This will be tested by BrdU pulse labeling of cells (followed by pulse chasing) for directly determining the order of γH2AX compartments in G_2.

REFERENCES

1 Farmer H, McCabe N, Lord CJ, Tutt AN, Johnson DA, Richardson TB, et al. *Targeting the DNA repair defect in BRCA mutant cells as a therapeutic strategy.* Nature 2005 Apr 14;434(7035):917-21.

2 Bryant HE, Schultz N, Thomas HD, Parker KM, Flower D, Lopez E, et al. *Specific killing of BRCA2-deficient tumours with inhibitors of poly(ADP-ribose) polymerase.* Nature 2005 Apr 14;434(7035):913-7.

3 Kaelin WG. *The Concept of Synthetic Lethality in the Context of Anticancer Therapy.* Nat Rev Cancer 2005 Sep;5(9):689-98.

4 Williamson CT, Muzik H, Turhan AG, Zamo A, O'Connor MJ, Bebb DG, et al. *ATM deficiency sensitizes mantle cell lymphoma cells to poly(ADP-ribose) polymerase-1 inhibitors.* Mol Cancer Ther 2010 Feb;9(2):347-57.

5 Menisser-de MJ, Mark M, Wendling O, Wynshaw-Boris A, de MG. *Early embryonic lethality in PARP-1 Atm double-mutant mice suggests a functional synergy in cell proliferation during development.* Mol Cell Biol 2001 Mar;21(5):1828-32.

6 Aguilar-Quesada R, Munoz-Gamez JA, Martin-Oliva D, Peralta A, Valenzuela MT, Matinez-Romero R, et al. *Interaction between ATM and PARP-1 in response to DNA damage and sensitization of ATM deficient cells through PARP inhibition.* BMC Mol Biol 2007;8:29.

7 Weston VJ, Oldreive CE, Skowronska A, Oscier DG, Pratt G, Dyer MJ, et al. *The PARP inhibitor olaparib induces significant killing of ATM-deficient lymphoid tumor cells in vitro and in vivo.* Blood 2010 Nov 25;116(22):4578-87.

8 Golla RM, Li M, Shen Y, Ji M, Yan Y, Fu K, et al. *Inhibition of poly(ADP-ribose) polymerase (PARP) and ataxia telangiectasia mutated (ATM) on the chemosensitivity of mantle cell lymphoma to agents that induce DNA strand breaks.* Hematol Oncol 2011 Dec 14.

9 Williamson CT, Kubota E, Hamill JD, Klimowicz A, Ye R, Muzik H, et al. *Enhanced cytotoxicity of PARP inhibition in mantle cell lymphoma harbouring mutations in both ATM and p53.* EMBO Mol Med 2012;n/a.

10 Lord CJ, McDonald S, Swift S, Turner NC, Ashworth A. *A high-throughput RNA interference screen for DNA repair determinants of PARP inhibitor sensitivity.* DNA Repair (Amst) 2008 Dec 1;7(12):2010-9.

11 Bryant HE, Petermann E, Schultz N, Jemth AS, Loseva O, Issaeva N, et al. *PARP is activated at stalled forks to mediate Mre11-dependent replication restart and recombination.* EMBO J 2009 Sep 2;28(17):2601-15.

12 Patel AG, Sarkaria JN, Kaufmann SH. *Nonhomologous end joining drives poly(ADP-ribose) polymerase (PARP) inhibitor lethality in homologous recombination-deficient cells.* Proceedings of the National Academy of Sciences 2011 Feb 22;108(8):3406-11.

13 Gottipati P, Vischioni B, Schultz N, Solomons J, Bryant HE, Djureinovic T, et al. *Poly(ADP-ribose) polymerase is hyperactivated in homologous recombination-defective cells.* Cancer Res 2010 Jul 1;70(13):5389-98.

14 Ström CE, Johansson F, Uhlen M, Szigyarto CA-K, Erixon K, Helleday T. *Poly (ADP-ribose) polymerase (PARP) is not involved in base excision repair but PARP inhibition traps a single-strand intermediate.* Nucleic Acids Research 2011 Apr 1;39(8):3166-75.

15 Williams ME, Connors JM, Dreyling MH, Gascoyne RD, Kahl BS, Leonard JP, et al. *Mantle cell lymphoma: report of the 2010 Mantle Cell Lymphoma Consortium Workshop.* Leuk Lymphoma 2010 Dec 6;52(1):24-33.

16 Schaffner C, Idler I, Stilgenbauer S, Dohner H, Lichter P. *Mantle cell lymphoma is characterized by inactivation of the ATM gene.* Proc Natl Acad Sci U S A 2000 Mar 14;97(6):2773-8.

17 Bullrich F, Rasio D, Kitada S, Starostik P, Kipps T, Keating M, et al. *ATM mutations in B-cell chronic lymphocytic leukemia.* Cancer Res 1999 Jan 1;59(1):24-7.

18 Dohner H, Stilgenbauer S, James MR, Benner A, Weilguni T, Bentz M, et al. *11q deletions identify a new subset of B-cell chronic lymphocytic leukemia characterized by extensive nodal involvement and inferior prognosis.* Blood 1997 Apr 1;89(7):2516-22.

19 Stankovic T, Weber P, Stewart G, Bedenham T, Murray J, Byrd PJ, et al. *Inactivation of ataxia telangiectasia mutated gene in B-cell chronic lymphocytic leukaemia.* Lancet 1999 Jan 2;353(9146):26-9.

20 Hartmann EM, Campo E, Wright G, Lenz G, Salaverria I, Jares P, et al. *Pathway discovery in mantle cell lymphoma by integrated analysis of high-resolution gene expression and copy number profiling.* Blood 2010 Aug 12;116(6):953-61.

21 Greiner TC, Dasgupta C, Ho VV, Weisenburger DD, Smith LM, Lynch JC, et al. *Mutation and genomic deletion status of ataxia telangiectasia mutated (ATM) and p53 confer specific gene expression profiles in mantle cell lymphoma.* Proc Natl Acad Sci U S A 2006 Feb 14;103(7):2352-7.

22 Ghielmini M, Zucca E. *How I treat mantle cell lymphoma.* Blood 2009 Aug 20;114(8):1469-76.

23 Cancer Registry of Norway. *Cancer in Norway 2009: Camcer incidence, mortality, survival and prevalence in Norway.* 2011. Oslo, Cancer Registry of Norway.

24 Statistics Norway. *Statistical Yearbook of Norway 2011.* 2011. Oslo, Statistics Norway.

25 Hanahan D, Weinberg RA. *The hallmarks of cancer.* Cell 2000 Jan 7;100(1):57-70.

26 Hanahan D, Weinberg RA. *Hallmarks of cancer: the next generation.* Cell 2011 Mar 4;144(5):646-74.

27 Raffeld M, Jaffe ES. *bcl-1, t(11;14), and mantle cell-derived lymphomas.* Blood 1991 Jul 15;78(2):259-63.

28 Weisenburger DD, Armitage JO. *Mantle cell lymphoma-- an entity comes of age.* Blood 1996 Jun 1;87(11):4483-94.

29 Bartek J, Lukas J. *DNA damage checkpoints: from initiation to recovery or adaptation.* Curr Opin Cell Biol 2007 Apr;19(2):238-45.

30 Lodish H, Berk A, Kaiser CA, et al. *Molecular Cell Biology, Sixth Edition.* 2008. New York, W.H. Freeman and company.

31 Zharkov DO. *Base excision DNA repair.* Cell Mol Life Sci 2008 May;65(10):1544-65.

32 Thompson LH, Brookman KW, Dillehay LE, Carrano AV, Mazrimas JA, Mooney CL, et al. *A CHO-cell strain having hypersensitivity to mutagens, a defect in DNA strand-break repair, and an extraordinary baseline frequency of sister-chromatid exchange.* Mutat Res 1982 Aug;95(2-3):427-40.

33 Cappelli E, Taylor R, Cevasco M, Abbondandolo A, Caldecott K, Frosina G. *Involvement of XRCC1 and DNA ligase III gene products in DNA base excision repair.* J Biol Chem 1997 Sep 19;272(38):23970-5.

34 Rogakou EP, Pilch DR, Orr AH, Ivanova VS, Bonner WM. *DNA Double-stranded Breaks Induce Histone H2AX Phosphorylation on Serine 139.* Journal of Biological Chemistry 1998 Mar 6;273(10):5858-68.

35 Rube CE, Lorat Y, Schuler N, Schanz S, Wennemuth G, Rube C. *DNA repair in the context of chromatin: new molecular insights by the nanoscale detection of DNA repair complexes using transmission electron microscopy.* DNA Repair (Amst) 2011 Apr 3;10(4):427-37.

36 Bekker-Jensen S, Lukas C, Melander F, Bartek J, Lukas J. *Dynamic assembly and sustained retention of 53BP1 at the sites of DNA damage are controlled by Mdc1/NFBD1.* J Cell Biol 2005 Jul 18;170(2):201-11.

37 MacPhail SH, Banáth JP, Yu Y, Chu E, Olive PL. *Cell Cycle-Dependent Expression of Phosphorylated Histone H2AX: Reduced Expression in Unirradiated but not X-Irradiated G1-Phase Cells.* Radiation Research 2003 Jun 1;159(6):759-67.

38 Tkacz-Stachowska K, Lund-Andersen C, Velissarou A, Myklebust JH, Stokke T, Syljuasen RG. *The amount of DNA damage needed to activate the radiation-induced G2 checkpoint varies between single cells.* Radiother Oncol 2011 Oct;101(1):24-7.

39 Huang X, Tanaka T, Kurose A, Traganos F, Darzynkiewicz Z. *Constitutive histone H2AX phosphorylation on Ser-139 in cells untreated by genotoxic agents is cell-cycle phase specific and attenuated by scavenging reactive oxygen species.* Int J Oncol 2006 Aug;29(2):495-501.

40 Difilippantonio S, Celeste A, Kruhlak MJ, Lee Y, Difilippantonio MJ, Feigenbaum L, et al. *Distinct domains in Nbs1 regulate irradiation-induced checkpoints and apoptosis.* J Exp Med 2007 May 14;204(5):1003-11.

41 Horejsi Z, Falck J, Bakkenist CJ, Kastan MB, Lukas J, Bartek J. *Distinct functional domains of Nbs1 modulate the timing and magnitude of ATM activation after low doses of ionizing radiation.* Oncogene 2003 Nov 7;23(17):3122-7.

42 Berkovich E, Monnat RJ, Kastan MB. *Roles of ATM and NBS1 in chromatin structure modulation and DNA double-strand break repair.* Nat Cell Biol 2007 Jun;9(6):683-90.

43 Cerosaletti K, Wright J, Concannon P. *Active role for nibrin in the kinetics of atm activation.* Mol Cell Biol 2006 Mar;26(5):1691-9.

44 Bakkenist CJ, Kastan MB. *DNA damage activates ATM through intermolecular autophosphorylation and dimer dissociation.* Nature 2003 Jan 30;421(6922):499-506.

45 Lukas C, Falck J, Bartkova J, Bartek J, Lukas J. *Distinct spatiotemporal dynamics of mammalian checkpoint regulators induced by DNA damage.* Nat Cell Biol 2003 Mar;5(3):255-60.

46 Chen K, Albano A, Ho A, Keaney JF, Jr. *Activation of p53 by oxidative stress involves platelet-derived growth factor-beta receptor-mediated ataxia telangiectasia mutated (ATM) kinase activation.* J Biol Chem 2003 Oct 10;278(41):39527-33.

47 Kitagawa R, Bakkenist CJ, McKinnon PJ, Kastan MB. *Phosphorylation of SMC1 is a critical downstream event in the ATM-NBS1-BRCA1 pathway.* Genes Dev 2004 Jun 15;18(12):1423-38.

48 Stucki M, Jackson SP. *gammaH2AX and MDC1: anchoring the DNA-damage-response machinery to broken chromosomes.* DNA Repair (Amst) 2006 May 10;5(5):534-43.

49 Adams KE, Medhurst AL, Dart DA, Lakin ND. *Recruitment of ATR to sites of ionising radiation-induced DNA damage requires ATM and components of the MRN protein complex.* Oncogene 2006 Jun 29;25(28):3894-904.

50 You Z, Shi LZ, Zhu Q, Wu P, Zhang YW, Basilio A, et al. *CtIP Links DNA Double-Strand Break Sensing to Resection.* Mol Cell 2009 Dec 24;36(6):954-69.

51 Jazayeri A, Falck J, Lukas C, Bartek J, Smith GC, Lukas J, et al. *ATM- and cell cycle-dependent regulation of ATR in response to DNA double-strand breaks.* Nat Cell Biol 2006 Jan;8(1):37-45.

52 Sorensen CS, Hansen LT, Dziegielewski J, Syljuasen RG, Lundin C, Bartek J, et al. *The cell-cycle checkpoint kinase Chk1 is required for mammalian homologous recombination repair.* Nat Cell Biol 2005 Feb;7(2):195-201.

53 Bahassi EM, Ovesen JL, Riesenberg AL, Bernstein WZ, Hasty PE, Stambrook PJ. *The checkpoint kinases Chk1 and Chk2 regulate the functional associations between hBRCA2 and Rad51 in response to DNA damage.* Oncogene 2008 Jun 26;27(28):3977-85.

54 Beucher A, Birraux J, Tchouandong L, Barton O, Shibata A, Conrad S, et al. *ATM and Artemis promote homologous recombination of radiation-induced DNA double-strand breaks in G2.* EMBO J 2009 Nov 4;28(21):3413-27.

55 Wold MS. *Replication protein A: a heterotrimeric, single-stranded DNA-binding protein required for eukaryotic DNA metabolism.* Annu Rev Biochem 1997;66:61-92.

56 Khanna KK, Jackson SP. *DNA double-strand breaks: signaling, repair and the cancer connection.* Nat Genet 2001 Mar;27(3):247-54.

57 Misteli T, Soutoglou E. *The emerging role of nuclear architecture in DNA repair and genome maintenance.* Nat Rev Mol Cell Biol 2009 Apr;10(4):243-54.

58 Kim JS, Krasieva TB, Kurumizaka H, Chen DJ, Taylor AM, Yokomori K. *Independent and sequential recruitment of NHEJ and HR factors to DNA damage sites in mammalian cells.* J Cell Biol 2005 Aug 1;170(3):341-7.

59 Xie A, Kwok A, Scully R. *Role of mammalian Mre11 in classical and alternative nonhomologous end joining.* Nat Struct Mol Biol 2009 Aug;16(8):814-8.

60 Helmink BA, Bredemeyer AL, Lee BS, Huang CY, Sharma GG, Walker LM, et al. *MRN complex function in the repair of chromosomal Rag-mediated DNA double-strand breaks.* J Exp Med 2009 Mar 16;206(3):669-79.

61 Rass E, Grabarz A, Plo I, Gautier J, Bertrand P, Lopez BS. *Role of Mre11 in chromosomal nonhomologous end joining in mammalian cells.* Nat Struct Mol Biol 2009 Aug;16(8):819-24.

62 Gottlieb TM, Jackson SP. *The DNA-dependent protein kinase: requirement for DNA ends and association with Ku antigen.* Cell 1993 Jan 15;72(1):131-42.

63 Smith GC, Divecha N, Lakin ND, Jackson SP. *DNA-dependent protein kinase and related proteins.* Biochem Soc Symp 1999;64:91-104.

64 DeFazio LG, Stansel RM, Griffith JD, Chu G. *Synapsis of DNA ends by DNA-dependent protein kinase.* EMBO J 2002 Jun 17;21(12):3192-200.

65 Ma Y, Pannicke U, Lu H, Niewolik D, Schwarz K, Lieber MR. *The DNA-dependent Protein Kinase Catalytic Subunit Phosphorylation Sites in Human Artemis.* Journal of Biological Chemistry 2005 Oct 7;280(40):33839-46.

66 Ahnesorg P, Smith P, Jackson SP. *XLF interacts with the XRCC4-DNA ligase IV complex to promote DNA nonhomologous end-joining.* Cell 2006 Jan 27;124(2):301-13.

67 Buck D, Malivert L, de CR, Barraud A, Fondaneche MC, Sanal O, et al. *Cernunnos, a novel nonhomologous end-joining factor, is mutated in human immunodeficiency with microcephaly.* Cell 2006 Jan 27;124(2):287-99.

68 Pierce AJ, Hu P, Han M, Ellis N, Jasin M. *Ku DNA end-binding protein modulates homologous repair of double-strand breaks in mammalian cells.* Genes Dev 2001 Dec 15;15(24):3237-42.

69 Adachi N, Ishino T, Ishii Y, Takeda S, Koyama H. *DNA ligase IV-deficient cells are more resistant to ionizing radiation in the absence of Ku70: Implications for DNA double-strand break repair.* Proc Natl Acad Sci U S A 2001 Oct 9;98(21):12109-13.

70 Sonoda E, Hochegger H, Saberi A, Taniguchi Y, Takeda S. *Differential usage of non-homologous end-joining and homologous recombination in double strand break repair.* DNA Repair (Amst) 2006 Sep 8;5(9-10):1021-9.

71 Mari PO, Florea BI, Persengiev SP, Verkaik NS, Brüggenwirth HT, Modesti M, et al. *Dynamic assembly of end-joining complexes requires interaction between Ku70/80*

and XRCC4. Proceedings of the National Academy of Sciences 2006 Dec 5;103(49):18597-602.

72 Blomen V, Boonstra J. *Cell fate determination during G1 phase progression.* Cellular and Molecular Life Sciences 2007 Dec 23;64(23):3084-104.

73 Hartwell LH, Weinert TA. *Checkpoints: controls that ensure the order of cell cycle events.* Science 1989 Nov 3;246(4930):629-34.

74 Boye E, Skjolberg HC, Grallert B. *Checkpoint regulation of DNA replication.* Methods Mol Biol 2009;521:55-70.

75 Mikhailov A, Cole RW, Rieder CL. *DNA damage during mitosis in human cells delays the metaphase/anaphase transition via the spindle-assembly checkpoint.* Curr Biol 2002 Oct 29;12(21):1797-806.

76 Monaco L, Kolthur-Seetharam U, Loury R, Murcia JM, de MG, Sassone-Corsi P. *Inhibition of Aurora-B kinase activity by poly(ADP-ribosyl)ation in response to DNA damage.* Proc Natl Acad Sci U S A 2005 Oct 4;102(40):14244-8.

77 Smith J, Mun Tho L, Xu N, Gillespie A. The ATM–Chk2 and ATR–Chk1 Pathways in DNA Damage Signaling and Cancer. In: George F, V, editor. Advances in Cancer Research. Volume 108 ed. Academic Press; 2010. p. 73-112.

78 Chehab NH, Malikzay A, Appel M, Halazonetis TD. *Chk2/hCds1 functions as a DNA damage checkpoint in G(1) by stabilizing p53.* Genes Dev 2000 Feb 1;14(3):278-88.

79 Blasina A, de Weyer IV, Laus MC, Luyten WH, Parker AE, McGowan CH. *A human homologue of the checkpoint kinase Cds1 directly inhibits Cdc25 phosphatase.* Curr Biol 1999 Jan 14;9(1):1-10.

80 Matsuoka S, Huang M, Elledge SJ. *Linkage of ATM to cell cycle regulation by the Chk2 protein kinase.* Science 1998 Dec 4;282(5395):1893-7.

81 Chaturvedi P, Eng WK, Zhu Y, Mattern MR, Mishra R, Hurle MR, et al. *Mammalian Chk2 is a downstream effector of the ATM-dependent DNA damage checkpoint pathway.* Oncogene 1999 Jul 15;18(28):4047-54.

82 Landsverk KS, Patzke S, Rein ID, Stokke C, Lyng H, De Angelis PM, et al. *Three independent mechanisms for arrest in G2 after ionizing radiation.* Cell Cycle 2011 Mar 1;10(5):819-29.

83 Kastan MB, Onyekwere O, Sidransky D, Vogelstein B, Craig RW. *Participation of p53 protein in the cellular response to DNA damage.* Cancer Res 1991 Dec 1;51(23 Pt 1):6304-11.

84 Kuerbitz SJ, Plunkett BS, Walsh WV, Kastan MB. *Wild-type p53 is a cell cycle checkpoint determinant following irradiation.* Proc Natl Acad Sci U S A 1992 Aug 15;89(16):7491-5.

85 Levine AJ. *p53, the Cellular Gatekeeper for Growth and Division.* Cell 1997 Feb 7;88(3):323-31.

86 Oren M. *Decision making by p53: life, death and cancer.* Cell Death Differ 0 AD;10(4):431-42.

87 Kroemer G, Galluzzi L, Vandenabeele P, Abrams J, Alnemri ES, Baehrecke EH, et al. *Classification of cell death: recommendations of the Nomenclature Committee on Cell Death 2009.* Cell Death Differ 2009 Jan;16(1):3-11.

88 Vakifahmetoglu H, Olsson M, Zhivotovsky B. *Death through a tragedy: mitotic catastrophe.* Cell Death Differ 2008 Apr 11;15(7):1153-62.

89 Peart MJ, Tainton KM, Ruefli AA, Dear AE, Sedelies KA, O'Reilly LA, et al. *Novel mechanisms of apoptosis induced by histone deacetylase inhibitors.* Cancer Res 2003 Aug 1;63(15):4460-71.

90 Castedo M, Perfettini JL, Roumier T, Andreau K, Medema R, Kroemer G. *Cell death by mitotic catastrophe: a molecular definition.* Oncogene 2004 Apr 12;23(16):2825-37.

91 Castedo M, Perfettini JL, Roumier T, Valent A, Raslova H, Yakushijin K, et al. *Mitotic catastrophe constitutes a special case of apoptosis whose suppression entails aneuploidy.* Oncogene 2004 May 27;23(25):4362-70.

92 Vakifahmetoglu H, Olsson M, Tamm C, Heidari N, Orrenius S, Zhivotovsky B. *DNA damage induces two distinct modes of cell death in ovarian carcinomas.* Cell Death Differ 2008 Mar;15(3):555-66.

93 Tsujimoto Y, Shimizu S. *Another way to die: autophagic programmed cell death.* Cell Death Differ 2005 Nov;12 Suppl 2:1528-34.

94 Vercammen D, Vandenabeele P, Beyaert R, Declercq W, Fiers W. *Tumour necrosis factor-induced necrosis versus anti-Fas-induced apoptosis in L929 cells.* Cytokine 1997 Nov;9(11):801-8.

95 Vercammen D, Brouckaert G, Denecker G, Van de Craen M, Declercq W, Fiers W, et al. *Dual signaling of the Fas receptor: initiation of both apoptotic and necrotic cell death pathways.* J Exp Med 1998 Sep 7;188(5):919-30.

96 Vercammen D, Beyaert R, Denecker G, Goossens V, Van LG, Declercq W, et al. *Inhibition of caspases increases the sensitivity of L929 cells to necrosis mediated by tumor necrosis factor.* J Exp Med 1998 May 4;187(9):1477-85.

97 Otto H, Reche PA, Bazan F, Dittmar K, Haag F, Koch-Nolte F. *In silico characterization of the family of PARP-like poly(ADP-ribosyl)transferases (pARTs).* BMC Genomics 2005;6:139.

98 Hassa PO, Haenni SS, Elser M, Hottiger MO. *Nuclear ADP-ribosylation reactions in mammalian cells: where are we today and where are we going?* Microbiol Mol Biol Rev 2006 Sep;70(3):789-829.

99 D'Amours D, Desnoyers S, D'Silva I, Poirier GG. *Poly(ADP-ribosyl)ation reactions in the regulation of nuclear functions.* Biochem J 1999 Sep 1;342 (Pt 2):249-68.

100 Ame JC, Spenlehauer C, de MG. *The PARP superfamily.* Bioessays 2004 Aug;26(8):882-93.

101 Wang ZQ, Auer B, Stingl L, Berghammer H, Haidacher D, Schweiger M, et al. *Mice lacking ADPRT and poly(ADP-ribosyl)ation develop normally but are susceptible to skin disease.* Genes Dev 1995 Mar 1;9(5):509-20.

102 de Murcia JM, Niedergang C, Trucco C, Ricoul M, Dutrillaux B, Mark M, et al. *Requirement of poly(ADP-ribose) polymerase in recovery from DNA damage in mice and in cells.* Proc Natl Acad Sci U S A 1997 Jul 8;94(14):7303-7.

103 Oliver FJ, Menissier-de MJ, Nacci C, Decker P, Andriantsitohaina R, Muller S, et al. *Resistance to endotoxic shock as a consequence of defective NF-kappaB activation in poly (ADP-ribose) polymerase-1 deficient mice.* EMBO J 1999 Aug 16;18(16):4446-54.

104 Mabley JG, Suarez-Pinzon WL, Hasko G, Salzman AL, Rabinovitch A, Kun E, et al. *Inhibition of poly (ADP-ribose) synthetase by gene disruption or inhibition with 5-iodo-6-amino-1,2-benzopyrone protects mice from multiple-low-dose-streptozotocin-induced diabetes.* Br J Pharmacol 2001 Jul;133(6):909-19.

105 Ha HC. *Defective transcription factor activation for proinflammatory gene expression in poly(ADP-ribose) polymerase 1-deficient glia.* Proc Natl Acad Sci U S A 2004 Apr 6;101(14):5087-92.

106 Miwa M, Hanai S, Poltronieri P, Uchida M, Uchida K. *Functional analysis of poly(ADP-ribose) polymerase in Drosophila melanogaster.* Mol Cell Biochem 1999 Mar;193(1-2):103-7.

107 Tulin A, Stewart D, Spradling AC. *The Drosophila heterochromatic gene encoding poly(ADP-ribose) polymerase (PARP) is required to modulate chromatin structure during development.* Genes Dev 2002 Aug 15;16(16):2108-19.

108 Tulin A, Spradling A. *Chromatin loosening by poly(ADP)-ribose polymerase (PARP) at Drosophila puff loci.* Science 2003 Jan 24;299(5606):560-2.

109 Menissier de Murcia J, Ricoul M, Tartier L, Niedergang C, Huber A, Dantzer F, et al. *Functional interaction between PARP-1 and PARP-2 in chromosome stability and embryonic development in mouse.* EMBO J 2003 May 1;22(9):2255-63.

110 Schreiber V, Dantzer F, Ame JC, de Murcia G. *Poly(ADP-ribose): novel functions for an old molecule.* Nat Rev Mol Cell Biol 2006 Jul;7(7):517-28.

111 Yelamos J, Schreiber V, Dantzer F. *Toward specific functions of poly(ADP-ribose) polymerase-2.* Trends in Molecular Medicine 2008 Apr;14(4):169-78.

112 Adamietz P. *Poly(ADP-ribose) synthase is the major endogenous nonhistone acceptor for poly(ADP-ribose) in alkylated rat hepatoma cells.* Eur J Biochem 1987 Dec 1;169(2):365-72.

113 Ohgushi H, Yoshihara K, Kamiya T. *Bovine thymus poly(adenosine diphosphate ribose) polymerase. Physical properties and binding to DNA.* Journal of Biological Chemistry 1980 Jul 10;255(13):6205-11.

114 Ferro AM, Olivera BM. *Poly(ADP-ribosylation) in vitro. Reaction parameters and enzyme mechanism.* Journal of Biological Chemistry 1982 Jul 10;257(13):7808-13.

115 Mendoza-Alvarez H, Alvarez-Gonzalez R. *Regulation of p53 sequence-specific DNA-binding by covalent poly(ADP-ribosyl)ation.* J Biol Chem 2001 Sep 28;276(39):36425-30.

116 Kanai M, Hanashiro K, Kim SH, Hanai S, Boulares AH, Miwa M, et al. *Inhibition of Crm1-p53 interaction and nuclear export of p53 by poly(ADP-ribosyl)ation.* Nat Cell Biol 2007 Oct;9(10):1175-83.

117 Kraus WL. *Transcriptional control by PARP-1: chromatin modulation, enhancer-binding, coregulation, and insulation.* Curr Opin Cell Biol 2008 Jun;20(3):294-302.

118 Wielckens K, Schmidt A, George E, Bredehorst R, Hilz H. *DNA fragmentation and NAD depletion. Their relation to the turnover of endogenous mono(ADP-ribosyl) and poly(ADP-ribosyl) proteins.* J Biol Chem 1982 Nov 10;257(21):12872-7.

119 Alvarez-Gonzalez R, Althaus FR. *Poly(ADP-ribose) catabolism in mammalian cells exposed to DNA-damaging agents.* Mutat Res 1989 Sep;218(2):67-74.

120 Zahradka P, Ebisuzaki K. *A shuttle mechanism for DNA-protein interactions. The regulation of poly(ADP-ribose) polymerase.* Eur J Biochem 1982 Oct;127(3):579-85.

121 Yamanaka H, Penning CA, Willis EH, Wasson DB, Carson DA. *Characterization of human poly(ADP-ribose) polymerase with autoantibodies.* J Biol Chem 1988 Mar 15;263(8):3879-83.

122 Koh DW, Lawler AM, Poitras MF, Sasaki M, Wattler S, Nehls MC, et al. *Failure to degrade poly(ADP-ribose) causes increased sensitivity to cytotoxicity and early embryonic lethality.* Proceedings of the National Academy of Sciences of the United States of America 2004 Dec 21;101(51):17699-704.

123 Niere M, Mashimo M, Agledal L, Doelle C, Kasamatsu A, Kato J, et al. *ADP-Ribosylhydrolase 3 (ARH3), not Poly-ADP-Ribose Glycohydrolase (PARG) Isoforms, are Responsible for Degradation of Mitochondrial Matrix-Associated Poly-ADP-Ribose.* J Biol Chem 2012 Mar 20.

124 Lazebnik YA, Kaufmann SH, Desnoyers S, Poirier GG, Earnshaw WC. *Cleavage of poly(ADP-ribose) polymerase by a proteinase with properties like ICE.* Nature 1994 Sep 22;371(6495):346-7.

125 Dantzer F, Schreiber V, Niedergang C, Trucco C, Flatter E, de la Rubia G, et al. *Involvement of poly(ADP-ribose) polymerase in base excision repair.* Biochimie 1999 Jan;81(1-2):69-75.

126 Trucco C, Oliver FJ, de MG, Menissier-de MJ. *DNA repair defect in poly(ADP-ribose) polymerase-deficient cell lines.* Nucleic Acids Res 1998 Jun 1;26(11):2644-9.

127 Allinson SL, Sleeth KM, Matthewman GE, Dianov GL. *Orchestration of base excision repair by controlling the rates of enzymatic activities.* DNA Repair (Amst) 2004 Jan 5;3(1):23-31.

128 Vodenicharov MD, Sallmann FR, Satoh MS, Poirier GG. *Base excision repair is efficient in cells lacking poly(ADP-ribose) polymerase 1.* Nucleic Acids Research 2000 Oct 15;28(20):3887-96.

129 Xanthoudakis S, Smeyne RJ, Wallace JD, Curran T. *The redox/DNA repair protein, Ref-1, is essential for early embryonic development in mice.* Proc Natl Acad Sci U S A 1996 Aug 20;93(17):8919-23.

130 Tebbs RS, Thompson LH, Cleaver JE. *Rescue of Xrcc1 knockout mouse embryo lethality by transgene-complementation.* DNA Repair (Amst) 2003 Dec 9;2(12):1405-17.

131 Wang M, Wu W, Wu W, Rosidi B, Zhang L, Wang H, et al. *PARP-1 and Ku compete for repair of DNA double strand breaks by distinct NHEJ pathways.* Nucleic Acids Research 2006 Dec 1;34(21):6170-82.

132 Durkacz BW, Irwin J, Shall S. *Inhibition of (ADP-ribose)n biosynthesis retards DNA repair but does not inhibit DNA repair synthesis.* Biochemical and Biophysical Research Communications 1981 Aug 31;101(4):1433-41.

133 Satoh MS, Lindahl T. *Role of poly(ADP-ribose) formation in DNA repair.* Nature 1992 Mar 26;356(6367):356-8.

134 Fisher AE, Hochegger H, Takeda S, Caldecott KW. *Poly(ADP-ribose) polymerase 1 accelerates single-strand break repair in concert with poly(ADP-ribose) glycohydrolase.* Mol Cell Biol 2007 Aug;27(15):5597-605.

135 El-Khamisy SF, Masutani M, Suzuki H, Caldecott KW. *A requirement for PARP-1 for the assembly or stability of XRCC1 nuclear foci at sites of oxidative DNA damage.* Nucleic Acids Res 2003 Oct 1;31(19):5526-33.

136 Haince JF, Kozlov S, Dawson VL, Dawson TM, Hendzel MJ, Lavin MF, et al. *Ataxia telangiectasia mutated (ATM) signaling network is modulated by a novel poly(ADP-ribose)-dependent pathway in the early response to DNA-damaging agents.* J Biol Chem 2007 Jun 1;282(22):16441-53.

137 Gagné JP, Rouleau Ml, Poirier GG. *PARP-1 Activation–Bringing the Pieces Together.* Science 2012 May 11;336(6082):678-9.

138 Haince JF, McDonald D, Rodrigue A, Dery U, Masson JY, Hendzel MJ, et al. *PARP1-dependent kinetics of recruitment of MRE11 and NBS1 proteins to multiple DNA damage sites.* J Biol Chem 2008 Jan 11;283(2):1197-208.

139 Menear KA, Adcock C, Boulter R, Cockcroft Xl, Copsey L, Cranston A, et al. *4-[3-(4-Cyclopropanecarbonylpiperazine-1-carbonyl)-4-fluorobenzyl]-2H-phthalazin-1-one: A Novel Bioavailable Inhibitor of Poly(ADP-ribose) Polymerase-1.* J Med Chem 2008 Sep 19;51(20):6581-91.

140 Mendeleyev J, Kirsten E, Hakam A, Buki KG, Kun E. *Potential chemotherapeutic activity of 4-iodo-3-nitrobenzamide: Metabolic reduction to the 3-nitroso derivative and induction of cell death in tumor cells in culture.* Biochemical Pharmacology 1995 Aug 25;50(5):705-14.

141 Fong PC, Boss DS, Yap TA, Tutt A, Wu P, Mergui-Roelvink M, et al. *Inhibition of poly(ADP-ribose) polymerase in tumors from BRCA mutation carriers.* N Engl J Med 2009 Jul 9;361(2):123-34.

142 Fong PC, Yap TA, Boss DS, Carden CP, Mergui-Roelvink M, Gourley C, et al. *Poly(ADP)-ribose polymerase inhibition: frequent durable responses in BRCA carrier ovarian cancer correlating with platinum-free interval.* J Clin Oncol 2010 May 20;28(15):2512-9.

143 Kummar S, Chen A, Ji J, Zhang Y, Reid JM, Ames M, et al. *Phase I study of PARP inhibitor ABT-888 in combination with topotecan in adults with refractory solid tumors and lymphomas.* Cancer Res 2011 Sep 1;71(17):5626-34.

144 Yamamoto N, Nokihara H, Yamada Y, Goto Y, Tanioka M, Shibata T, et al. *A Phase I, dose-finding and pharmacokinetic study of olaparib (AZD2281) in Japanese patients with advanced solid tumors.* Cancer Sci 2012 Mar;103(3):504-9.

145 Dean E, Middleton MR, Pwint T, Swaisland H, Carmichael J, Goodege-Kunwar P, et al. *Phase I study to assess the safety and tolerability of olaparib in combination with bevacizumab in patients with advanced solid tumours.* Br J Cancer 2012 Jan 5.

146 Tutt A, Robson M, Garber JE, Domchek SM, Audeh MW, Weitzel JN, et al. *Oral poly(ADP-ribose) polymerase inhibitor olaparib in patients with BRCA1 or BRCA2 mutations and advanced breast cancer: a proof-of-concept trial.* Lancet 2010 Jul 24;376(9737):235-44.

147 Audeh MW, Carmichael J, Penson RT, Friedlander M, Powell B, Bell-McGuinn KM, et al. *Oral poly(ADP-ribose) polymerase inhibitor olaparib in patients with BRCA1 or BRCA2 mutations and recurrent ovarian cancer: a proof-of-concept trial.* Lancet 2010 Jul 24;376(9737):245-51.

148 O'Shaughnessy J, Osborne C, Pippen JE, Yoffe M, Patt D, Rocha C, et al. *Iniparib plus Chemotherapy in Metastatic Triple-Negative Breast Cancer.* N Engl J Med 2011 Jan 5;364(3):205-14.

149 Gelmon KA, Tischkowitz M, Mackay H, Swenerton K, Robidoux A, Tonkin K, et al. *Olaparib in patients with recurrent high-grade serous or poorly differentiated ovarian carcinoma or triple-negative breast cancer: a phase 2, multicentre, open-label, non-randomised study.* Lancet Oncol 2011 Sep;12(9):852-61.

150 Ledermann J, Harter P, Gourley C, Friedlander M, Vergote I, Rustin G, et al. *Olaparib maintenance therapy in platinum-sensitive relapsed ovarian cancer.* N Engl J Med 2012 Apr 12;366(15):1382-92.

151 Turner NC, Lord CJ, Iorns E, Brough R, Swift S, Elliott R, et al. *A synthetic lethal siRNA screen identifying genes mediating sensitivity to a PARP inhibitor.* EMBO J 2008 May 7;27(9):1368-77.

152 Shiobara M, Miyazaki M, Ito H, Togawa A, Nakajima N, Nomura F, et al. *Enhanced polyadenosine diphosphate-ribosylation in cirrhotic liver and carcinoma tissues in patients with hepatocellular carcinoma.* J Gastroenterol Hepatol 2001 Mar;16(3):338-44.

153 Wielckens K, Garbrecht M, Kittler M, Hilz H. *ADP-ribosylation of nuclear proteins in normal lymphocytes and in low-grade malignant non-Hodgkin lymphoma cells.* Eur J Biochem 1980 Feb;104(1):279-87.

154 Nosho K, Yamamoto H, Mikami M, Taniguchi H, Takahashi T, Adachi Y, et al. *Overexpression of poly(ADP-ribose) polymerase-1 (PARP-1) in the early stage of colorectal carcinogenesis.* Eur J Cancer 2006 Sep;42(14):2374-81.

155 Dobzhansky T. *Genetics of natural populations; recombination and variability in populations of Drosophila pseudoobscura.* Genetics 1946 May;31:269-90.

156 Hartwell LH, Szankasi P, Roberts CJ, Murray AW, Friend SH. *Integrating genetic approaches into the discovery of anticancer drugs.* Science 1997 Nov 7;278(5340):1064-8.

157 Liu X, Shi Y, Maag DX, Palma JP, Patterson MJ, Ellis PA, et al. *Iniparib nonselectively modifies cysteine-containing proteins in tumor cells and is not a Bona Fide PARP inhibitor.* Clin Cancer Res 2012 Jan 15;18(2):510-23.

158 Patel AG, De Lorenzo SB, Flatten KS, Poirier GG, Kaufmann SH. *Failure of iniparib to inhibit poly(ADP-Ribose) polymerase in vitro.* Clin Cancer Res 2012 Mar 15;18(6):1655-62.

159 Helleday T. *The underlying mechanism for the PARP and BRCA synthetic lethality: clearing up the misunderstandings.* Mol Oncol 2011 Aug;5(4):387-93.

160 Strumberg D, Pilon AA, Smith M, Hickey R, Malkas L, Pommier Y. *Conversion of topoisomerase I cleavage complexes on the leading strand of ribosomal DNA into 5'-phosphorylated DNA double-strand breaks by replication runoff.* Mol Cell Biol 2000 Jun;20(11):3977-87.

161 Aly A, Ganesan S. *BRCA1, PARP, and 53BP1: conditional synthetic lethality and synthetic viability.* J Mol Cell Biol 2011 Feb;3(1):66-74.

162 Schlacher K, Christ N, Siaud N, Egashira A, Wu H, Jasin M. *Double-strand break repair-independent role for BRCA2 in blocking stalled replication fork degradation by MRE11.* Cell 2011 May 13;145(4):529-42.

163 Petermann E, Orta ML, Issaeva N, Schultz N, Helleday T. *Hydroxyurea-stalled replication forks become progressively inactivated and require two different RAD51-mediated pathways for restart and repair.* Mol Cell 2010 Feb 26;37(4):492-502.

164 Yang YG, Cortes U, Patnaik S, Jasin M, Wang ZQ. *Ablation of PARP-1 does not interfere with the repair of DNA double-strand breaks, but compromises the reactivation of stalled replication forks.* Oncogene 2004 May 6;23(21):3872-82.

165 Ying S, Hamdy FC, Helleday T. *Mre11-dependent degradation of stalled DNA replication forks is prevented by BRCA2 and PARP1.* Cancer Research 2012 Mar 23.

166 Morrison C, Smith GC, Stingl L, Jackson SP, Wagner EF, Wang ZQ. *Genetic interaction between PARP and DNA-PK in V(D)J recombination and tumorigenesis.* Nat Genet 1997 Dec;17(4):479-82.

167 Hochegger H, Dejsuphong D, Fukushima T, Morrison C, Sonoda E, Schreiber V, et al. *Parp-1 protects homologous recombination from interference by Ku and Ligase IV in vertebrate cells.* EMBO J 2006 Mar 22;25(6):1305-14.

168 Mansour WY, Rhein T, hm-Daphi J. *The alternative end-joining pathway for repair of DNA double-strand breaks requires PARP1 but is not dependent upon microhomologies.* Nucleic Acids Research 2010 Oct 1;38(18):6065-77.

169 Cheng Q, Barboule N, Frit P, Gomez D, Bombarde O, Couderc B, et al. *Ku counteracts mobilization of PARP1 and MRN in chromatin damaged with DNA double-strand breaks.* Nucleic Acids Research 2011 Dec 1;39(22):9605-19.

170 Hochegger H, Dejsuphong D, Fukushima T, Morrison C, Sonoda E, Schreiber V, et al. *Parp-1 protects homologous recombination from interference by Ku and Ligase IV in vertebrate cells.* EMBO J 2006 Mar 22;25(6):1305-14.

171 Bunting SF, Callen E, Wong N, Chen HT, Polato F, Gunn A, et al. *53BP1 Inhibits Homologous Recombination in Brca1-Deficient Cells by Blocking Resection of DNA Breaks.* Cell 2010 Apr 16;141(2):243-54.

172 Wang B, Matsuoka S, Carpenter PB, Elledge SJ. *53BP1, a mediator of the DNA damage checkpoint.* Science 2002 Nov 15;298(5597):1435-8.

173 Orsburn B, Escudero B, Prakash M, Gesheva S, Liu G, Huso DL, et al. *Differential Requirement for H2AX and 53BP1 in Organismal Development and Genome Maintenance in the Absence of Poly(ADP)ribosyl Polymerase 1.* Molecular and Cellular Biology 2010 May 15;30(10):2341-52.

174 Rosenfeld C, Goutner A, Venuat AM, Choquet C, Pico JL, Dore JF, et al. *An effective human leukaemic cell line: Reh.* European Journal of Cancer (1965) 2004 Apr;13(4-5):377-9.

175 Nilsson K, Sundström C. *Establishment and characteristics of two unique cell lines from patients with lymphosarcoma.* International Journal of Cancer 1974;13(6):808-23.

176 Melo JV, Foroni L, Brito-Babapulle V, Luzzatto L, Catovsky D. *The establishment of cell lines from chronic B cell leukaemias: evidence of leukaemic origin by karyotypic abnormalities and Ig gene rearrangement.* Clin Exp Immunol 1988 Jul;73(1):23-8.

177 Ruchlemer R, Parry-Jones N, Brito-Babapulle V, Attolico I, Wotherspoon AC, Matutes E, et al. *B-prolymphocytic leukaemia with t(11;14) revisited: a splenomegalic form of mantle cell lymphoma evolving with leukaemia.* Br J Haematol 2004 May;125(3):330-6.

178 Jadayel DM, Lukas J, Nacheva E, Bartkova J, Stranks G, De Schouwer PJ, et al. *Potential role for concurrent abnormalities of the cyclin D1, p16CDKN2 and p15CDKN2B genes in certain B cell non-Hodgkin's lymphomas. Functional studies in a cell line (Granta 519).* Leukemia 1997 Jan;11(1):64-72.

179 Rudolph C, Steinemann D, Von NN, Gadzicki D, Ripperger T, Drexler HG, et al. *Molecular cytogenetic characterization of the mantle cell lymphoma cell line GRANTA-519.* Cancer Genet Cytogenet 2004 Sep;153(2):144-50.

180 Vorechovsky I, Luo L, Dyer MJS, Catovsky D, Amlot PL, Yaxley JC, et al. *Clustering of missense mutations in the ataxia-telanglectasia gene in a sporadic T-cell leukaemia.* Nat Genet 1997 Sep;17(1):96-9.

181 Hickson I, Zhao Y, Richardson CJ, Green SJ, Martin NM, Orr AI, et al. *Identification and characterization of a novel and specific inhibitor of the ataxia-telangiectasia mutated kinase ATM.* Cancer Res 2004 Dec 15;64(24):9152-9.

182 Jordan MA, Thrower D, Wilson L. *Effects of vinblastine, podophyllotoxin and nocodazole on mitotic spindles. Implications for the role of microtubule dynamics in mitosis.* Journal of Cell Science 1992 Jul 1;102(3):401-16.

183 Waters JC, Chen RH, Murray AW, Salmon ED. *Localization of Mad2 to Kinetochores Depends on Microtubule Attachment, Not Tension.* The Journal of Cell Biology 1998 Jun 1;141(5):1181-91.

184 Taylor SS, McKeon F. *Kinetochore localization of murine Bub1 is required for normal mitotic timing and checkpoint response to spindle damage.* Cell 1997 May 30;89(5):727-35.

185 Mitchell LA, De Iuliis GN, Aitken RJ. *The TUNEL assay consistently underestimates DNA damage in human spermatozoa and is influenced by DNA compaction and cell vitality: development of an improved methodology.* International Journal of Andrology 2011;34(1):2-13.

186 Bradbury EM, Inglis RJ, Matthews HR, Sarner N. *Phosphorylation of very-lysine-rich histone in Physarum polycephalum. Correlation with chromosome condensation.* Eur J Biochem 1973 Feb 15;33(1):131-9.

187 Gurley LR, Walters RA, Tobey RA. *Cell cycle-specific changes in histone phosphorylation associated with cell proliferation and chromosome condensation.* J Cell Biol 1974 Feb;60(2):356-64.

188 Rea S, Eisenhaber F, O'Carroll D, Strahl BD, Sun ZW, Schmid M, et al. *Regulation of chromatin structure by site-specific histone H3 methyltransferases.* Nature 2000 Aug 10;406(6796):593-9.

189 Aebi U, Cohn J, Buhle L, Gerace L. *The nuclear lamina is a meshwork of intermediate-type filaments.* Nature 1986 Oct 9;323(6088):560-4.

190 Watson JV, Chambers SH, Smith PJ. *A pragmatic approach to the analysis of DNA histograms with a definable G1 peak.* Cytometry 1987 Jan;8(1):1-8.

191 Fox MH. *A model for the computer analysis of synchronous DNA distributions obtained by flow cytometry.* Cytometry 1980 Jul;1(1):71-7.

192 Neil MA, Juskaitis R, Wilson T. *Method of obtaining optical sectioning by using structured light in a conventional microscope.* Opt Lett 1997 Dec;22(24):1905-7.

193 Lines RW, Haslop D, Spence J, Matthews BR. *Instrumental methods for particle detection.* Anal Proc 1981;18(12):514-28.

194 Harfield JG, Wharton RT, Lines RW. *Response of the Coulter Counter-« Model ZM to Spheres.* Part Part Syst Charact 1984;1(1-4):32-6.

195 Grover NB, Naaman J, Ben-Sasson S, Doljanski F. *Electrical Sizing of Particles in Suspensions: III. Rigid Spheroids and Red Blood Cells.* Biophysical Journal 1972 Sep;12(9):1099-116.

196 Chou TC. *Theoretical Basis, Experimental Design, and Computerized Simulation of Synergism and Antagonism in Drug Combination Studies.* Pharmacological Reviews 2006 Sep 1;58(3):621-81.

197 Rogakou EP, Pilch DR, Orr AH, Ivanova VS, Bonner WM. *DNA Double-stranded Breaks Induce Histone H2AX Phosphorylation on Serine 139.* Journal of Biological Chemistry 1998 Mar 6;273(10):5858-68.

198 Sedelnikova OA, Rogakou EP, Panyutin IG, Bonner WM. *Quantitative detection of (125)IdU-induced DNA double-strand breaks with gamma-H2AX antibody.* Radiat Res 2002 Oct;158(4):486-92.

199 Ichijima Y, Sakasai R, Okita N, Asahina K, Mizutani S, Teraoka H. *Phosphorylation of histone H2AX at M phase in human cells without DNA damage response.* Biochemical and Biophysical Research Communications 2005 Oct 28;336(3):807-12.

200 Zakikhani M, Bazile M, Hashemi S, Pollak MN. *Antiproliferative effect of the Ataxia Telangiectasia Mutated (ATM) Inhibitor KU-55933, involves energy stress due to mitochondrial dysfunction.* 6-9-2011. 3rd Norwegian Cancer symposium.

201 Viniegra JG, Martinez N, Modirassari P, Losa JH, Parada CC, Lobo VJ, et al. *Full activation of PKB/Akt in response to insulin or ionizing radiation is mediated through ATM.* J Biol Chem 2005 Feb 11;280(6):4029-36.

202 Khalil A, Morgan RN, Adams BR, Golding SE, Dever SM, Rosenberg E, et al. *ATM-dependent ERK signaling via AKT in response to DNA double-strand breaks.* Cell Cycle 2011 Feb 1;10(3):481-91.

203 Chen WS, Xu PZ, Gottlob K, Chen ML, Sokol K, Shiyanova T, et al. *Growth retardation and increased apoptosis in mice with homozygous disruption of the Akt1 gene.* Genes Dev 2001 Sep 1;15(17):2203-8.

204 Li Y, Yang DQ. *The ATM Inhibitor KU-55933 Suppresses Cell Proliferation and Induces Apoptosis by Blocking Akt In Cancer Cells with Overactivated Akt.* Molecular Cancer Therapeutics 2010 Jan 1;9(1):113-25.

205 McFarlin DE, Strober W, Waldmann TA. *Ataxia-telangiectasia.* Medicine (Baltimore) 1972 Jul;51(4):281-314.

206 Schalch DS, McFarlin DE, Barlow MH. *An unusual form of diabetes mellitus in ataxia telangiectasia.* N Engl J Med 1970 Jun 18;282(25):1396-402.

207 Stiff T, O'Driscoll M, Rief N, Iwabuchi K, L+¦brich M, Jeggo PA. *ATM and DNA-PK Function Redundantly to Phosphorylate H2AX after Exposure to Ionizing Radiation.* Cancer Research 2004;64(7):2390-6.

208 Landsverk KS, Lyng H, Stokke T. *The response of malignant B lymphocytes to ionizing radiation: cell cycle arrest, apoptosis and protection against the cytotoxic effects of the mitotic inhibitor nocodazole.* Radiat Res 2004 Oct;162(4):405-15.

209 Lyng H, Landsverk KS, Kristiansen E, DeAngelis PM, Ree AH, Myklebost O, et al. *Response of malignant B lymphocytes to ionizing radiation: gene expression and genotype.* Int J Cancer 2005 Jul 20;115(6):935-42.

210 Lopez-Royuela N, Perez-Galan P, Galan-Malo P, Yuste VJ, Anel A, Susin SA, et al. *Different contribution of BH3-only proteins and caspases to doxorubicin-induced apoptosis in p53-deficient leukemia cells.* Biochem Pharmacol 2010 Jun 15;79(12):1746-58.

211 Steimer DA, Boyd K, Takeuchi O, Fisher JK, Zambetti GP, Opferman JT. *Selective roles for antiapoptotic MCL-1 during granulocyte development and macrophage effector function.* Blood 2009 Mar 19;113(12):2805-15.

212 Tucker CA, Bebb G, Klasa RJ, Chhanabhai M, Lestou V, Horsman DE, et al. *Four human t(11;14)(q13;q32)-containing cell lines having classic and variant features of Mantle Cell Lymphoma.* Leukemia Research 2006 Apr;30(4):449-57.

213 Bosco R, Rabusin M, Voltan R, Celeghini C, Corallini F, Capitani S, et al. *Anti-leukemic activity of Dasatinib in both p53-wild-type and p53-mutated B malignant cells.* Investigational New Drugs 2012 Feb 1;30(1):417-22.

214 Stokke T, Smedshammer L, Jonassen TS, Blomhoff HK, Skarstad K, Steen HB. *Uncoupling of the order of the S and M phases: effects of staurosporine on human cell cycle kinases.* Cell Prolif 1997 May;30(5):197-218.

215 Celton-Morizur S, Desdouets C. *Polyploidization of liver cells.* Adv Exp Med Biol 2010;676:123-35.

216 Saxena A, Wong LH, Kalitsis P, Earle E, Shaffer LG, Choo KH. *Poly(ADP-ribose) polymerase 2 localizes to mammalian active centromeres and interacts with PARP-1, Cenpa, Cenpb and Bub3, but not Cenpc.* Hum Mol Genet 2002 Sep 15;11(19):2319-29.

217 Saxena A, Saffery R, Wong LH, Kalitsis P, Choo KH. *Centromere proteins Cenpa, Cenpb, and Bub3 interact with poly(ADP-ribose) polymerase-1 protein and are poly(ADP-ribosyl)ated.* J Biol Chem 2002 Jul 26;277(30):26921-6.

218 Kanai M, Tong WM, Sugihara E, Wang ZQ, Fukasawa K, Miwa M. *Involvement of poly(ADP-Ribose) polymerase 1 and poly(ADP-Ribosyl)ation in regulation of centrosome function.* Mol Cell Biol 2003 Apr;23(7):2451-62.

219 Castiel A, Visochek L, Mittelman L, Dantzer F, Izraeli S, Cohen-Armon M. *A phenanthrene derived PARP inhibitor is an extra-centrosomes de-clustering agent exclusively eradicating human cancer cells.* BMC Cancer 2011;11:412.

220 Bryant HE, Helleday T. *Inhibition of poly (ADP-ribose) polymerase activates ATM which is required for subsequent homologous recombination repair.* Nucleic Acids Research34(6):1685-91.

221 Zhang J, Willers H, Feng Z, Ghosh JC, Kim S, Weaver DT, et al. *Chk2 Phosphorylation of BRCA1 Regulates DNA Double-Strand Break Repair.* Molecular and Cellular Biology 2004 Jan 15;24(2):708-18.

222 Yuan SS, Lee SY, Chen G, Song M, Tomlinson GE, Lee EYH. *BRCA2 Is Required for Ionizing Radiation-induced Assembly of Rad51 Complex in Vivo.* Cancer Research 1999 Aug 1;59(15):3547-51.

223 Senra JM, Telfer BA, Cherry KE, McCrudden CM, Hirst DG, O'Connor MJ, et al. *Inhibition of PARP-1 by olaparib (AZD2281) increases the radiosensitivity of a lung tumor xenograft.* Mol Cancer Ther 2011 Oct;10(10):1949-58.

224 van Vuurden DG, Hulleman E, Meijer OL, Wedekind LE, Kool M, Witt H, et al. *PARP inhibition sensitizes childhood high grade glioma, medulloblastoma and ependymoma to radiation.* Oncotarget 2011 Dec;2(12):984-96.

225 Miura K, Sakata KI, Someya M, Matsumoto Y, Matsumoto H, Takahashi A, et al. *The combination of olaparib and camptothecin for effective radiosensitization.* Radiat Oncol 2012 Apr 23;7(1):62.

Appendix

1 MATERIALS

Table S1: List of materials used, ordered alphabetically by product. N/A = Not applicable

Product	Product number	Manufacturer	City	Country/ US state
0,9% NaCl	0123	B. Braun	Melsungen	Germany
10xTris Buffered Saline-0,5% Tween20 (TBS-T)	sc-24953	Santa Cruz Biotechnology	Santa Cruz	CA
7,5% 10 well MiniPROTEAN-TGX gel	456-1023	Bio-Rad	Hercules	CA
Amersham Cy5-Streptavidin	PA45001	GE Healthcare	Little Chalfont	UK
Aproteinin	A6279	Sigma-Aldrich	St.Louis	MO
ATM inhibitor, KU-55933	S1092	Selleck Chemicals	Houston	TX
BD Cell Viability Kit	349480	BD Biosciences	San Jose	CA
Benzonase	1016940001	Merck Chemicals	Damstadt	Germany
Biotin-16-dUTP	11093070910	Roche Diagnostics	Mannheim	Germany
Bromophenol Blue	B0126	Sigma-Aldrich	St.Louis	MO
Dimethyl Sulfoxide (DMSO)	41639	Sigma-Aldrich	St.Louis	MO
Dithiothreitol (DTT)	Y00147	Life Technologies	Carlsbad	CA
Dulbecco's Modified Eagle Medium (DMEM)	31966	Gibco	Paisley	UK
Fat free Powdered Dry Milk	N/A	TMA	Brumundal	Norway
Fetal Bovine Serum (FBS)	10270	Gibco	Paisley	UK
Glycine	G8898	Sigma-Aldrich	St.Louis	MO
Glyserol	G5516	Sigma-Aldrich	St.Louis	MO
Hoechst 33258	861405	Sigma-Aldrich	St.Louis	MO

Appendix

Product	Product number	Manufacturer	City	Country/ US state
Immobilion-P, 0.45µm, transfer membrane	IPVH00010	Millipore	Temecula	CA
L-Glutamine	M11-004	PAA	Pasching	Austria
LumiGLO Chemiluminescent substrate system	54-61-00	KPL	Gaithersburg	MD
Methanol	20864.320	VWR	Radnor	PA
Nocodazole	M1404	Sigma-Aldrich	St. Louis	MO
PARP inhibitor, AZD-2281	S1060	Selleck Chemicals	Houston	TX
Penicillin-Streptomycin	P11-010	PAA	Pasching	Austria
Phophatase inhibitor cocktail(PIC) II	P5726	Sigma-Aldrich	St.Louis	MO
Phophatase inhibitor cocktail(PIC) III	P0004	Sigma-Aldrich	St.Louis	MO
Phosphate Buffered Saline (PBS)	H15-002	PAA	Pasching	Austria
Precision Plus Protein Dual Color Standard	161-0374	Bio-Rad	Hercules	CA
ProLong Gold Antifade Reagent	P-36930	Life Technologies	Carlsbad	CA
Recombinant Terminal Transferase kit	03333574001	Roche Diagnostics	Mannheim	Germany
Roswell Park Memorial Institute (RPMI) 1640	R8758	Sigma-Aldrich	St.Louis	MO
Sodium dodecyl sulfate (SDS)	161-0302	Bio-Rad	Hercules	CA
SuperSignal West Dura Chemiluminescent substrate system	34075	Thermo Fisher Scientific	Waltham	MA
Tris/Glycine/SDS buffer (10x)	161-0772	Bio-Rad	Hercules	CA
Trizma-hydrochloride	T5941	Sigma-Aldrich	St.Louis	MO

SOLUTIONS

<u>BD Cell Viability kit:</u>

The kit was allowed to reach room temperature before use.

Per ml sample:

- 1 µl Propidium iodide (4.3 mM)
- 2 µl Thiazole Orange (42 µM)

Each sample was added thoroughly mixed 50 µl BD Liquid Counting Beads, using the reverse pipetting technique for better accuracy.

<u>TUNEL-assay:</u>

The Recombinant Terminal Transferase kit, Biotin-16-dUTPs and DTT solution was allowed to reach room temperature before use.

Table S2: One sample recipe for a TUNEL reaction, optimized for minimal reagent use.

Reagent volume		
2.00	µl	5x TdT Reaction Buffer (1M $C_2H_6AsKO_2$, 125mM Tris-HCl, 1.25mg/ml BSA)
0.08	µl	TdT enzyme (400 U/µl)
1.20	µl	$CoCl_2$ (25mM)
0.20	µl	Biotin-16-dUTP (1mM)
0.20	µl	DTT (10mM)
16.32	µl	ddH_20 **for a total reaction volume of 20 µl**

Appendix

Western Blotting

2x Loading buffer:

- 4.0 ml 10% (w/v) SDS
- 2.0 ml Glycerol
- 0.1% (w/v) Bromophenol Blue
- 2.5 ml Tris-HCl (0.5M) pH 6.8
- 0.5 ml DTT (0.1M)
- 2 ml ddH_2O for a total volume of 10 ml

10x Blotting salts:

- 30.0 g Trizma Hydrochloride
- 144.0 g Glycine
- Dissolved in ddH_2O for a total volume of 1000 ml

Transfer buffer:

- 1:10 10x Blotting salts
- 2:10 Methanol
- 7:10 ddH_2O

PRIMARY ANTIBODIES

Table S3: List of primary antibody specifications, dilution and secondary antibody used for immunofluorescence (IF), or Western blotting (WB). Immunoflourescence methods used were flow cytometry analysis and sorting and fluorescense microscopy. For IF all antibodies were diluted in PBS containing 5%(w/v) dry milk. Antibodies used for WB were diluted in TBS-T with 5% dry milk. Primary antibody = 1°Ab, secondary antibody = 2°Ab. *For optimalized phospho-ATM signal the amount of antibody-solution used during incubation was twice the normal volume.

Use	Antigen	Antibody Host&Type	1°Ab dilution	Product number	Producer	Secondary antibody	2°Ab dilution
IF	**Phospho-Histone H3 (Ser10)**	Rabbit polyclonal	1:500	06-570	Millipore, Temecula, CA	R-PE Goat anti-rabbit	1:50
IF	**Phospho-HISTONE H2AX (Ser139)**	Mouse monoclonal	1:500	05-636	Millipore, Temecula, CA	FITC Rabbit anti-mouse	1:50
IF	**LAMIN B2**	Mouse monoclonal	1:200	MAB 3536	Merck Chemicals, Damstadt, Germany	FITC Rabbit anti-mouse	1:50
WB	**Phospho-ATM (Ser1981)**	Mouse monoclonal	1:1000 *	4526	Cell signaling, Danvers, MA	HRP Donkey anti-mouse	1:10000
WB	**Phospho-CHEK2 (Thr68)**	Rabbit polyclonal	1:1000	2661	Cell signaling, Danvers, MA	HRP Goat anti-rabbit	1:10000
WB	**γ-TUBULIN (GTU-88)**	Mouse monoclonal	1:5000	T6557	Sigma-Aldrich, St.Louis, MO	HRP Donkey anti-mouse	1:10000

SECONDARY ANTIBODIES

Table S4: Specifications of the secondary antibodies used in immunofluorescense or Western blotting.

Label	Antibody	Antibody Host&Type	Product number	Manufacturer	City	Country
R-phycoerythrin (PE)	Anti-rabbit IgG	Goat polyclonal	P-2771MP	Life Technologies	Carlsbad	CA
Fluorescein isothiocyanate isomer 1 (FITC)	Anti-mouse IgG	Rabbit polyclonal	F0232	Dako	Carpinteria	CA
Horseradish Peroxidase (HRP)	Anti-mouse IgG	Donkey polyclonal	715-035-150	Jackson Immuno-Research	West Grove	PA
Horseradish Peroxidase (HRP)	Anti-rabbit IgG	Goat polyclonal	111-035-144	Jackson Immuno-Research	West Grove	PA

2 CALCULATIONS

Linear Regression Coefficients[a]

Model		Unstandardized Coefficients B	Unstandardized Coefficients Std. Error	Standardized Coefficients Beta	t	Sig.	95,0% Confidence Interval for B Lower Bound	95,0% Confidence Interval for B Upper Bound
1	(Constant)	1.224	.370		3.306	.003	.456	1.992
	Reh Apoptotic	1.385	.073	.971	19.049	.000	1.234	1.536

a. Dependent Variable: Reh Dead

Model		Unstandardized Coefficients B	Unstandardized Coefficients Std. Error	Standardized Coefficients Beta	t	Sig.	95,0% Confidence Interval for B Lower Bound	95,0% Confidence Interval for B Upper Bound
1	(Constant)	-.626	.489		-1.282	.213	-1.640	.387
	U698 Apoptotic	3.613	.272	.943	13.276	.000	3.049	4.178

a. Dependent Variable: U698 Dead

Model		Unstandardized Coefficients B	Unstandardized Coefficients Std. Error	Standardized Coefficients Beta	t	Sig.	95,0% Confidence Interval for B Lower Bound	95,0% Confidence Interval for B Upper Bound
1	(Constant)	1.507	1.540		.979	.338	-1.686	4.700
	JVM-2 Apoptotic	2.855	.266	.916	10.737	.000	2.304	3.407

a. Dependent Variable: JVM-2 Dead

Model		Unstandardized Coefficients B	Unstandardized Coefficients Std. Error	Standardized Coefficients Beta	t	Sig.	95,0% Confidence Interval for B Lower Bound	95,0% Confidence Interval for B Upper Bound
1	(Constant)	3.563	.665		5.354	.000	2.183	4.943
	Granta-519 Apoptotic	.944	.046	.975	20.499	.000	.848	1.039

a. Dependent Variable: Granta-519 Dead

Figure S1: SPSS output after linear regression of dead cells as a function of apoptotic cells.

3 SUPPLEMENTARY MATERIAL

144 HOUR TREATMENT OF U698 CELLS

As there were only a few % diploid G_1 cells after 144h treatment with 10µM ATMi and 3 µM PARPi, a 50:50 mixture with the 144h control sample was analyzed using flow cytometry (figure 2). The persistant 8n and 16n populations prove that the treatment causes endoreduplication in U698 cells.

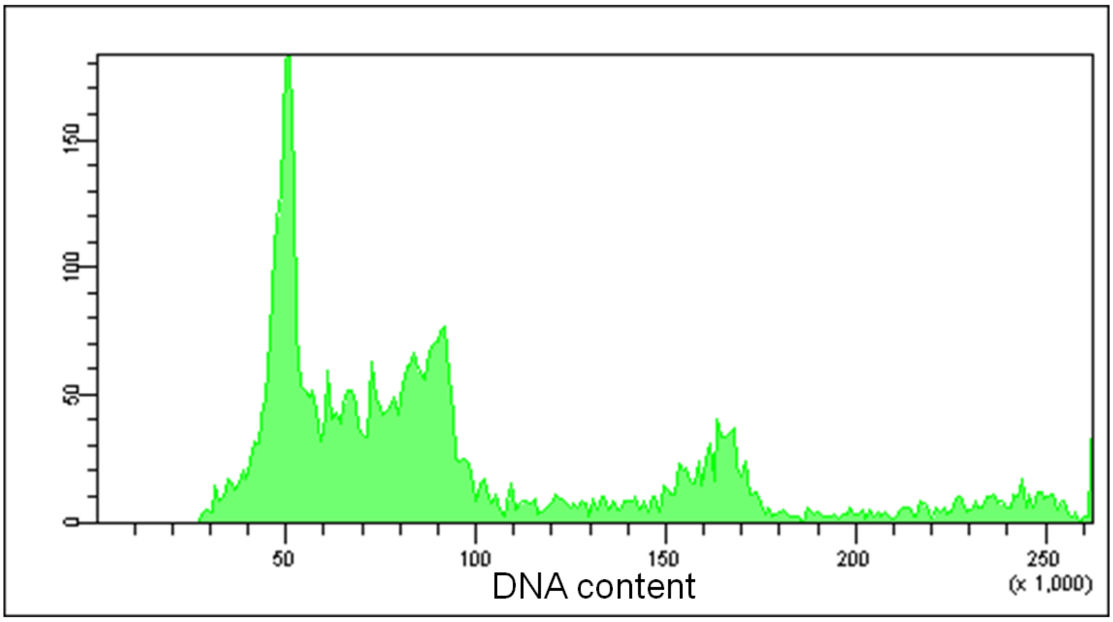

Figure S2: U698 cells after 144h treatment. Mixed sample-control of the mock-treated sample and sample treated with 3µM PARPi and 10µM ATMi.

MITOTIC AND APOPTOTIC CELLS DURING ENDOREDUPLICATION IN THE U698 CELL LINE

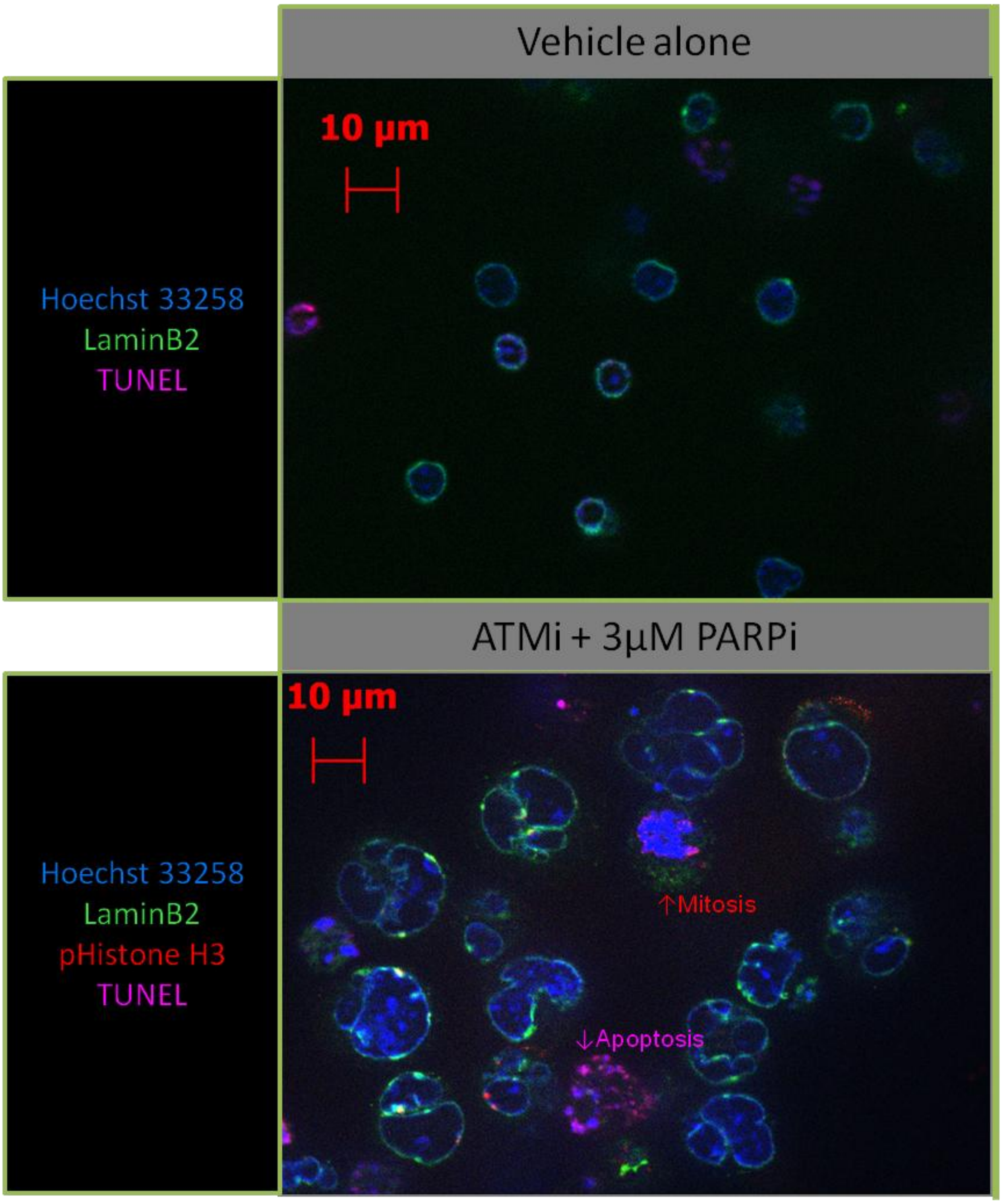

Figure S3: Fluorescence microscopy images of U698 cells after 144h treatment with PARPi (olaparib) and 10µM ATMi (KU-55933).

γH2AX INTENSITY DURING G_1, S AND G_2

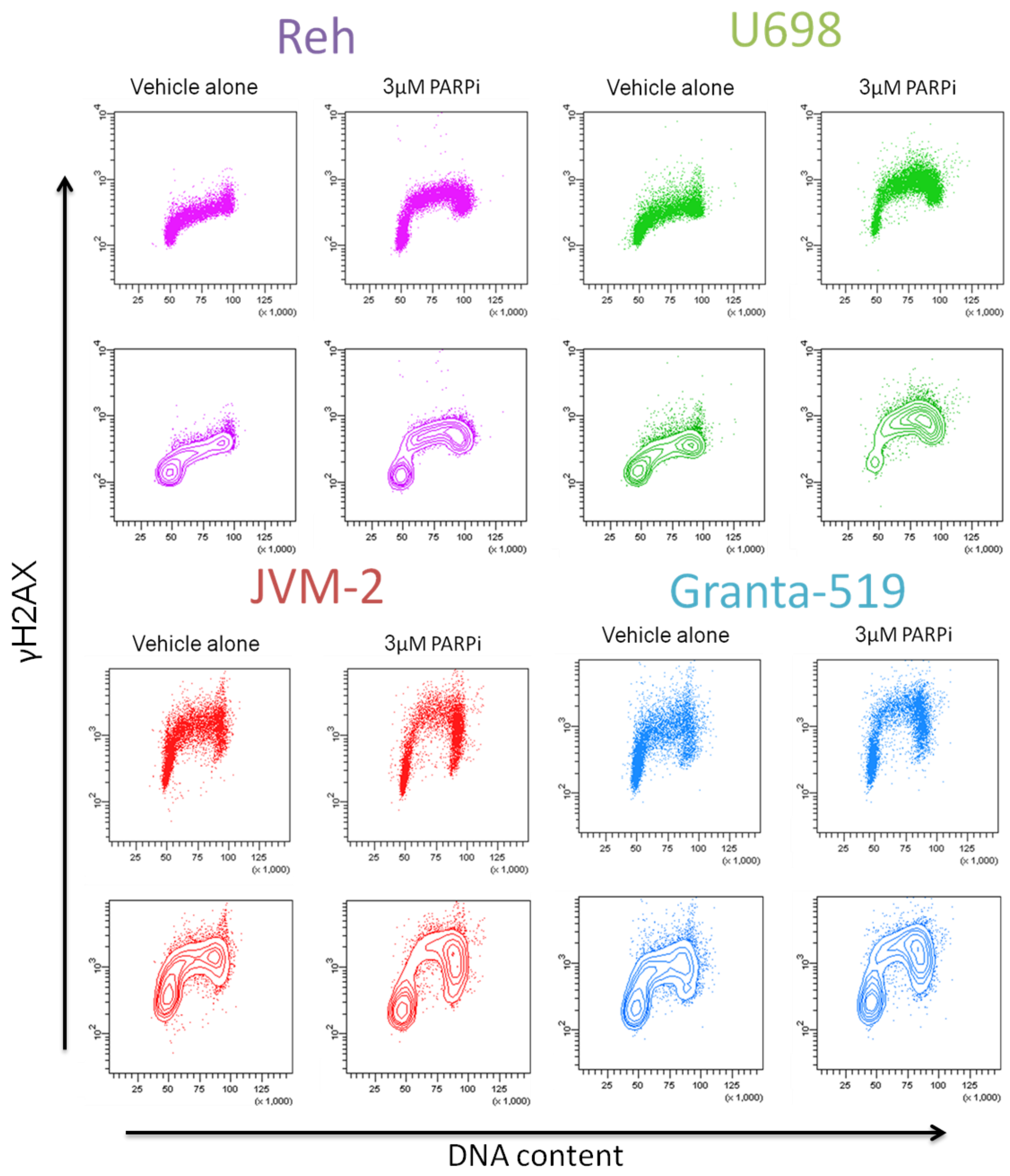

Figure S4: Flow cytometry analysis of γH2AX intensity relative to DNA content (doublets, mitotic and apoptotic cells are excluded) after 48h treatment with PARP inhibitor (olaparib). Dot plots and corresponding contour plots are shown for all cell lines.